



Available online at www.sciencedirect.com



ScienceDirect

International Journal of Fatigue 00 (2017) 1–72

Journal
Logo

www.elsevier.com/locate/procedia

A new strategy for fatigue analysis in presence of general multiaxial time varying loadings

Ma Zepeng^{a,*}, Patrick Le Tallec^b, Habibou Maitournam^c

^a*Laboratory of Solid Mechanics, Ecole Polytechnique, 91128 Palaiseau Cedex, France*

^b*Laboratory of Solid Mechanics, Ecole Polytechnique, 91128 Palaiseau Cedex, France*

^c*IMSIA, ENSTA ParisTech, CNRS, CEA, EDF, Université Paris-Saclay, 828 bd des Maréchaux, 91762 Palaiseau cedex France*

Abstract

The purpose of this paper is to propose an energy based multiscale fatigue approach which handles multi-dimensional time varying loading histories.

Our fundamental thought is to assume that the energy dissipated at small scales governs fatigue at failure. We follow the Dang Van paradigm at macro scale. The structure is elastic at the macroscopic scale. At each material points, there is a stochastic distribution of weak points which will undergo strong plastic yielding, which contribute to energy dissipation without affecting the overall macroscopic stress. The basis of our model is to consider a plastic behavior at the mesoscopic scales with a dependence of the yield function not only on the deviatoric part of the stress but also on the hydrostatic part. A kinematic hardening under the assumption of associative plasticity is also considered.

Instead of using the number of cycles, we use the concept of damage accumulation during the considered load history. Non-linear damage accumulation law based on plastic dissipation is also considered in our model. Fatigue will then be determined from the plastic shakedown cycle and from a phenomenological fatigue law linking lifetime and accumulated mesoscopic plastic dissipation.

Keywords: Fatigue; Energy; High cycle; Plasticity; Mean stress

^{*}Corresponding author. Email address: zepeng.ma@polytechnique.edu

Nomenclature

| | |
|--|--|
| S_a | maximum deviatoric stress during the loading cycles, |
| s_{-1} | the second principal invariant of the stress deviatoric tensor |
| b | tensile fatigue limit for $R = -1$ |
| \dot{w} | back stress |
| \dot{W} | energy dissipation rate at a certain scale |
| W | energy dissipation rate at all scales |
| W_{cyc} | dissipated energy at all scales per unit time |
| N | dissipated energy at all scales per cycle |
| N_F | current number of cycles |
| $\dot{\varepsilon}_p$ | number of cycles to failure |
| W_0 | rate of effective plastic strain |
| E | reference density of damage energy |
| $k = 500 \sim 800 \text{ MPa}$ | Young's modulus |
| $\beta = 1 \sim 50$ | hardening parameter |
| $\gamma = 0 \sim 50$ | weakening scales distribution exponent |
| $\alpha = 1 - a \left(\frac{\frac{1}{2}J_2(t) - \sigma_{-1}(1 - 3c\sigma_{H,max}(t))}{\sigma_u - J_2(t)} \right)$ | material parameter from Chaboche law |
| J_2 | characterizes non-linearity of damage accumulation(c is constant) |
| a | The second principal invariant of the stress deviatoric tensor |
| σ_y | material parameter from Chaboche law |
| $\lambda = 0 \sim 5$ | macroscopic yield stress(normal or shear) |
| $\underline{\underline{S}} = \text{dev} \dot{\underline{\underline{\Sigma}}}$ | hydrostatic pressure sensitivity |
| $\underline{\underline{\Sigma}}_H$ | deviatoric part of the stress tensor |
| $A_{II} = \tau_{oct,a} = \sqrt{\frac{1}{6}J_2}$ | macroscopic hydrostatic pressure |
| $\sigma_{VM} = \sqrt{3J_2}$ | the amplitude of octahedral shear stress |
| $\langle \rangle$ | Von Mises stress |
| | Macaulay bracket symbol. $\langle \rangle$ is defined as $\langle m \rangle = 0$ if $m \leq 0$ |

1 Weakening scales and yield function

1.1. The concept of weakening scales

We follow the Dang Van paradigm. The structure is elastic at the macroscopic scale. At each material points, there is a stochastic distribution of weak points which will undergo strong plastic yielding, without contributing to the overall macroscopic stress. From a microscopic point of view, there is a distribution of weakening scales, namely $s \in [1, \infty)$. In order to introduce our concept, let us imagine that we can measure the macroscopic stress intensity at present time by a given value S_a . Let σ_y be the yield limit before weakening. Then we imagine that for a given scale s :

- either $1 \leq s \leq \sigma_y/S_a$, then $S_a \leq \sigma_y/s$, the material stays in the elastic regime and there is no energy dissipation at this scale.
- or $\sigma_y/S_a \leq s \leq \infty$, then $S_a \geq \sigma_y/s$, the material is in plastic regime at this scale, which evolves through kinematic hardening, say from zero initial plastic strain $\underline{\underline{\varepsilon}}_p(s)$ and zero initial backstress $b(s)$ at initial time t_0 . There is then dissipated energy at scale s contributing to the fatigue limit.

1.2. Distribution of weakening scales

We assume the weakening scales have a probability distribution function following a power law:

$$P(s) = Hs^{-\beta} = (\beta - 1)s^{-\beta}, \quad (1)$$

where β is a material constant. The choice of a power law comes with two reasons: on one hand, this type of distribution corresponds to a scale invariant process, on the other hand it leads in cyclic loading to a prediction of a number of cycles to life limit as a power law function of the stress intensity. More general laws can also be proposed, without changing the spirit of the model.

The probability of weakening scales is shown in Fig. 1 and Fig. 2. We can see that smaller β leads to larger probability of weakening for large s .

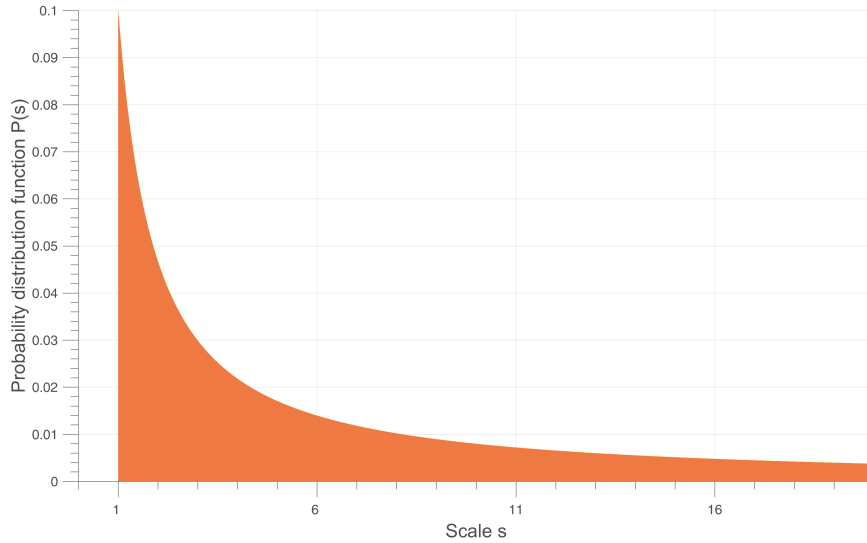


Fig. 1: Weakening scales s probability distribution curve when $\beta = 1.5$

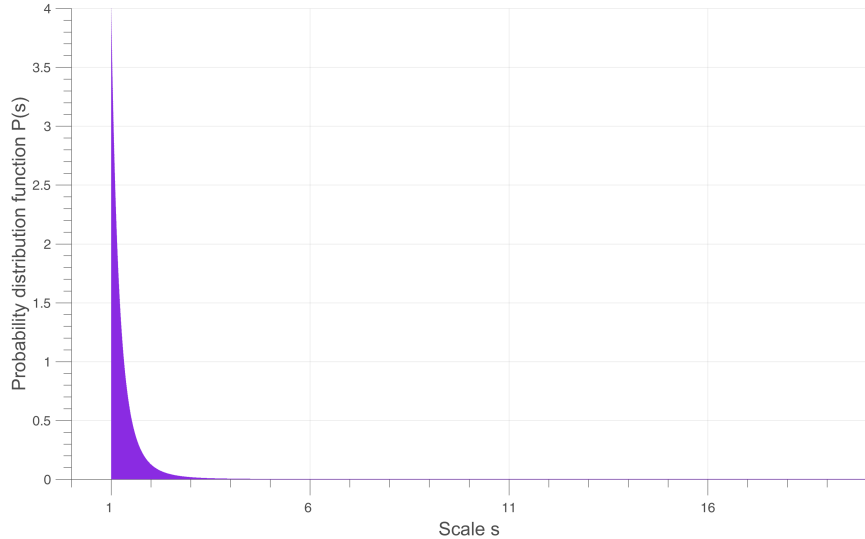


Fig. 2: Weakening scales s probability distribution curve when $\beta = 5$

1.3. Yield function with mean stress effect

Positive mean stress clearly reduces the fatigue life of the material. In design evaluation of multiaxial fatigue with mean stress, a simplified, conservative relation between mean stress and equivalent alternating stress is necessary. We can improve the model to come by modifying the yield function σ_y and the localization tensor.

Present choice

In the model to come, our idea is to consider as in [1] that the yield limit σ_y can be reduced in presence of positive mean stress. The mesoscopic yield function can therefore be written as:

$$f(s) = \|\underline{\underline{S}}(s) - \underline{\underline{b}}(s)\| + (\lambda \Sigma_H - \sigma_y) / s \leq 0 \quad (2)$$

with $\underline{\underline{S}}$ denoting the deviatoric part of the stress tensor at microscale, and $\underline{\underline{b}}(s)$ the corresponding backstress at the same scale. The material remain in elastic regime when $f < 0$ and in plastic regime when $f = 0$. The parameter λ can itself be a function of Σ_H with a different value in traction(λ_+) than in compression(λ_-).

1.4. Local plastic model

We can now describe the mesoscopic stress state. The model considers a plastic behavior at the mesoscopic scale. The mesoscopic stress evolution equations are thus:

$$\dot{\underline{\underline{S}}}(s, M, t) = dev \dot{\underline{\underline{\Sigma}}}(M, t) - \frac{E}{1 + \nu} \dot{\underline{\underline{\epsilon}}}^p(s, M, t), \quad (3)$$

which defines a Taylor-Lin scale transition model with unit localization tensor ([2]). The mesoscopic deviatoric strain rate tensor is thus equal to the macroscopic strain rate tensor $dev \dot{\underline{\underline{\Sigma}}} = \frac{1 + \nu}{E} dev \dot{\underline{\underline{\epsilon}}}$ with $dev \underline{\underline{\Sigma}}$ the deviatoric part of the macroscopic stress tensor. It is complemented by

$$\dot{\underline{\underline{b}}}(s, M, t) = \frac{kE}{E - k} \dot{\underline{\underline{\epsilon}}}^p(s, M, t), \quad (4)$$

which is our kinematic hardening model, and by

$$\dot{\underline{\underline{\varepsilon}}}^p(s, M, t) = C \frac{\partial f(s, M, t)}{\partial \underline{\underline{S}}}, \quad (5)$$

which is the associated plastic flow rule assuming $C = 0$ when $f < 0$ and $C \geq 0$ when $f = 0$.

Here E denotes the Young's modulus and k the hardening parameter. The local dissipated energy rate per unit volume at weakening scales s is given by the local entropy dissipation:

$$\dot{w}(s, M, t) = (\underline{\underline{S}} - \underline{\underline{b}})(s, M, t) : \dot{\underline{\underline{\varepsilon}}}^p(s, M, t). \quad (6)$$

2 Construction of an energy based fatigue approach

In a preliminary step, we will consider a simple macroscopic loading history $\underline{\underline{\Sigma}}(M, t)$ which is uniaxial along direction $\underline{\underline{s}}_1$, with $\underline{\underline{s}}_1$ a given stress tensor of unit norm. In traction there is

$$\underline{\underline{s}}_1 = \sqrt{\frac{3}{2}} \begin{pmatrix} 2/3 & 0 & 0 \\ 0 & -1/3 & 0 \\ 0 & 0 & -1/3 \end{pmatrix}.$$

Time periodic of deviatoric amplitude S_a , constant mean stress Σ_H and a Von Mises flow rule are taken into account to see if we get a prediction of local failure for a number of cycles N_F varying as $S_a^{-\gamma}$.

In uniaxial cyclic loading, there will be 3 kinds of loading patterns, as is shown in Fig. 3:

1. Elastic regime, in phase 2 and 4, where we have no plastic flow $\dot{\underline{\underline{\varepsilon}}}^p(s, M, t) = \dot{\underline{\underline{b}}} = 0$, and where the stress is below the yield limit $|\underline{\underline{S}} - \underline{\underline{b}}| < (\sigma_y - \lambda \Sigma_H) / s$, and where we have therefore $\dot{\underline{\underline{S}}} = \text{dev} \dot{\underline{\underline{\Sigma}}}$.
2. Plastic regime according to plastic flow rule, with increasing plastic deformation, in phase 5 and 1, where $\dot{\underline{\underline{\varepsilon}}}^p(s, M, t) = \xi \frac{\underline{\underline{S}}(s) - \underline{\underline{b}}(s)}{\|\underline{\underline{S}}(s) - \underline{\underline{b}}(s)\|} > 0$ with $\xi = \left| \text{dev} \dot{\underline{\underline{\Sigma}}} \right| \left(\frac{kE}{E - k} + \frac{E}{1 + \nu} \right)^{-1}$ (detailed in annex), $\underline{\underline{S}} - \underline{\underline{b}} = \underline{\underline{s}}_1 (\sigma_y - \lambda \Sigma_H) / s$ and $\dot{\underline{\underline{S}}} - \dot{\underline{\underline{b}}} = 0$.
3. Plastic regime in the other direction, in phase 3, where we now have $\dot{\underline{\underline{\varepsilon}}}^p(s, M, t) < 0$, then $\underline{\underline{S}} - \underline{\underline{b}} = -\underline{\underline{s}}_1 (\sigma_y - \lambda \Sigma_H) / s$ and $\dot{\underline{\underline{S}}} - \dot{\underline{\underline{b}}} = 0$.

In phase 1, a direct analysis yields the energy dissipation at scale s :

$$dW = (S - b) d\underline{\underline{\varepsilon}}^p = \frac{(E - k)(1 + \nu)}{E(E + k\nu)} \frac{(\sigma_y - \lambda \Sigma_H)}{s} \left(S_a - \frac{(\sigma_y - \lambda \Sigma_H)}{s} \right). \quad (7)$$

A similar analysis yields

$$dW(\text{phase1}) = dW(\text{phase5}) = \frac{1}{2} dW(\text{phase3}).$$

We can then calculate the local dissipated energy W at point M during one cycle by cumulating

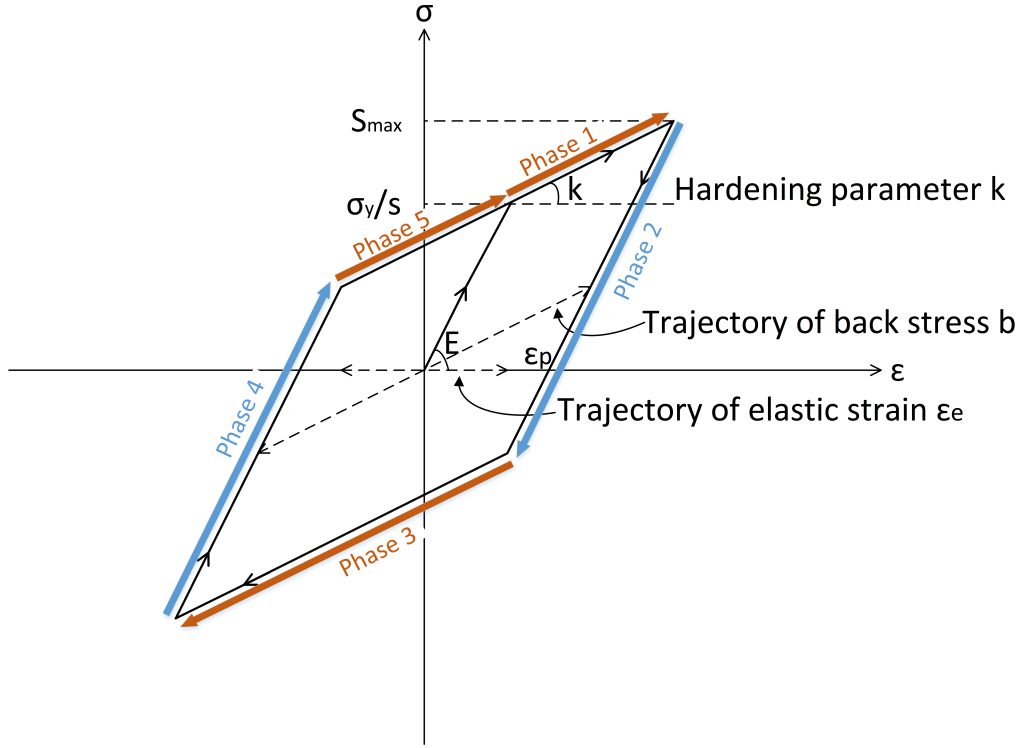


Fig. 3: Uniaxial load with plastic dissipation

the input of all sub-scales plastic regime with their probabilities ([3]).

$$\begin{aligned}
 W_{cyc} &= 4 \int_{(\sigma_y - \lambda \Sigma_H)/S_a}^{\infty} dW(s, M, t) P(s) ds \\
 &= 4 \int_{(\sigma_y - \lambda \Sigma_H)/S_a}^{\infty} \frac{(E - k)(1 + \nu)}{E(E + k\nu)} \frac{(\sigma_y - \lambda \Sigma_H)}{s} \left(S_a - \frac{(\sigma_y - \lambda \Sigma_H)}{s} \right) (\beta - 1) s^{-\beta} ds \\
 &= \frac{4(E - k)(1 + \nu)(\beta - 1)}{E(E + k\nu)\beta(\beta + 1)} \frac{S_a^{\beta+1}}{(\sigma_y - \lambda \Sigma_H)^{\beta-1}}.
 \end{aligned} \quad (8)$$

So we have a power law relationship between stress intensity and the dissipated energy per cycle.

$$W_{cyc} = C_1 S_a^{\beta+1}, \quad (9)$$

with

$$C_1 = f(\lambda, \beta) = \frac{4(E - k)(1 + \nu)(\beta - 1)}{E(E + k\nu)\beta(\beta + 1)(\sigma_y - \lambda \Sigma_H)^{\beta-1}}.$$

If the dissipated energy accumulates until a failure value W_0 , we can get directly the number of cycles to failure from Eq.(9) as:

$$N_F = \frac{W_0}{W_{cyc}} = \frac{W_0}{C_1} S_a^{-\beta-1}. \quad (10)$$

As for the time to failure in cyclic loading, it will be:

$$T_F = N_F t_{cyc}.$$

From Eq.(8), we then obtain that in uniaxial cyclic loading the model predicts as expected (Chapter ??) a power law dependence of the number of cycles to failure in function of S_a . However, experiments shows that the damage or the energy accumulation of a material evolves non-linearly in time and present a load dependent cycle (Chapter ??). We should introduce below a method to handle such a nonlinearity.

3 Nonlinearity of damage accumulation

3.1. Energy approach with Chaboche law

The Chaboche law ([4]) is essentially a damage incremental law for cyclic loads with a deviatoric stress intensity A_{II} and hydrostatic mean part Σ_H , defining the damage increase by:

$$\delta D = \left(1 - (1 - D)^{\gamma+1}\right)^\alpha \left(\frac{A_{II}}{M(\sigma_H)(1 - D)}\right)^\gamma \delta N, \quad (11)$$

using an effective intensity $A_{II}^* = A_{II}/(1 - D)$ evolving with damage D . And the mean stress effect is present both in exponential factor α and in denominator $M(\sigma_H)$.

$$\alpha = 1 - a \left\langle \frac{\frac{1}{2}A_{II} - \sigma_{-1}M(\sigma_H)}{\sigma_u - A_{II}} \right\rangle,$$

$$M(\sigma_H) = M_0 (1 - 3c\sigma_{H,max}).$$

Eq.(11) writes equivalently:

$$\delta[1 - (1 - D)^{\gamma+1}]^{1-\alpha} = (1 - \alpha)(\gamma + 1) \left(\frac{A_{II}}{M(\Sigma_H)}\right)^\gamma \delta N = \frac{1}{N_F(\sigma)} \delta N. \quad (12)$$

Here $N_F(\sigma)$ denotes the number of cycles at intensity σ to failure as obtained by integration of Eq.(12) from $D = 0$ to $D = 1$.

Similar to Eq.(12), we define here the “equivalent damage” \tilde{D} (Fig. 13) :

$$\tilde{D} = 1 - (1 - D)^{\gamma+1}, \quad (13)$$

with D the damage variable introduced by Chaboche in its model to scale the stress intensity:

$$A_{II} \longrightarrow \frac{A_{II}}{1 - D}.$$

We have

• $\tilde{D} = 0$ when $D = 0$ (undamaged material),

• $\tilde{D} = 1$ when $D = 1$ (failure of material),

and a nonlinear relation in between as in Fig. 4:

$$\delta\tilde{D} = (\gamma + 1) (1 - D)^\gamma \delta D.$$

Change of damage measure $\tilde{D} = 1 - (1 - D)^{\gamma+1}$ makes the evolution (11) explicit. It writes

$$\frac{d\tilde{D}}{dN} = c_D \tilde{D}^\alpha \left(\frac{A_{II}}{M(\Sigma_H)}\right)^\gamma, \quad (14)$$

yielding after integration from $\tilde{D} = 0$ to $\tilde{D} = 1$ a number of cycles to fatigue at constant load given by

$$N_F = \frac{1}{(1 - \alpha)} \left(\frac{A_{II}}{M(\Sigma_H)}\right)^{-\gamma}.$$

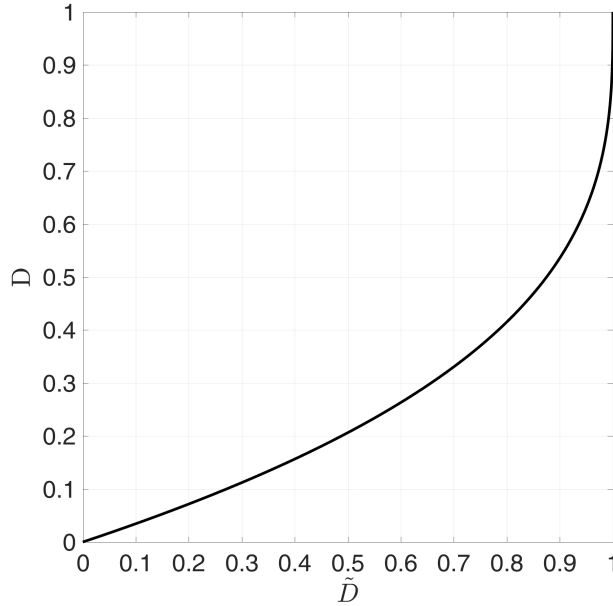


Fig. 4: The relation between \tilde{D} and D when $\gamma = 2$

This method as written requires cycle counting which is difficult and technical for complex load histories. In addition, it allows only a limited influence of multiaxiality.

Now in our model we use the same growth rule as in Chaboche in cyclic load regime, but replace stress intensity by multiscale dissipated energy in Eq.(14), which removes cycle counting.

The evolution (14) then writes

$$\frac{d\tilde{D}}{dt} = \tilde{D}^\alpha \dot{W}/W_0,$$

or in a differential form

$$d\tilde{D} = \tilde{D}^\alpha \frac{dW}{W_0} = \tilde{D}^\alpha \frac{W_{cyc} dN}{W_0}. \quad (15)$$

The replacement of dW by $W_{cyc} dN$ is only introduced to handle cyclic loadings if they occur. The number of cycles to failure in constant loading case, obtained by integrating \tilde{D} from \tilde{D}_0 to 1 is then:

$$N_F = \frac{W_0}{(1-\alpha) W_{cyc}} (1 - D_0^{1-\alpha}).$$

With initial damage $D_0 = 0$, we finally get with our proposed expression Eq.(9) of cyclic energy dissipation:

$$N_F = \frac{W_0}{(1-\alpha) W_{cyc}} = \frac{W_0}{(1-\alpha) C_1} S_a^{-\beta-1}. \quad (16)$$

From Eq.(16), we see $(-\beta - 1) = -\gamma$ is related to the slope in S-N curve and that $\frac{W_0}{(1-\alpha) C_1}$ defines the number of cycles to failure.

3.2. Sequence effect

Experiments show fatigue tests started with high stress then change to low stress has less fatigue life than the combination of high stress life proportion plus the low one. This phenomenon of sequence effect is load history dependent, so we need a stress induced parameter to describe it.

This is done in Chaboche with three ingredients:

1. a damage sensitive effective stress:

$$\sigma_D^{eff} = J_2(\underline{\Sigma})/(1 - D) = A_{II}/(1 - D);$$

2. a $(\sigma_D^{eff})^\gamma$ controlled law for damage growth

$$\frac{dD}{dN} = c_\gamma \tilde{D}^\alpha (\sigma_D^{eff})^\gamma;$$

3. a load dependence of exponent α (from 1 at zero load to 0 at large loads). In Chaboche model, the proposition of α is

$$\alpha = 1 - a \left(\frac{\sigma_{eq} - \sigma_{fatigue}}{\sigma_u - \sigma_{eq}} \right) \quad (17)$$

in order to recover the proper high-low sequencing effect.

Many fatigue damage accumulation models are based on the two level loading experiments which is one of the basic random loading analysis. To facilitate the validation and interpretation of an α dependence on stress we will also use two-stress level loading, the specimen is firstly loaded at stress Σ_1 for T_1 cycles and then at stress Σ_2 for T_2 cycles until failure. We can then observe if the experimental results are satisfactory.

During a loading time T_1 , we cycle from $\tilde{D} = 0$ to $\tilde{D} = \tilde{D}_1$. By integrating Eq.(15) of our proposed approach, we get:

$$(1 - \tilde{D}_1)^{1-\alpha_1} = \frac{T_1}{T_{F1}}, \quad (18)$$

with T_{F1} the time to failure with this loading.

Then we cycle from $\tilde{D} = \tilde{D}_1$ to failure $\tilde{D} = 1$, which yields

$$1 - (1 - \tilde{D}_1)^{1-\alpha_2} = \frac{T_2}{T_{F2}}. \quad (19)$$

From Eq.(18) and Eq.(19), after elimination of $(1 - D_1)$ we get:

$$\frac{T_2}{T_{F2}} = 1 - \left(\frac{T_1}{T_{F1}} \right)^\eta, \quad (20)$$

with

$$\eta = \frac{1 - \alpha_2}{1 - \alpha_1}. \quad (21)$$

In the case of high-low loading sequence we have $\Sigma_1 > \Sigma_2$, which gives $\alpha_1 < \alpha_2$, so it comes to:

$$\eta = \frac{1 - \alpha_2}{1 - \alpha_1} < 1 \implies \frac{T_2}{T_{F2}} = 1 - \left(\frac{T_1}{T_{F1}} \right)^\eta < 1 - \frac{T_1}{T_{F1}} \implies \frac{T_1}{T_{F1}} + \frac{T_2}{T_{F2}} < 1.$$

The α dependence on stress intensity does therefore predict a sequencing effect where a low loading sequence following a high one will reduce the life of the structure if α decreases when the load increases.

To get the same effect in our construction, we propose here to introduce s_{min} , which is the minimum scale that experiences plastic dissipation thus causes energy loss:

$$s_{min} = \frac{(\sigma_y - \lambda \Sigma_H)}{S_a}. \quad (22)$$

We propose a load dependent α through s_{min} . Possible choice of α is expressed as Eq.(23):

$$\alpha = 1 - a \left(\frac{\frac{1}{s_{min}}}{1 - \frac{1}{s_{min}}} \right). \quad (23)$$

There is no notion of fatigue limit in our model, $\sigma_{fatigue} = 0$. The intensity of loading

$$\frac{\sigma_{eq} - \sigma_{fatigue}}{\sigma_u - \sigma_{eq}} = \frac{1}{\frac{\sigma_u}{\sigma_{eq}} - 1}$$

is measured by

$$\left(\frac{\frac{1}{s_{min}}}{1 - \frac{1}{s_{min}}} \right) = (s_{min} - 1)^{-1}.$$

This means that we measure the distance of load to ultimate failure by local variable s_{min} through

$$\frac{\sigma_u}{\sigma_{eq}} - 1 \longrightarrow (s_{min} - 1)$$

We can see from Fig. 5 that with our proposition, cycling 1 for fifty percent of its failure time leaves a reserve before failure to cycling 2 of much less than fifty percent. To conclude, the cumulative damage under high-low loading sequence, as we deduced, has the addition of partial lives less than unit. Similarly, the cumulative damage under low-high loading sequence has addition of partial lives more than 1:

$$\frac{T_1}{T_{F1}} + \frac{T_2}{T_{F2}} > 1.$$

The curve in both cases is depicted in Fig. 5. For constant two-level stress loading, $\alpha_1 = \alpha_2$, the

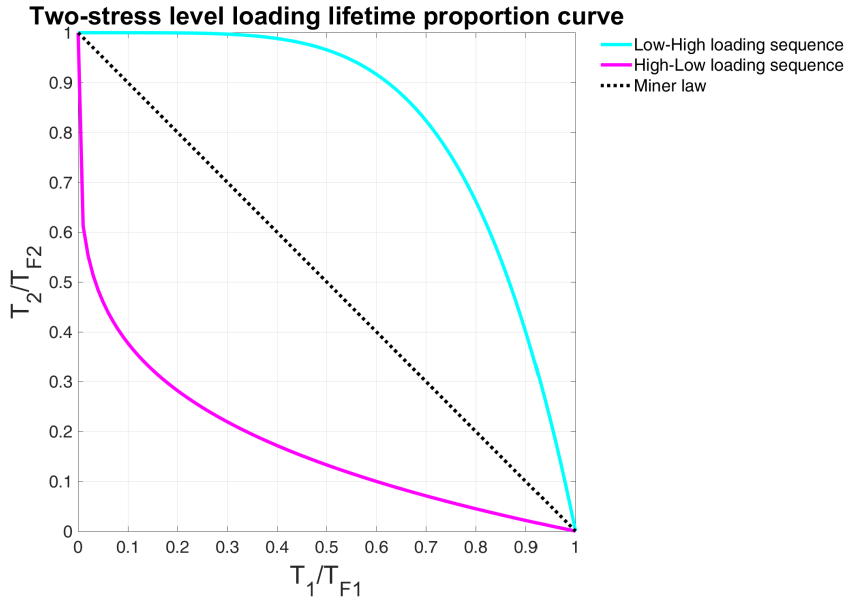


Fig. 5: High to low and low to high loading sequence comparison in 4-point bending ($F_{low} = 5000N, F_{high} = 30000N, Radius = 0.2m, \Sigma_u = 1.67E8$), with the proposed damage accumulation law (Eq.(15)) induced equation Eq.(20) and Chaboche type α (Eq.(17)) containing Crossland criterion

Chaboche law returns to the Miner rule when $F_{low} = F_{high}$ where:

$$\frac{T_1}{T_{F1}} + \frac{T_2}{T_{F2}} = 1.$$

3.3. The final model

In summary, our damage based fatigue life criterion using a damage evolution governed by a multiscale plastic energy dissipation, has four ingredients.

- a scale dependent yield limit

$$\frac{1}{s}(\sigma_y - \lambda \Sigma_H^{macro})$$

associated to a microscopic plastic evolution governed by the standard plastic evolution laws Eq.(3) - Eq.(5);

- a multiscale plastic energy dissipation obtained by summing plastic dissipation across our power law scale distribution

$$\dot{W}(M, t) = \int_{s=1}^{\infty} \left(\underline{S} - \underline{b} \right) (s, M, t) : \underline{\dot{\varepsilon}}^p (s, M, t) s^{-\beta} ds; \quad (24)$$

- a load intensity sequencing effect that we have represented by the formula :

$$1 - \alpha = a(s_{min} - 1)^{-f}; \quad (25)$$

- a exponential damage evolution law with load dependent exponent α given by the above formula and coefficient \dot{W}/W_0 governed by the multiscale plastic dissipation rate:

$$\frac{d\tilde{D}}{dt} = \tilde{D}^\alpha \dot{W}/W_0. \quad (26)$$

In this model we have five independent coefficients in addition to the construction of the local plastic model Eq.(3) - Eq.(5) :

1. reference density of damage energy : W_0 (in MPa)
2. mean stress effect coefficient : λ
3. slope of SN curve : $\beta + 1$
4. sensitivity to load intensity a .
5. exponent in the load sequence effect f .

4 Numerical strategy

4.1. Scale discretization

We now need to propose a practical implementation strategy for our final model of section 3.3. Our first approach takes one cycle as unit time. We compute analytically by Eq.(8) the energy dissipation at each scale during this cycle. The method is valid for simple loading history and which includes the integration on all weakening scales. The damage \tilde{D} is then accumulated after each cycle by numerical integration of Eq.(26) until we get to the fatigue limit of $\tilde{D} = 1$.

However, there are certain limitations of this method. Firstly we need a load history decomposition in cycles. Secondly in real life the perfect close loop cycle is hardly applicable. Finally, we need to approximate α by its average value per cycle which is computed numerically and can not be done analytically.

Thus we propose in a more general method which can be integrated by a step by step strategy. We compute numerically the dissipation at different scales using an implicit Euler time integration of the constitutive laws of section 4.2. After which we make a numerical integration on different scales. Then we can update the damage and go to next time step.

Instead of doing the scale integration directly which can be difficult for complex loading, the Gaussian Quadrature rule with Legendre points is used to give the value of local dissipated energy rate. To use the Gaussian quadrature rule the limit range of integral must be from -1 to 1 , while the total dissipated energy is expressed by integrating all the weakening scale s ranging from 1 to infinity with their occurrence probabilities:

$$\dot{W} = \int_1^\infty \dot{w}(s)(\beta - 1)(s)^{-\beta} ds.$$

To change the limit range of integral from $[1, \infty]$ to $[1, 0]$ we take as new integration variable $u(s) = s^{1-\beta}$. Therefore the dissipated energy summed on all scales is:

$$\begin{aligned} \dot{W} &= \int_1^\infty \dot{w}(s)(\beta - 1)(s)^{-\beta} ds \\ &= \int_0^1 \dot{w}(u^{1-\beta}) du \\ &= \frac{1}{2} \int_{-1}^1 \dot{w}\left[\left(\frac{x+1}{2}\right)^{\frac{1}{1-\beta}}\right] dx \end{aligned} \quad (27)$$

given $u = \frac{x+1}{2}$. So the dissipated energy rate integrated over all scales takes the form of Eq.(28):

$$\dot{W} = \frac{1}{2} \int_{-1}^1 \dot{w}\left[\left(\frac{x+1}{2}\right)^{\frac{1}{1-\beta}}, t\right] dx \approx \frac{1}{2} \sum_i \omega_i \dot{w}\left[\left(\frac{x_i+1}{2}\right)^{\frac{1}{1-\beta}}, t\right], \quad (28)$$

where ω_i and x_i are respectively the weights and nodes of the Gauss Legendre integration rule used for the numerical integration. In this work, we used a 64 points Gaussian Legendre integration rule ([5]) with $s_i = \left(\frac{x_i+1}{2}\right)^{\frac{1}{1-\beta}}$ being the associated scale.

4.2. Calculation of local plastic dissipation

The material could be both in elastic and plastic regime depending on the considered scale. To be more elaborate, we reuse the fundamental equations in different regimes. At scale s , we have a dissipation rate given by:

$$\dot{w}(s) = \left(\underline{S} - \underline{b}\right) : \underline{\dot{\varepsilon}}^p,$$

which differs between plastic and elastic regime.

Elastic regime:

There we have plastic strain rate $\underline{\dot{\varepsilon}}^p = 0$, back stress rate $\underline{\dot{b}} = 0$ and deviatoric stress rate $\dot{\underline{\underline{S}}} = \text{dev} \dot{\underline{\underline{\Sigma}}}$, leading to

$$\dot{\underline{\underline{S}}} - \underline{\dot{b}} = \text{dev} \dot{\underline{\underline{\Sigma}}},$$

meaning

$$(\underline{\underline{S}} - \underline{\dot{b}})(t + dt) = (\underline{\underline{S}} - \underline{\dot{b}})(t) + \text{dev} \dot{\underline{\underline{\Sigma}}} dt.$$

At each time step we define a trial stress:

$$(\underline{\underline{S}} - \underline{\dot{b}})_{\text{trial}} := (\underline{\underline{S}} - \underline{\dot{b}})(t + dt). \quad (29)$$

We are in elastic regime at scale s as long as we satisfy

$$\left\| \underline{\underline{S}} - \underline{\dot{b}} \right\|_{\text{trial}} \leq (\sigma_y - \lambda \Sigma_H) / s. \quad (30)$$

Plastic regime:

When we leave elastic regime at scale s , i.e. when the above inequality Eq.(30) is violated, we have:

$$\left\{ \begin{array}{ll} \underline{\dot{\varepsilon}}^p = \xi \frac{\underline{\underline{S}} - \underline{\dot{b}}}{\left\| \underline{\underline{S}} - \underline{\dot{b}} \right\|}, \xi > 0, & \text{plastic flow,} \\ \left\| \underline{\underline{S}} - \underline{\dot{b}} \right\| = (\sigma_y - \lambda \Sigma_H) / s, & \text{yield limit,} \end{array} \right. \quad (31)$$

$$\left\{ \begin{array}{ll} (\underline{\underline{S}} - \underline{\dot{b}}) : (\dot{\underline{\underline{S}}} - \dot{\underline{\dot{b}}}) = 0, & \text{yield limit time invariance,} \end{array} \right. \quad (32)$$

$$\left\{ \begin{array}{ll} \dot{\underline{\dot{b}}} = \frac{kE}{E - k\underline{\dot{\varepsilon}}^p}, & \text{kinematic hardening rule,} \end{array} \right. \quad (33)$$

$$\left\{ \begin{array}{ll} \dot{\underline{\underline{S}}} = \text{dev} \dot{\underline{\underline{\Sigma}}} - \frac{E}{1 + \nu} \dot{\underline{\dot{\varepsilon}}^p}, & \text{localisation rule.} \end{array} \right. \quad (34)$$

$$\left\{ \begin{array}{ll} & \end{array} \right. \quad (35)$$

In all cases, we get by integrating Eq.35, Eq.34 with the use of Eq.31.

$$(\underline{\underline{S}} - \underline{\dot{b}})(s, t + dt) = \frac{(\underline{\underline{S}} - \underline{\dot{b}})_{\text{trial}}(s, t + dt)}{1 + \eta}, \quad (36)$$

and because of the yield condition Eq.32, we have

$$\eta = \max \left\{ \underbrace{0}_{\text{elastic regime}}, \underbrace{\frac{\left\| \underline{\underline{S}} - \underline{\dot{b}} \right\|_{\text{trial}}}{(\sigma_y - \lambda \Sigma_H) / s} - 1}_{\substack{\text{plastic regime when this number is positive}}} \right\},$$

That is to say, when the structure is in elastic regime at time t and scale s , we have $(\underline{\underline{S}} - \underline{\dot{b}})(s, t) = (\underline{\underline{S}} - \underline{\dot{b}})_{\text{trial}}(s, t)$. Otherwise, if the norm of $(\underline{\underline{S}} - \underline{\dot{b}})_{\text{trial}}(s, t)$ is greater than the local yield limit $(\sigma_y - \lambda \Sigma_H) / s$, $(\underline{\underline{S}} - \underline{\dot{b}})(s, t)$ will be projected on the yield limit.

Knowing the distinction between elastic and plastic regime under multiple scales, we compute the general expression of the dissipated energy rate at scale s .

$$\dot{w}(s) = \left(\underline{\underline{S}} - \underline{\underline{b}} \right) : \dot{\underline{\underline{\epsilon}}}^p = \gamma \frac{(\sigma_y - \lambda \Sigma_H)}{s}. \quad (37)$$

From Eq.(??) and Eq.(??) in annex, we get:

$$\begin{aligned} E\gamma dt &= \left\langle \left| \underline{\underline{S}} - \underline{\underline{b}} \right|_{trial} - \frac{(\sigma_y - \lambda \Sigma_H)}{s} \right\rangle / \left(\frac{1}{1+\nu} + \frac{k}{E-k} \right) \\ &= \left\langle \left| \underline{\underline{S}} - \underline{\underline{b}} \right|_{trial} - \frac{(\sigma_y - \lambda \Sigma_H)}{s} \right\rangle \frac{(E-k)(1+\nu)}{(E+k\nu)}, \end{aligned} \quad (38)$$

where $\langle \rangle$ is Macaulay bracket symbol defined as $\langle m \rangle = 0$ if $m \leq 0$, otherwise $\langle m \rangle = m$. Thus the dissipated energy rate only depends on the evolution of the variable $(\underline{\underline{S}} - \underline{\underline{b}})$, which must therefore be mentioned during the whole cycle under study.

We replace γ deduced from Eq.(38) in Eq.(37) to give the expression of local energy dissipation rate at scale s :

$$\dot{w}(s)dt = \frac{(E-k)(1+\nu)}{E(E+k\nu)} \left\langle \left| \underline{\underline{S}} - \underline{\underline{b}} \right|_{trial} - \frac{(\sigma_y - \lambda \Sigma_H)}{s} \right\rangle \frac{(\sigma_y - \lambda \Sigma_H)}{s}. \quad (39)$$

With Eq.(28), the final expression of energy dissipation W during time step dt writes:

$$\begin{aligned} W &= \dot{W}dt \\ &= \frac{1}{2} \sum_i \omega_i \dot{w} \left[\left(\frac{x_i + 1}{2} \right)^{\frac{1}{1-\beta}} \right] dt \\ &= \frac{(E-k)(1+\nu)}{2E(E+k\nu)} \sum_i \omega_i \left\langle \left| \underline{\underline{S}} - \underline{\underline{b}} \right|_{trial} - \frac{(\sigma_y - \lambda \Sigma_H)}{\left(\frac{x_i + 1}{2} \right)^{\frac{1}{1-\beta}}} \right\rangle \frac{(\sigma_y - \lambda \Sigma_H)}{\left(\frac{x_i + 1}{2} \right)^{\frac{1}{1-\beta}}}. \end{aligned} \quad (40)$$

The mean stress effect term in Chaboche model is $s_{-1} \left(1 - 3 \frac{\sigma_H}{\sigma_u} \right)$, where the fatigue limit at zero mean stress s_{-1} is reduced in the presence of σ_H . In our model, the yield limit decreases with positive mean stress. Because of the presence of the term $\lambda \Sigma_H$ which will be positive when Σ_H is positive. In Eq.40, the coefficient λ can change values if Σ_H changes sign (see section 1.3).

4.3. Damage integration algorithm

Numerically the change of α is extremely nonlinear with time. From Fig. 6 we can see the mean value of α depends on loading pattern.

Because of the possible large variations in time of α , the evolution problem in damage is very nonlinear and thus, one needs to develop and validate an improved numerical time integration strategy at least for two specific cases: the constant amplitude case and the random load case.

We propose in constant amplitude load with very small evolution of damage per cycle to numerically calculate W_{cyc} and the mean values of α through one cycle or several cycles(out-of-phase condition) and apply the result to life prediction by using Eq.(16):

$$N_F = \frac{W_0}{(1 - \alpha_m) W_{cyc}}, \quad (41)$$

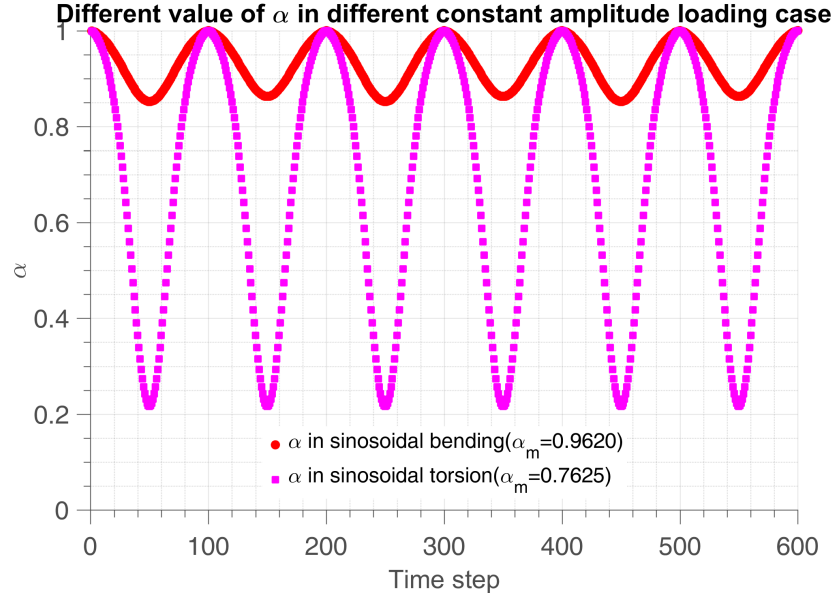


Fig. 6: The evolution of α in bending and torsion with $\Sigma_y = 1080 \text{ MPa}$, $\Sigma_{bending} = \Sigma_{torsion} = 500 \text{ MPa}$, $a = 0.3$ and 200 time steps in one cycle

which is obtained by direct integration of our damage law assuming time uniform dissipation in one cycle and frozen α . In this way the numerical cost is not as high as for the numerical implementation of all the loading points in random loading case. Because of the symmetrical shape of the evolution of α , numerically the mean value of α does not strongly depend on the number of steps per cycle. In the verification process we have compared 100 ~ 1000 time steps per cycle (Fig. 8).

For complex cyclic load cases, the idea is to accurately compute the history of plastic dissipation during one cycle (multiscale calculation with time refinement), and to use this precomputed result in the time integration of the scalar damage evolution law with a time stepping which is adapted to the time variation of α .

If α varies significantly, we use optimal time step numerical method to update D during one time step. In more details, let us suppose that our first few cycles calculation with fine time steps Δt has produced a sequence $\alpha(i)$ and $W_{cyc}(i)$ of exponent and dissipation at time $i\Delta t$. We then construct an adaptive time stepping strategy with variable time steps $\Delta t_{ref}(j)$, reference exponent $\alpha_{ref}(j)$ and dissipated energy $W_{ref}(j)$ by regrouping together adjacent time steps $\Delta t(i)$ with similar exponents $\alpha(i)$. This sequence is incremented as follows.

For $t_{ref}(j)$ and $\alpha_{ref}(j) = \alpha(t_{ref}(j))$ given, we set

$$\Delta t_{ref}(j) = \sum_{\substack{t(i) \geq t_{ref}(j) \\ \|\alpha(i) - \alpha_{ref}(j)\| \leq \Delta \alpha}} \Delta t, \quad t_{ref}(j+1) = t_{ref}(j) + \Delta t_{ref}(j).$$

The same goes for the dissipated energy:

$$\Delta W_{ref}(j) = \sum_{\substack{t(i) \geq t_{ref}(j) \\ \|\alpha(i) - \alpha_{ref}(j)\| \leq \Delta \alpha}} W_{cyc}(i), \quad W_{ref}(j+1) = W_{ref}(j) + \Delta W_{ref}(j).$$

We finally use these new time steps with corresponding α_{ref} and W_{ref} to update the damage by looping on all the following cycles with the new optimal time steps j and cycles N , and updating

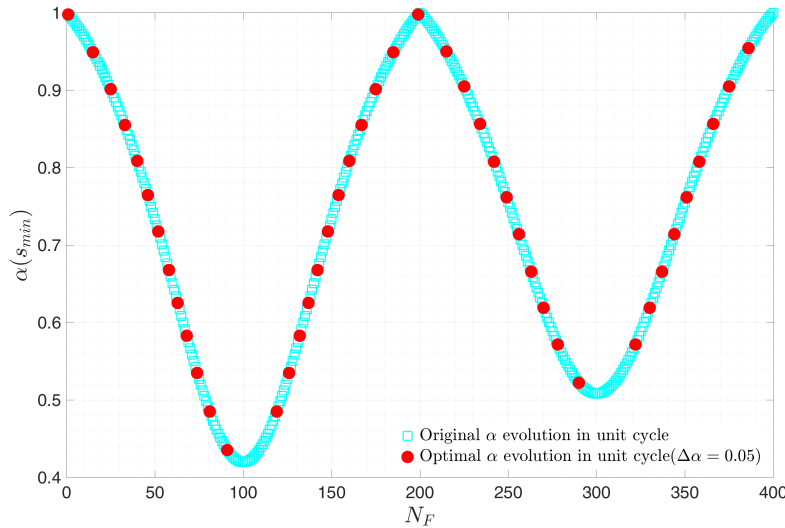


Fig. 7: Comparing numerical strategy with optimal time steps in one cycle with the old one, in this way the number of steps in unit cycle is reduced from 400 to 35, meaning a cost reduction factor of 0.0875 (with $\Delta\alpha = 0.05$, $a = 0.4$, $\lambda = 0.1$, $\Sigma_y = 230\text{ MPa}$, $\Sigma_{bending} = 225\text{ MPa}$)

damage in each cycle by:

$$D = D + D^{\alpha_{ref}(j)} \frac{\Delta W_{ref}(j)}{W_0}, \quad (42)$$

with values $\alpha_{ref}(j)$ and $\Delta W_{ref}(j)$ precomputed in the first few cycles. This strategy is validated in Fig. 7.

Complexity analysis

The optimal time step method clearly reduces the numerical cost. Typically, we assume the material has fatigue life of 1×10^6 cycles to failure and we implement 1000 time steps in unit cycle. The reduction factor of points in unit cycle for example as in Fig. 7 equals $35/400 = 0.0875$. We can then compare the cost between full numerical strategy and the new one.

| | |
|---------------------------------|---|
| Full numerical strategy: | $1000 \text{ time steps} \times 64 \text{ scales} \times 1 \times 10^6 \text{ cycles}$ |
| Optimal cyclic strategy: | $1000 \text{ time steps} \times 64 \text{ scales} \times 5 \text{ cycles until stabilization} + 1 \times 10^6 \text{ cycles} \times (1000 \text{ time steps} \times \text{reduction factor})$ |
| Ratio between optimal and full: | $\approx \frac{\text{reduction factor}}{64 \text{ scales}} = \frac{1}{731}$ |

The same strategy is applied to random loading situations which are made of repeated sequence of random loads:

- calculation of dissipated energy and exponent on one sequence;
- time coarsening;
- repeated integration of damage through the different sequences.

In such a strategy, the extra cost of introducing multiple scales in the calculation becomes negligible as compared to the time integration of damage in the evolution process.

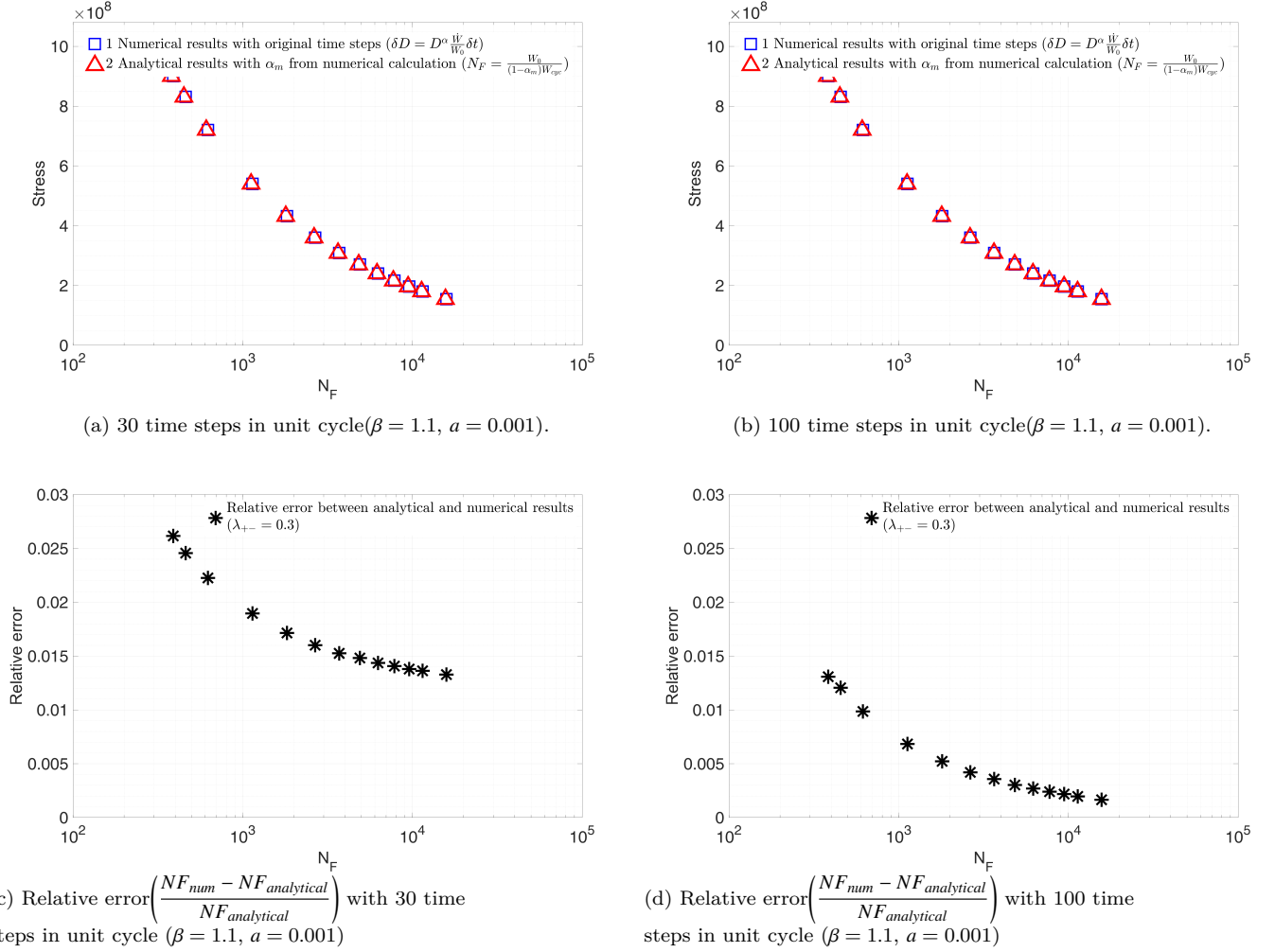


Fig. 8: S-N curve of bending test on 30NCD16 steel using numerical and analytical method (Eq.(41)) with different time steps. Data are those of table.1

Altogether, we have three numerical approaches for integrating damage.

1. Numerical results with varying α (equally divide time in unit cycle), and do the scale integration all along the fatigue life time, which can be of high numerical cost

$$\delta D = D^\alpha \frac{\dot{W}}{W_0} \delta t.$$

This method only serves for qualification purposes.

2. Numerical results with optimal time steps(equally divide α in unit cycle), here we have $\Delta\alpha = 0.01$, to reduce time steps needed, after several cycles adaptation we iterate using the recorded scalar values of α_{ref} , W_{ref} and t_{ref} to decide fatigue life time.

$$\delta D = D^{\alpha_{ref}} \frac{W_{ref}}{W_0} \delta t_{ref}.$$

3. Analytical results after integration of D (with mean alpha from numerical strategy)

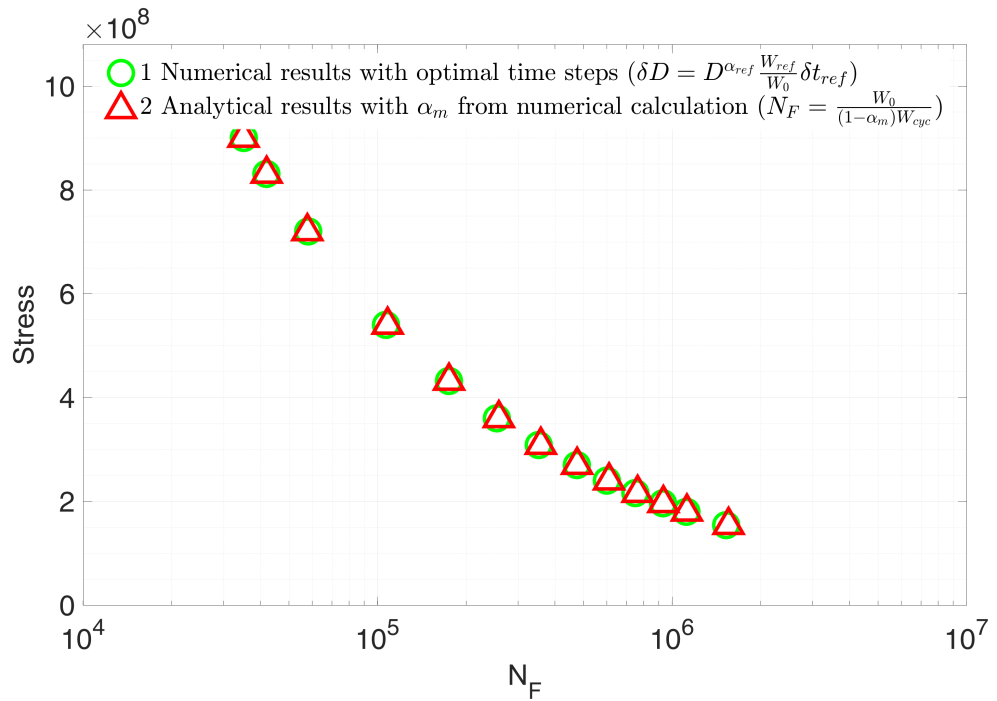
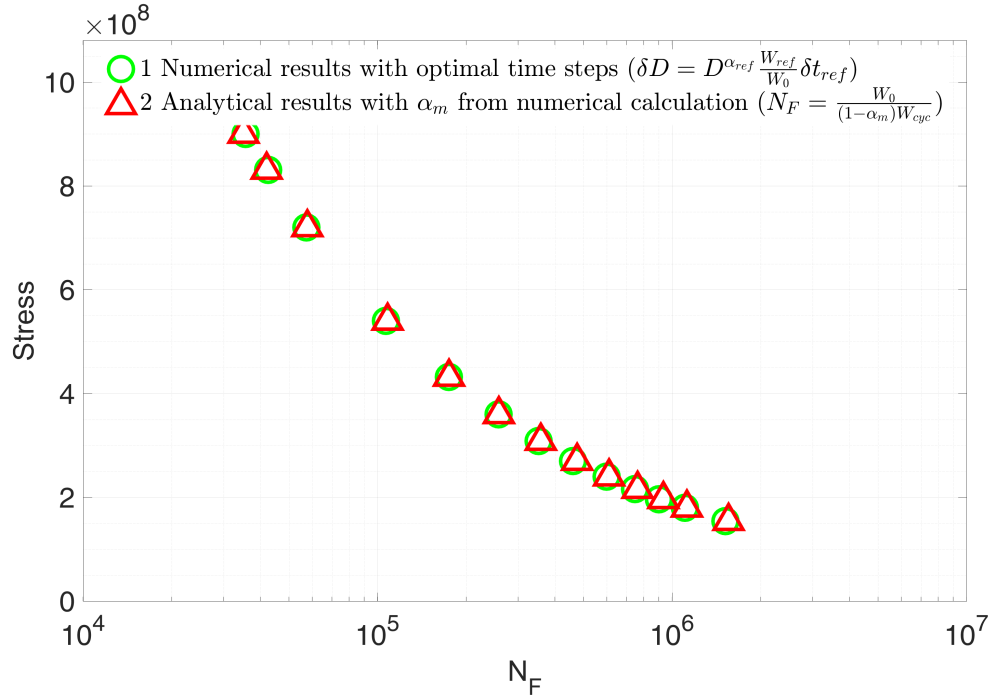
$$N_F = \frac{W_0}{(1 - \alpha_m)W_{cyc}},$$

which is derived from the differential equation

$$\delta D = D^{\alpha_m} \frac{W_{cyc}}{W_0} \delta N.$$

Although method 2 is much more numerically efficient than the original numerical method 1, it is still not cheap in the experimental fitting process. We need the analytical formula method 3 to do the fitting process. To validate the feasibility, we now compare only the analytical(method 3) one and optimal time steps(method 2) one. The results are shown in Fig. 9 and Fig. 10, the relation ship between relative error and $\Delta\alpha$ with 2000 time steps in unit cycle is shown in Fig. 11 and Fig. 12.

Now we can conclude that with more time steps in unit cycle, we get closer results with the original numerical method(method 2) in HCF regime. With smaller $\Delta\alpha$ value, we get less relative error between numerical(method 3) and analytical(method 1) results. This indicates that in constant amplitude cyclic loading, with moderate values of β it is feasible to use the analytical formula, given α_m is calculated using sufficient large time steps and small $\Delta\alpha$ in the first several cycles.



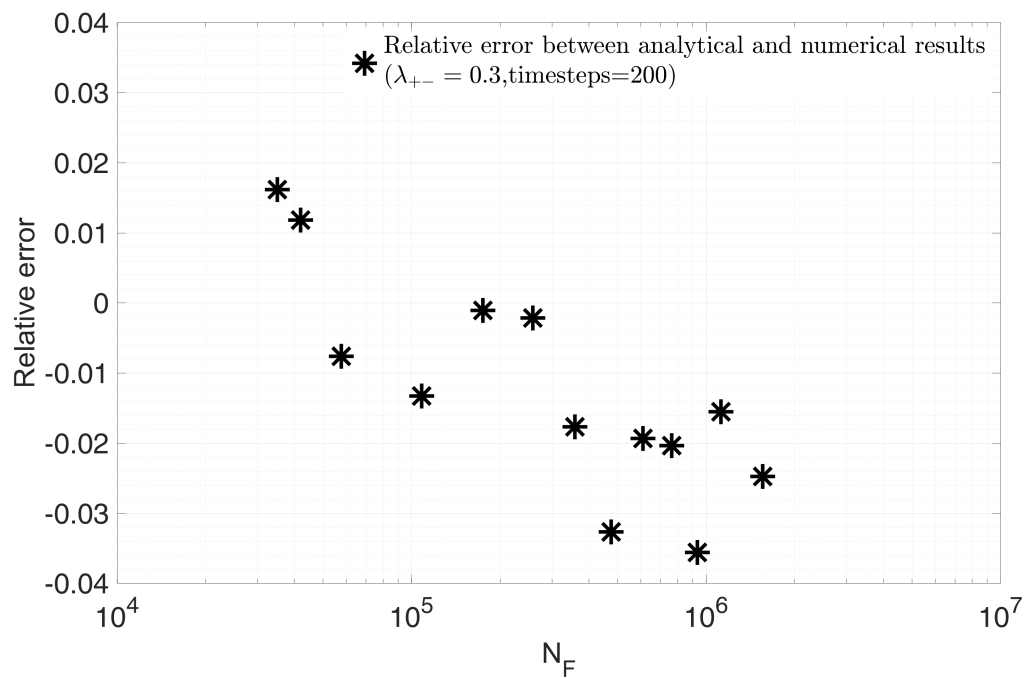


Fig. 11: Relative error $\left(\frac{NF_{opt} - NF_{analytical}}{NF_{analytical}} \right)$ between analytical and numerical results with optimal time steps methods
 $(\beta = 1.1, a = 0.01, \Delta\alpha = 2 \times 10^{-5} \text{ in unit cycle})$

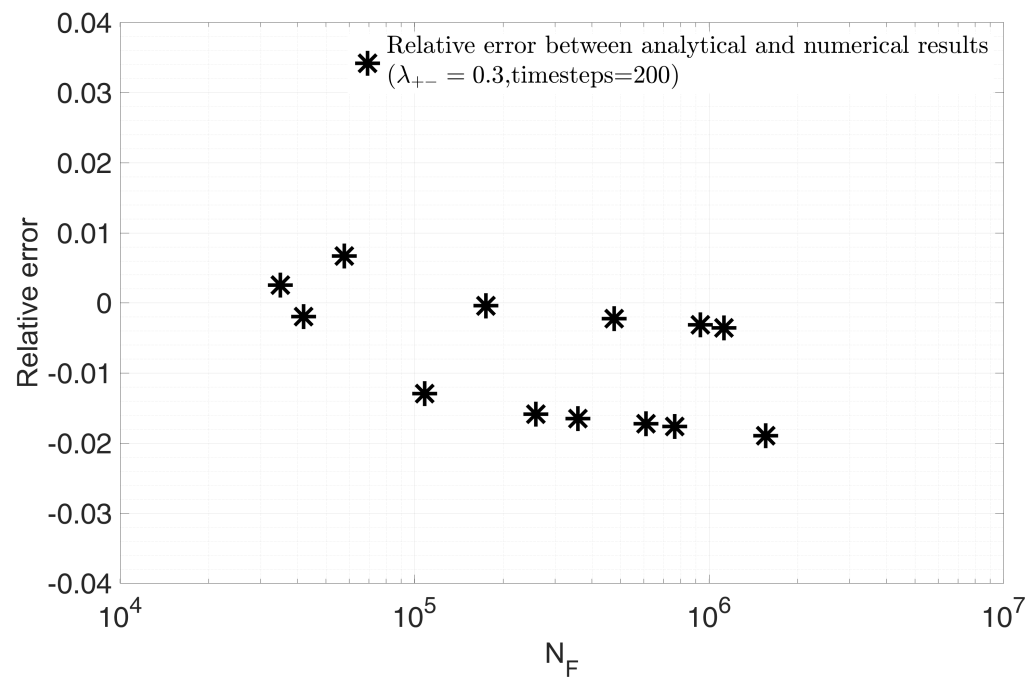


Fig. 12: Relative error $\left(\frac{NF_{opt} - NF_{analytical}}{NF_{analytical}} \right)$ between analytical and numerical results with optimal time steps methods ($\beta = 1.1$, $a = 0.01$, $\Delta\alpha = 1 \times 10^{-5}$ in unit cycle)

5 Validation on recovery tests

5.1. Recovery of Chaboche law on cyclic loading

The test is first performed on a sinusoidal uniaxial load $\Sigma_{11}(t) = A\sin(t)$, giving a deviatoric amplitude $S_a(t) = \sqrt{J_{2,a}(\text{dev}\Sigma(t))}$ so that $S_a(t) = \left\| \sqrt{\frac{1}{3}}\Sigma_{11}(t) \right\|$. We use parameters in Table 1 to recover the classic Chaboche law in cyclic loading.

| Parameters | Value |
|--|-------------------------------|
| Young's modulus | $E = 191 \text{ GPa}$ |
| Hardening parameter | $k = 1 \text{ GPa}$ |
| Weakening scales distribution exponent | $\beta = 1.5$ |
| Hydrostatic pressure sensitivty | $\lambda_{+-} = 0.6$ |
| Macroscopic yield stress | $\sigma_y = 1080 \text{ MPa}$ |
| Sequencing effect sensitivty | $a = 0.1$ |
| Dissipated energy to failure per unit volume | $W_0 = 5 \text{ MJ(MPa)}$ |

Table 1: Material parameters in a simple cyclic load

We use matlab to numerically realize our method. The plot of $\left\| \underline{\underline{S}} - \underline{\underline{b}} \right\|_{\text{trial}}$ and $\left\| \underline{\underline{S}} - \underline{\underline{b}} \right\|$ during the first cycles at two different scales ($s_3 = 1.21$ and $s_{10} = 1.13$) are shown in Fig. 13 and Fig. 14. We use here a fixed value of λ ($\lambda_+ = \lambda_-$), thus the local yield limit is reduced in traction and increased in compression.

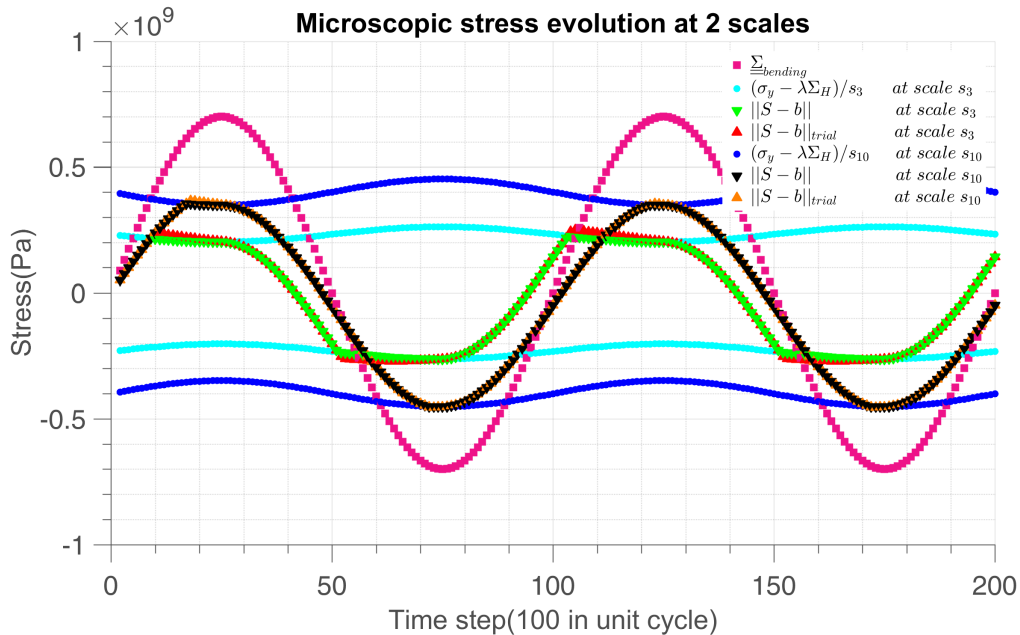


Fig. 13: Microscopic $\left\| \underline{\underline{S}} - \underline{\underline{b}} \right\|_{\text{trial}}$ and $\left\| \underline{\underline{S}} - \underline{\underline{b}} \right\|$ evolution with time under different weakening scales ($s_3 = 1.21$ and $s_{10} = 1.13$) in sinusoidal load with zero mean stress

The time history of dissipated energy is depicted in Fig. 15. We scale S_a in the plot to see more clearly the relation between energy dissipation and stress intensity. The choice of α does not affect W ; it only concerns damage accumulation rate. Smaller α causes faster accumulation.

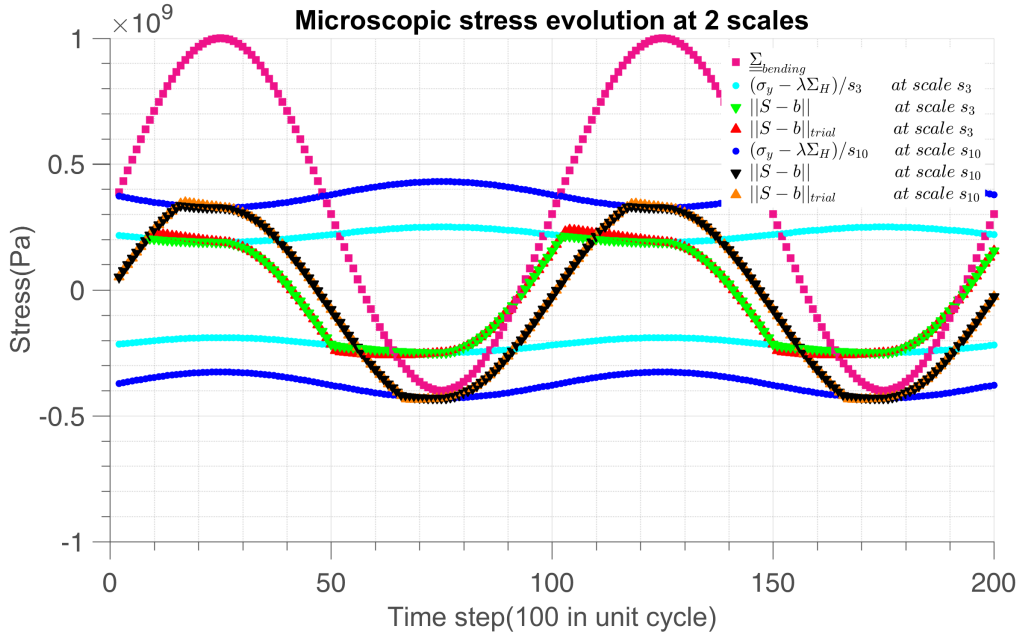


Fig. 14: Microscopic $(\underline{S} - \underline{b})_{trial}$ and $(\underline{S} - \underline{b})$ evolution with time under different weakening scales ($s_3 = 1.21$ and $s_{10} = 1.13$) in sinusoidal load with mean stress=300 MPa

The “jump” in energy evolution is due to activation of new scales while in-between two scales the dissipated energy follows the stress increment at each time step. In other words, because in our method the dissipated energy W (Fig. 15), sums energy dissipation at all scales, any additional violation of $\|S - b\|_{trial}$ at local yield limit (Fig. 13) introduces an additional dissipation.

We take the mean value of α during all the iteration process of numerical method as α_m . The energy and damage accumulation is shown in Fig. 17 and Fig. 20. Here we give 100 time steps in one cycle to see the relative difference between changing α and α_m , also \dot{W} and $W_{cyc}/stepnumber$ method. The more time steps we give, the more precision we get. The relative difference between analytical energy loss and numerical one is shown in Fig. 19 from which we conclude that the three methods converge in terms of elastic energy dissipation, but due to nonlinear effects the damage evolution does not have the same history per cycle. The frozen α delays damage, the varying α increases damage during the phase of strong loading. The difference has a significant impact if damage occurs with very few cycles. It will not when computing on a large number of cycles.

The cyclic load calculation is only valid for very simple such as proportional loading in fatigue. However, the convergence of the two methods is based on the small value of β (close to 1), in case of large values of β (typically around 5), the numerical strategy gives shorter life than the analytical one due to extreme non-linearity in the energy dissipation history per cycle. The relative error is around 20% as shown in Fig. 23 and Fig. 24. Nevertheless the analytical formula can still be used as a comparison group to verify the numerical results. And in the identification process we need the analytical form to fit the $S - N$ curve of a certain material. The outcome is satisfactory. Hence, to be more general for any loading history, we adopt the numerical method after identification of β .

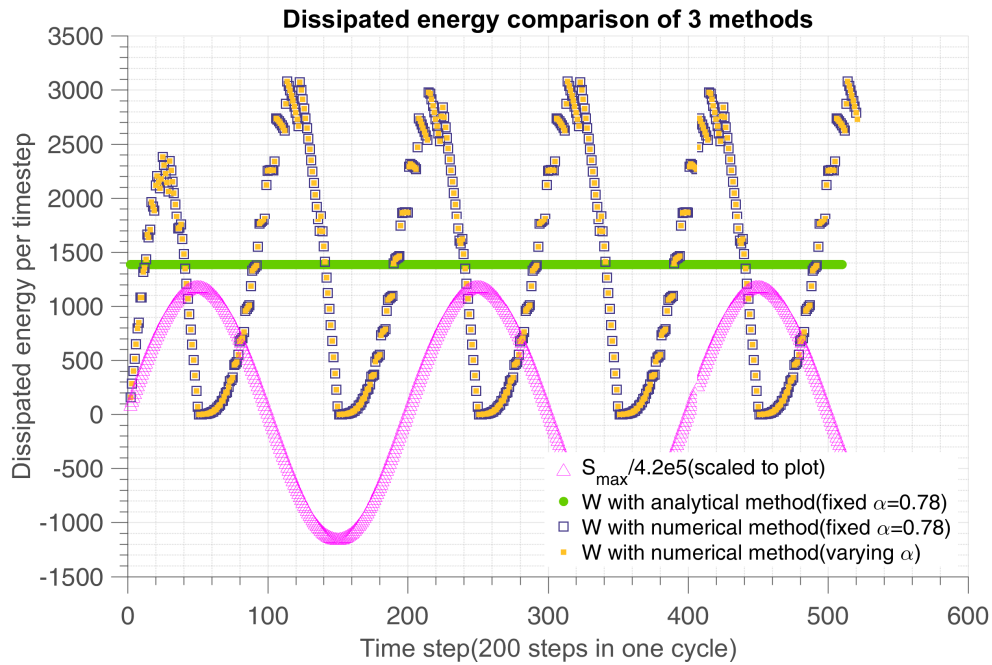


Fig. 15: Validation of dissipated energy in all scales with analytical(method 3) and numerical method(method 1) with $\beta = 1.1, \Sigma = 0.85\sigma_y$. The time evolution of α does not play a role in the dissipation calculation which is normal since α does not enter in the dissipation calculation

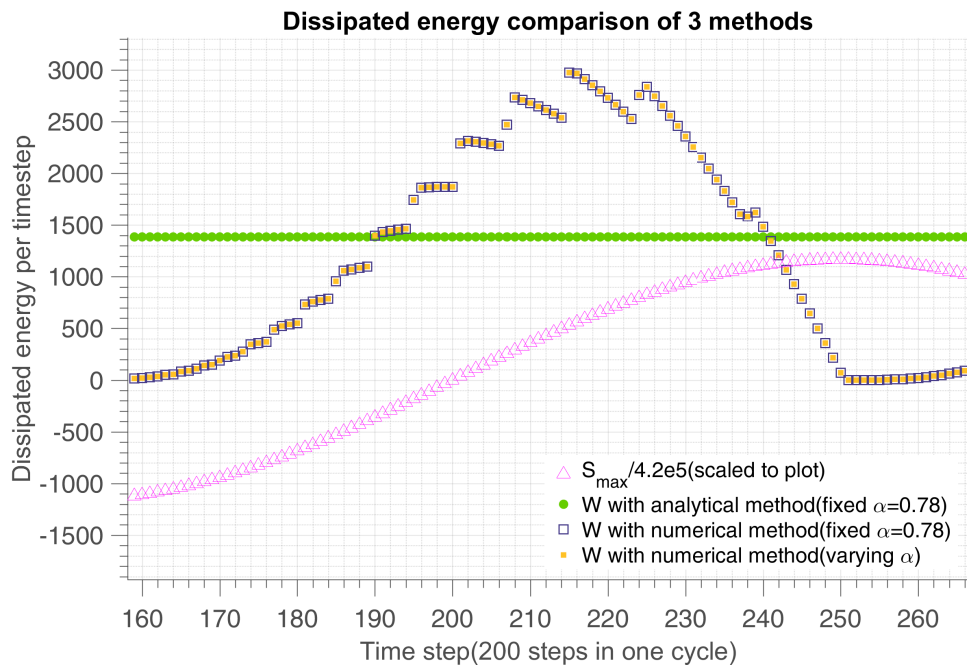


Fig. 16: Validation of dissipated energy in all scales with analytical and numerical method(enlargement of Fig. 15)

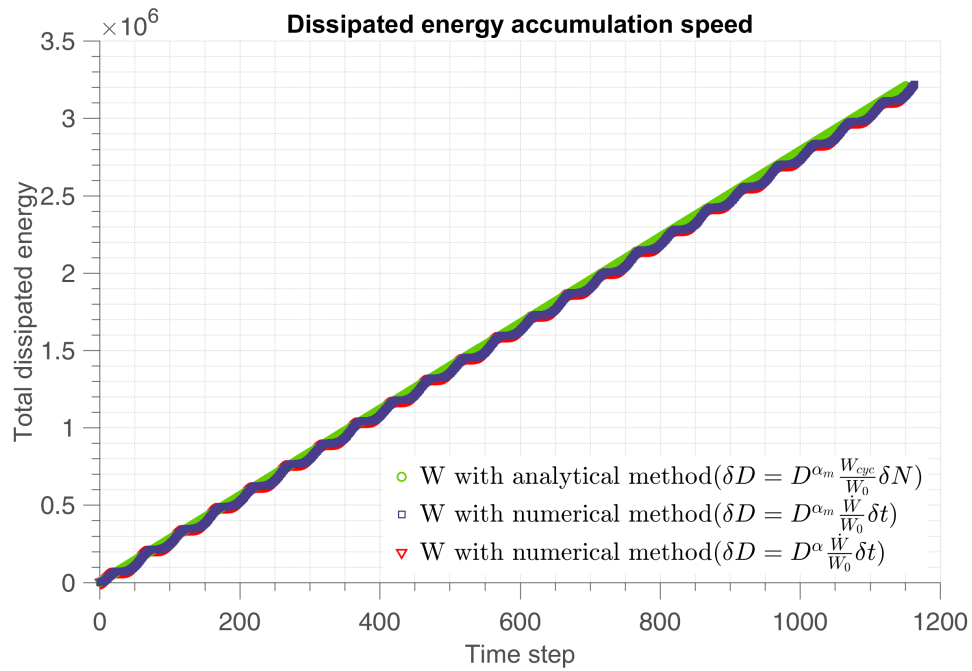


Fig. 17: Dissipated energy accumulation through time with different methods, there are 100 time steps in unit cycle

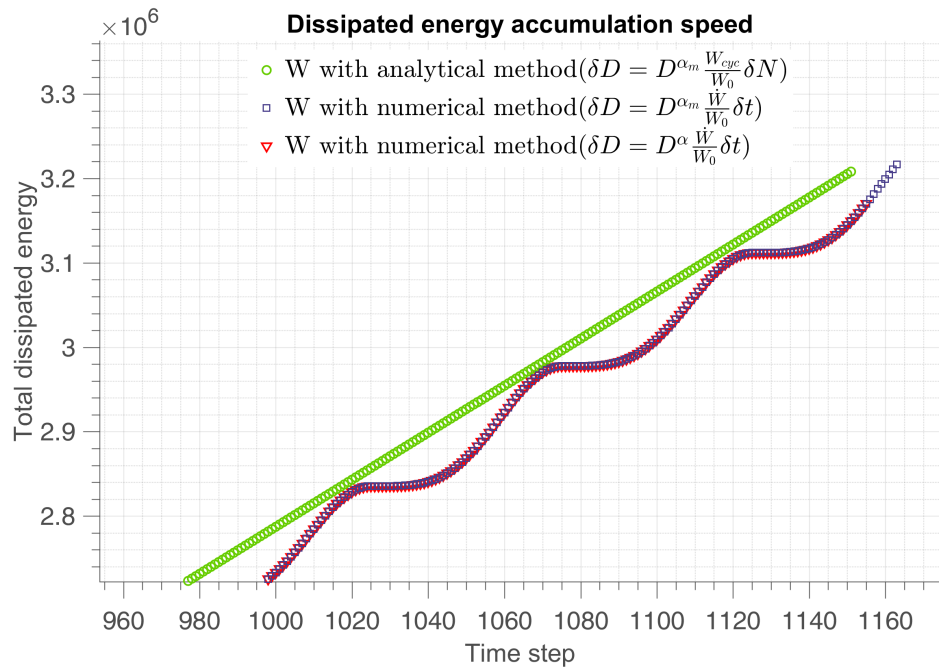


Fig. 18: Dissipated energy accumulation through time with of 3 methods(enlargement of Fig. 17)

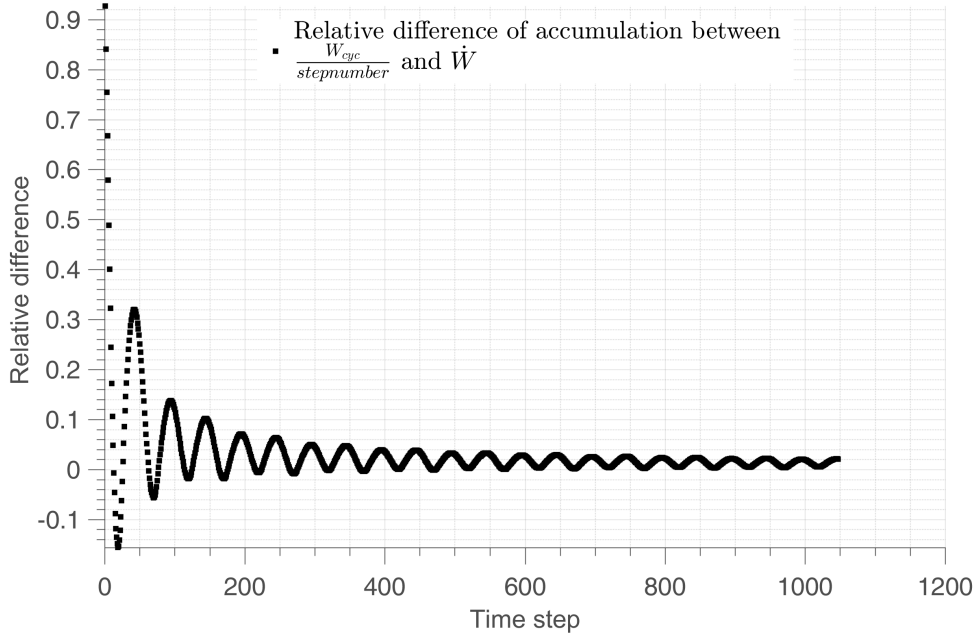


Fig. 19: Relative difference $\frac{W_{analytical} - W_{numerical}}{W_{analytical}}$ between analytical energy loss and numerical one with α varying with time of Fig. 17

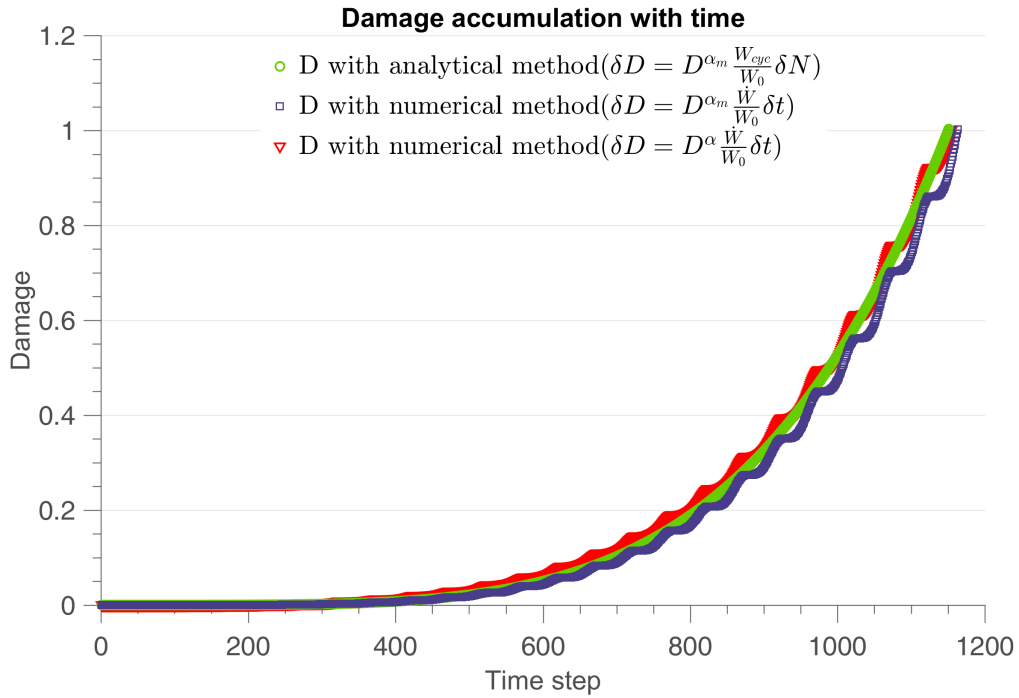


Fig. 20: Damage evolution with time under sinusoidal load with different methods, there are 100 time steps in unit cycle($\beta = 1.1, \Sigma = 0.85\sigma_y$)

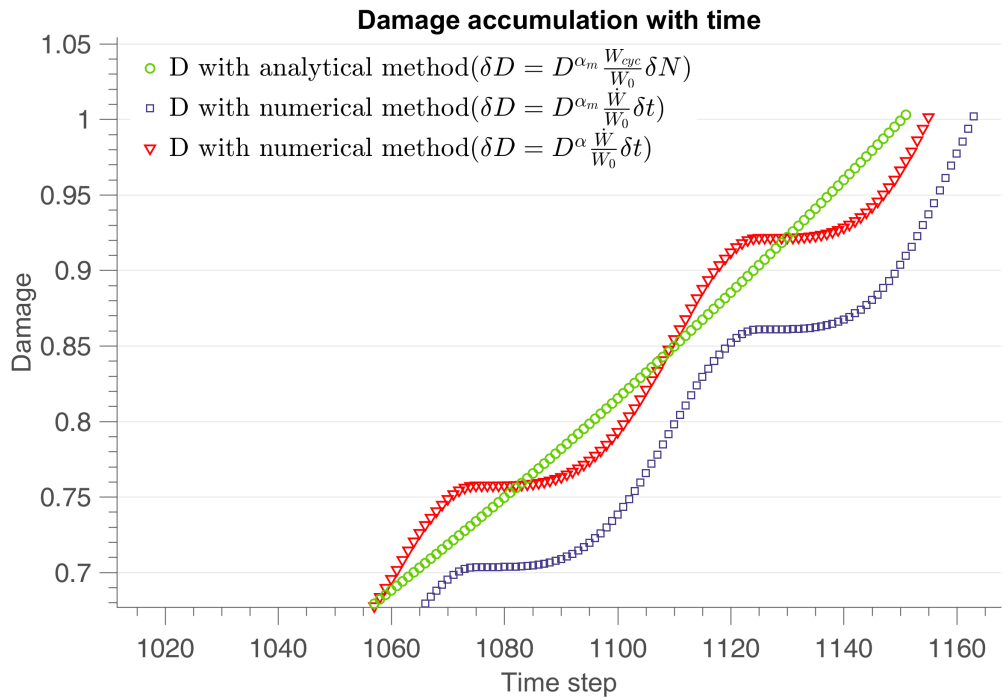


Fig. 21: Damage evolution with time under sinusoidal load with two different methods(enlargement of Fig. 20)

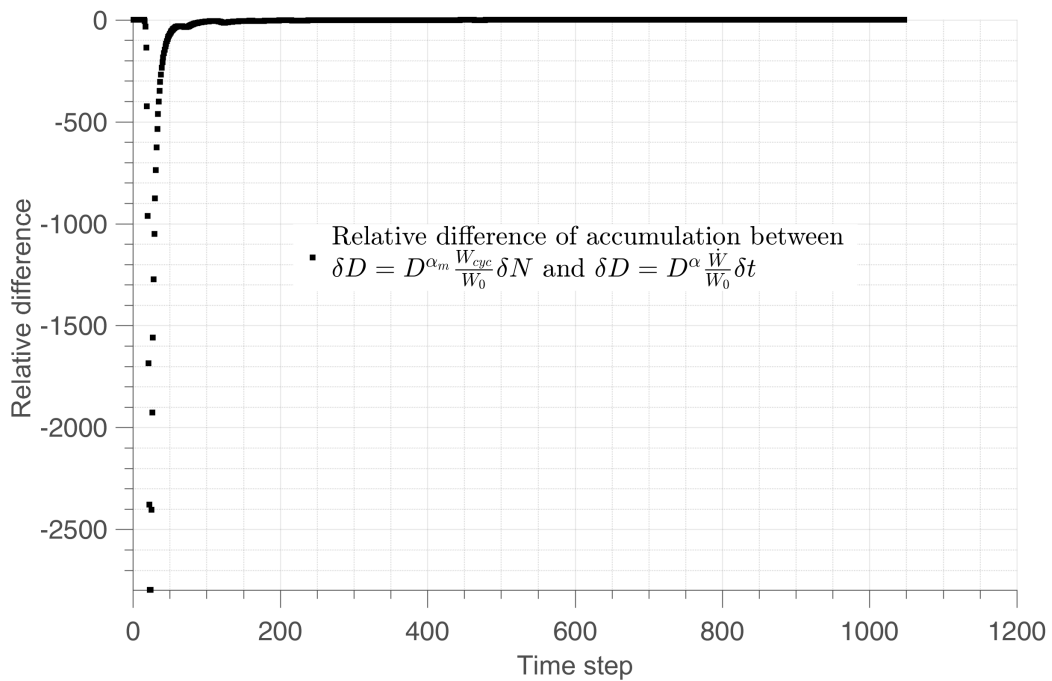


Fig. 22: Relative difference $\frac{D_{analytical} - D_{numerical}}{D_{analytical}}$ evolution with time of Fig. 20

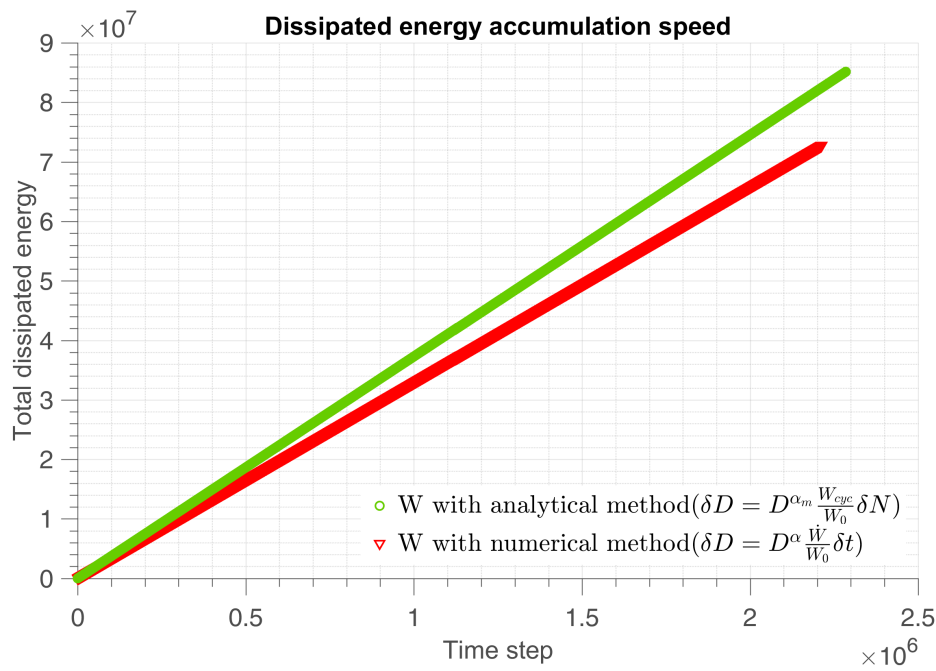


Fig. 23: Validation of dissipated energy in all scales with analytical and numerical method with $\beta = 5$, $\Sigma = 0.4\sigma_y$

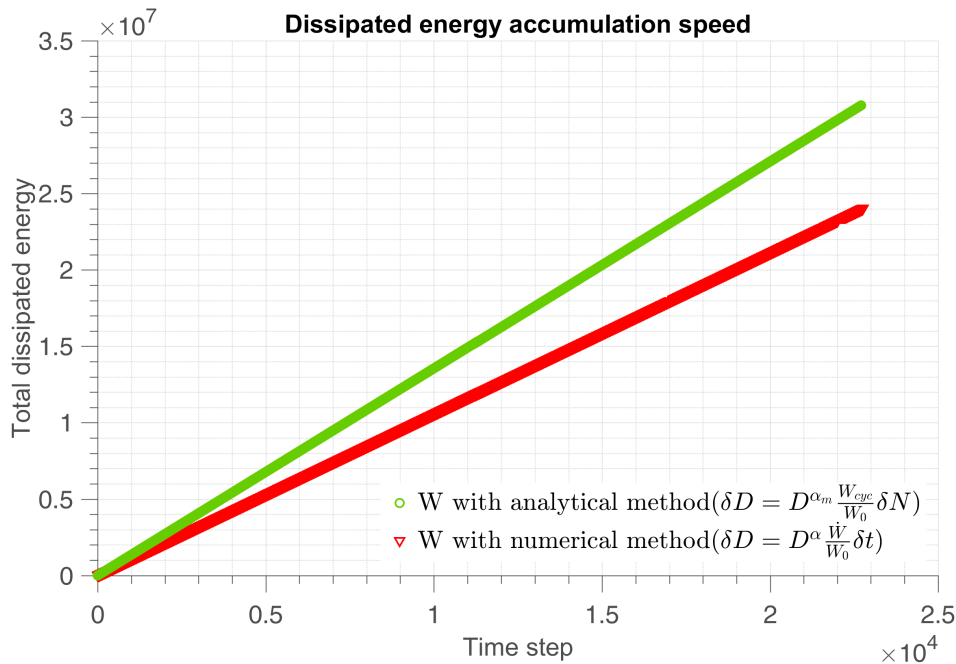


Fig. 24: Validation of dissipated energy in all scales with analytical and numerical method with $\beta = 5$, $\Sigma = 0.8\sigma_y$

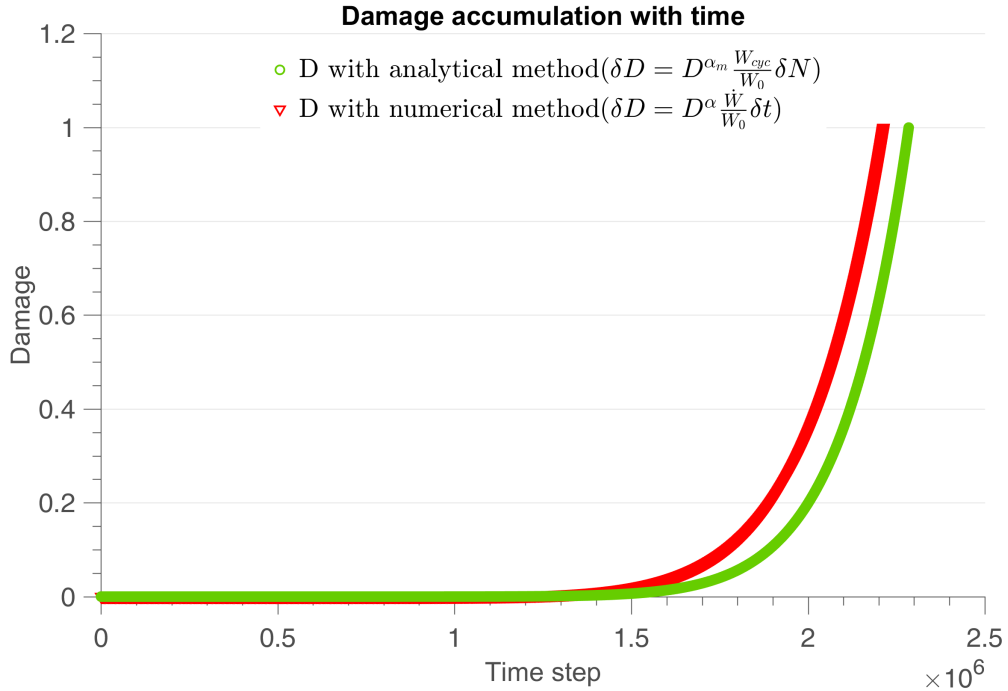


Fig. 25: Damage evolution with time under sinusoidal load with $\beta = 5$, $\Sigma = 0.4\sigma_y$. In such a severe loading and with extreme non-linearity, the simple Chaboche like formula with frozen α departs from the outcome of the full numerical model

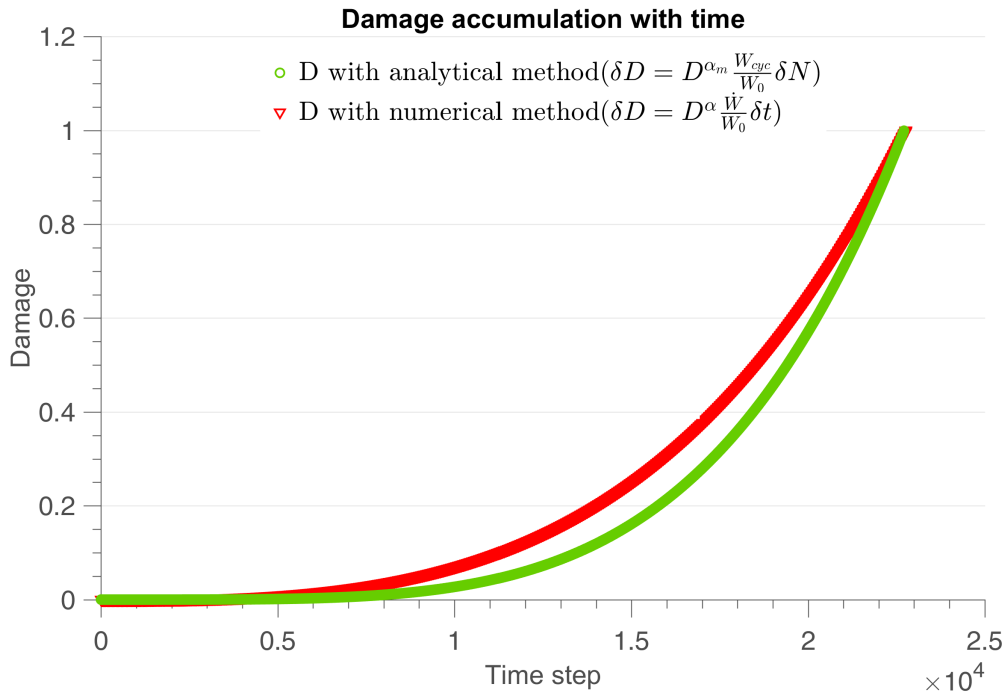


Fig. 26: Damage evolution with time under sinusoidal load with $\beta = 5$, $\Sigma = 0.8\sigma_y$

5.2. Numerical recovery of sequence effect

We adopt the parameter α to take into account the sequence effect. The high-low loading sequence clearly reduces the fatigue life, as depicted in Fig. 27. In order to cover this phenomenon, we let α change with time($\alpha = 1 - a(s_{min}(t) - 1)^{-f}$). Here a is the sequence effect sensitivity. According to Eq.(22), we have:

$$s_{min}(t) = \frac{\Sigma_y - \lambda \Sigma_H(t)}{S_a(t)},$$

which is the minimum weakening scale that activates energy loss. We use a general law for α of the type $\alpha = \alpha(s_{min})$ with the idea that for us s_{min} is a measure of present intensity of macroscopic stress. It is therefore a mechanical based stress norm. The impact of this construction of α can be seen on Fig. 28, on a test case specifically built to illustrate such a sequence effect.

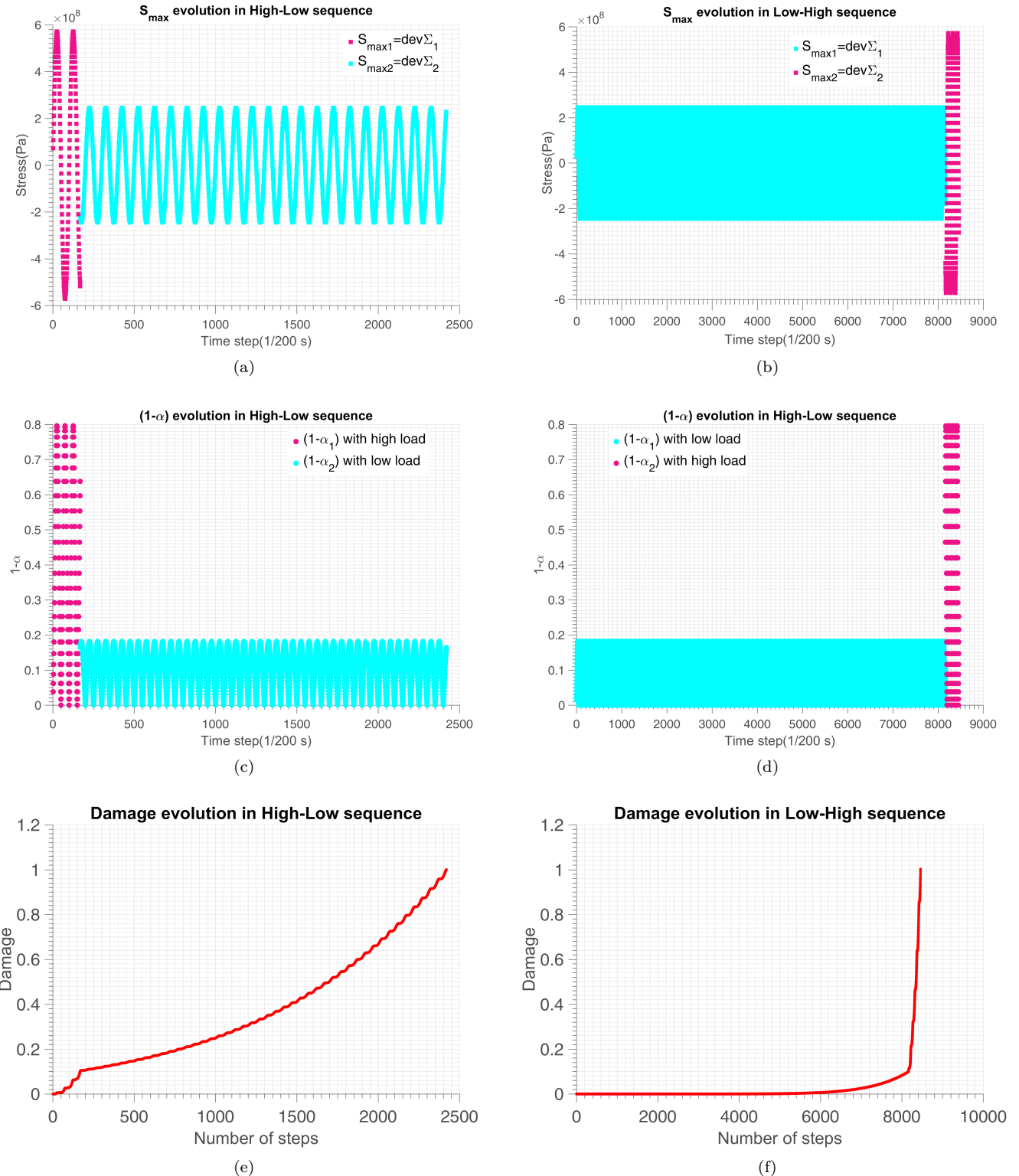


Fig. 27: Two level sequence effect. By comparing the vertical figures we can see high stress gives high $(1-\alpha)$ value which causes fast damage accumulation speed. The evolution of $(1-\alpha)$ is highly nonlinear and follows the value of stress at each time step.

5.2.1. Major damage effect

To see the influence of sequence effect factor of α , we first fix α for all tests to see the results. When α is fixed, it becomes denominator in the final expression of N_F (Eq.(16)) and has the same impact as W_0 . We find that the fatigue life of random loading is widely dispersed (Fig. 28). In this case we need to use $\alpha = f(s_{min})$ which evolves with time to make large stress intensity bring more damage.

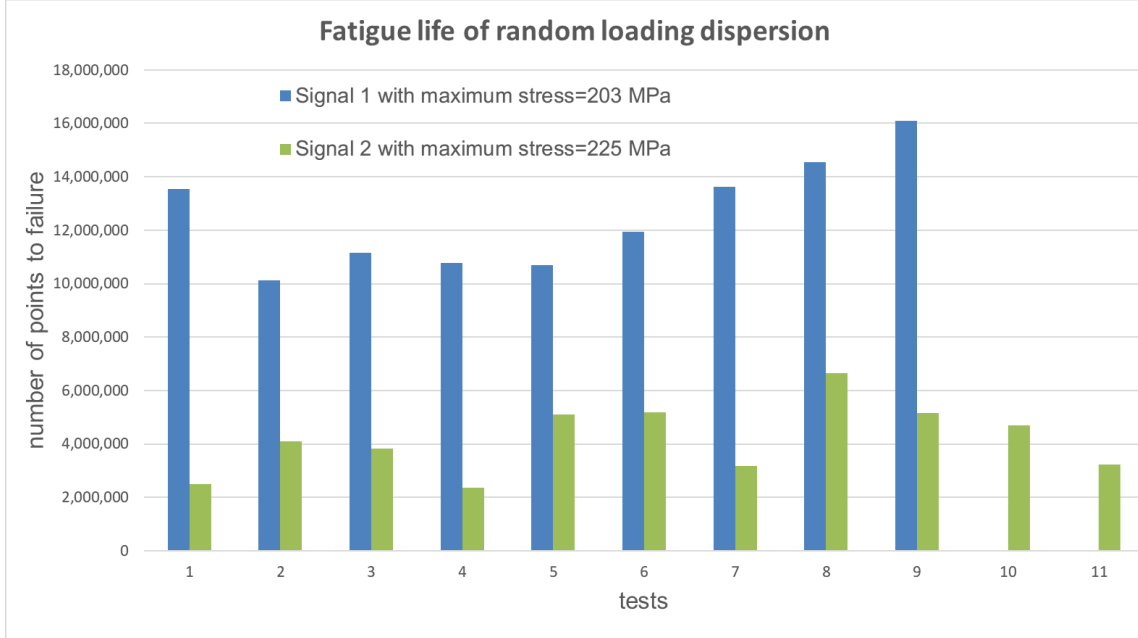


Fig. 28: Fatigue life of random loading dispersion

After comparison with the experimental data we find out that large stresses cause much more damage than the smaller ones. It is necessary to include this major stress induced damage to our stress intensity parameter α . With the new α used in Eq.(25) compared to Eq.(23) we are able to calibrate our model better with the experimental results by using

$$\alpha = 1 - a \left(\frac{\frac{1}{s_{min}}}{1 - \frac{1}{s_{min}}} \right)^f. \quad (43)$$

With $f = 1.1$, we use the power to magnify large stress impact and minify lower stress damage. The demonstration of major damage effect using magnification power is depicted in Fig. 29. With larger value of power, the sequence effect is more significant(bigger dispersion between high-low and low-high sequence).

The larger value of S_a causes more damage in the presence of the power β , leading to faster increase of

$$(1 - \alpha) = a \left(\frac{\frac{1}{s_{min}}}{1 - \frac{1}{s_{min}}} \right)^f = a(s_{min} - 1)^{-f}.$$

which causes faster damage accumulation. We can also see this effect in Fig. 30.

To assess large stress correctly we define the larger stress intensity as the value of stress which makes expression in the bracket in the second term of α greater than $1(\frac{1}{s_{min}(t) - 1} > 1)$, then we use power β to magnify this term. In this way the damage is accelerated for large stresses. The

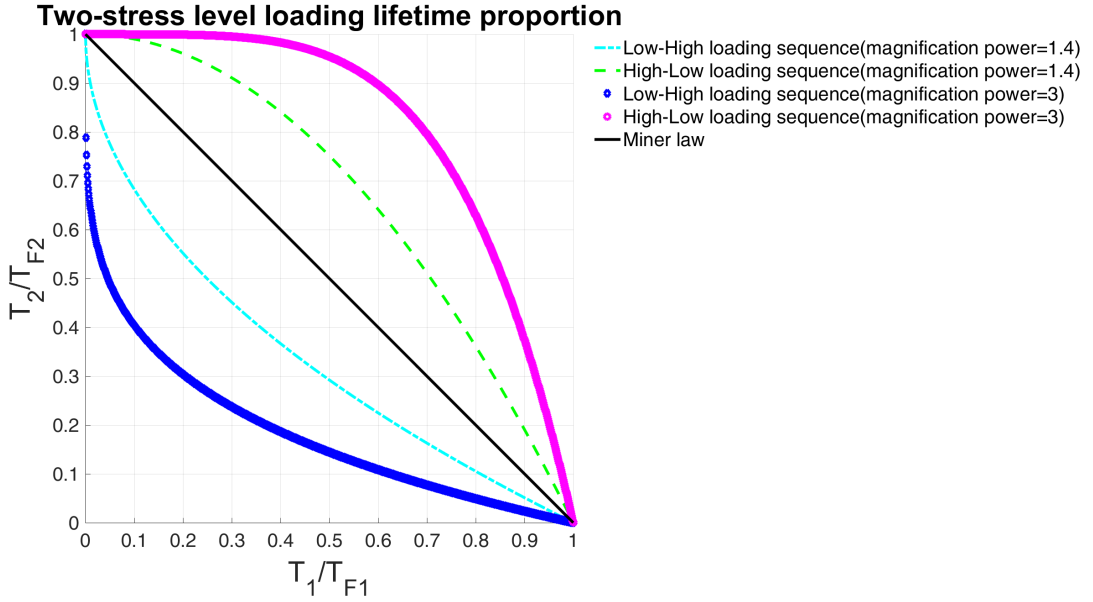


Fig. 29: Major damage effect using different magnification power of Eq.(43) on sequence effect. Here high stress is 1MPa and low stress is 0.8MPa. We see that using a large power f in Eq.(43) induces a stronger sequence effect.

deviatoric stress S_a , above which the damage is magnified, is determined from:

$$\alpha(t) = 1 - a \left(\frac{1}{s_{min}(t) - 1} \right)^{1.1},$$

$$s_{min}(t) = \frac{\Sigma_y - \lambda \Sigma_H(t)}{S_a(t)} < 2,$$

$$S_{large}(t) > \frac{\Sigma_y - \lambda \Sigma_H(t)}{2}.$$

The major damage effect can be seen in Fig. 30, which occurs when S is more than half the macroscopic yield stress of the material.

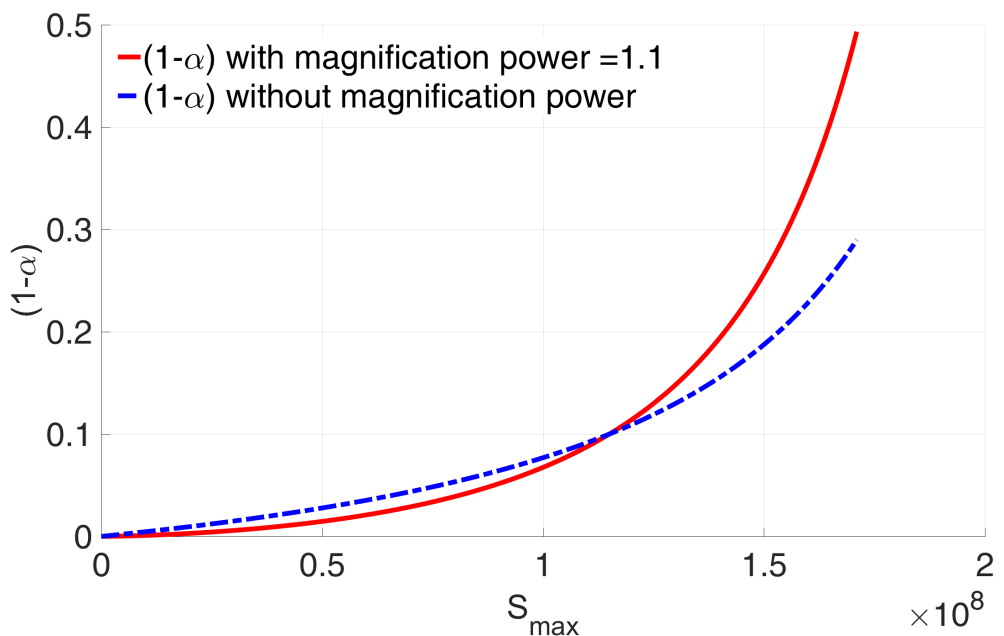


Fig. 30: $(1-\alpha)$ term which stands for the load intensity evolution, both with and without the magnification power f

6 Identification strategy

In our tests we keep $f = 1.1$ (justified in Chapter ?? by Fig. 34 and Fig. 35). The positive hydrostatic stress and negative one have different effect on the yield limit. It is necessary to adopt 2 parameters to describe this behavior. So we divide the hydrostatic sensitivity λ into 2 parts. λ_+ and λ_- . In the analytical formula, the amplitude of the stress intensity is adopted and the average value of tension hydrostatic stress(+) and compressive hydrostatic stress(-) is introduced.

For a good lifetime prediction, it is necessary to first identify the appropriate parameters of the model. For this purpose, we use the analytical formula Eq.(41) obtained in uniaxial cyclic loading case. With distinction of the hydrostatic stress in the presence of non-zero mean stress and since in fully reversed uniaxial loading we spend an equal time in compression and in traction, Eq.(8) now writes:

$$W_{cyc} = \frac{2(E - k)(1 + \nu)(\beta - 1)}{E(E + k\nu)\beta(\beta + 1)} \left[\frac{S_a^{\beta+1}}{(\sigma_y - \lambda_+ \bar{\Sigma}_{H+}(t))^{\beta-1}} + \frac{S_a^{\beta+1}}{(\sigma_y - \lambda_- \bar{\Sigma}_{H-}(t))^{\beta-1}} \right]. \quad (44)$$

$$N_{Fnum} = \frac{W_0}{(1 - \alpha)} \frac{E(E + k\nu)\beta(\beta + 1)}{2(E - k)(1 + \nu)(\beta - 1)} \frac{1}{\frac{S_a^{\beta+1}}{(\sigma_y - \lambda_+ \bar{\Sigma}_{H+}(t))^{\beta-1}} + \frac{S_a^{\beta+1}}{(\sigma_y - \lambda_- \bar{\Sigma}_{H-}(t))^{\beta-1}}}. \quad (45)$$

To use our analytical model Eq.(45) to fit the experiments, we employ matlab Least-Squares (model fitting) algorithm.

The best fitted parameters in uniaxial cyclic loading case are deduced from the minimization of the sum of square of difference between uniaxial numerical and experimental results:

$$\min_{\beta, \lambda, W_0} \left\{ \sum_i (N_{Fnum} - N_{Fexp(i)})^2 \right\} \quad (46)$$

Assume there are i sets of experimental data. To clarify the identification process, let us separate the parameters into:

- Experimental data: $S_{a(i)}$, $\Sigma_{H(i)}$, $N_{Fexp(i)}$, σ_y , E , k , ν .
- Material constants: β , λ_{+-} , W_0 (to be fitted)
- Input data from experimental data: $S_{max(i)}$, $\Sigma_{H(i)}$
- Input data from experimental data and parameter constants: $\alpha_{(i)}$
- Output data: $N_{Fnum(i)}$

In this process, σ_y , E , k and ν are given elastoplastic material constants. For each test (i), the load parameters are maximum amplitude $S_{a(i)}$, mean hydrostatic stress $\bar{\Sigma}_{H(i)}$, and the experimental number of cycles to failure is given by $N_{Fexp(i)}$.

The exponent $\alpha_{(i)}$ is cycle average obtained by

$$\alpha_{(i)} = \text{mean} \left[1 - a \left(\frac{1}{\frac{\Sigma_y - \lambda_{+-} \bar{\Sigma}_H(t)}{S_a(t)} - 1} \right)^{1.1} \right] (i). \quad (47)$$

The parameters to be calibrated are W_0 , β and λ . Since the exponent $\alpha_{(i)}$ depends on β and λ , we proceed iteratively by:

1. We first identify the S-N curve slope β and the energy scale W_0 using the analytical formula with torsion tests because there is no λ_{+-} impact in this kind of loading. We start from an initial guess β from which we can deduce $\alpha_{(i)}$ by numerical calculation of Eq.47 and identify β and W_0 by least squares. Because our analytical formula is not derivable in all ranges, when the identified value of β or W_0 get stuck in local minimum value, we regenerate a random β or W_0 in their range so as to get the global least square value.
2. Then, the parameter λ_+ are identified from numerical bending tests and we keep $\lambda_- = 0$. The final parameters correspond to the λ leading to the lowest identification error in β and W_0 . This strategy handles the nonlinearity in β and is well adapted to the low sensitivity in λ .

The analytical formula Eq.(45) with mean stress effect converges with the numerical method very well in the case of small β and λ_{+-} .

Parameter sensitivity analysis

The parameters we introduced during the deduction need to be calibrated. The source of the parameter identification are listed in Table.2. We perform a sensitivity analysis to see the influence of each parameter by comparing the results obtained respectively for the reference value, an upper bound and a lower bound of each parameter.

| Parameters | Strategy |
|--|--|
| Hydrostatic pressure sensitivity λ_+ | hydrostatic stress sensitivity (identified) |
| Non-linearity of damage accumulation a | amplification factor of load intensity (guessed) |
| Weakening scales distribution exponent β | to be calibrated (identified) |
| Dissipated energy to failure per defect W_0 | energy scaling (identified) |

Table 2: Parameters concerned

We analyze the sensitivity of parameters separately as in Table.3(uniaxial) and Table.7(random loading). The parameter β has more influence on the random loading case because it acts not only as the S-N curve slope but also the power magnification factor of large stress intensity. The λ has little influence because both tests are conducted on very small or zero mean stress load history.

In Miner's law the parameter α is zero, the maximum value is below 1. For $\alpha = 1$ the damage accumulation line becomes flat and there will be unlimited lifetime. To keep α in the range of $[0, 1]$ where in random amplitude tests there is $S_a = 163.3\text{MPa}$; we set the sensitivity of load intensity a to a maximum value of 0.29 to keep α positive.

The weakening scale distribution exponent(also the slope of S-N curve of the material) β ranges from 1 to 5. The hydrostatic pressure sensitivity λ is from positive mean stress test, which has the range of $0 \sim 0.8$. In constant amplitude cyclic loading, the dissipated energy to failure per defect W_0 (in MPa) is related to fatigue lifetime of the material.

| Constant amplitude sensitivity test with $f(\beta) = \beta$ | | | | | | |
|---|--------|--------|--------|--------|--------|-------------|
| Ref | Min | Max | Ref_n | Min_n | Max_n | Sensitivity |
| β | 1.1 | 1.05 | 1.50 | 414233 | 783723 | 243300 |
| λ_+ | 0.1 | 0.05 | 0.50 | 414233 | 449598 | 443376 |
| W_0 | 3.27e8 | 1.00e8 | 5.00e8 | 414233 | 137498 | 687209 |
| a | 0.1 | 0.05 | 0.15 | 414233 | 672869 | 324754 |

Table 3: Example of parameters sensitivity at cyclic loading of BATCH_A_02 on AW-6106 T6 aluminum (table.5)

7 Experimental verification

7.1. Introduction

The aim of this chapter is to validate the predictive model proposed. This consists in simulating tests available in the literature to determine the lifetime at initiation of crack by the application of the model and to compare these with the experimental lifetimes. The validation of the model involves a wide variety of metallic materials. The loads tested are of two types: cyclic loading of multiaxial stress of constant amplitude and repeated sequences of uniaxial stresses of variable amplitudes. The fatigue data of the materials used and the loads tested are taken from laboratory experiments or the literature.

7.2. Random amplitude 1D tests from Cetim on AW-6106 T6 aluminum

What makes automobile fatigue so difficult to predict is that, unlike standard tests done in a laboratory, an automobile's structure has to endure a complex, mostly random, set of static as well as cyclical stresses when in service. For example in Fig. 31 which could represent load data from testing or measurement, extracting the cyclic information can be challenging.

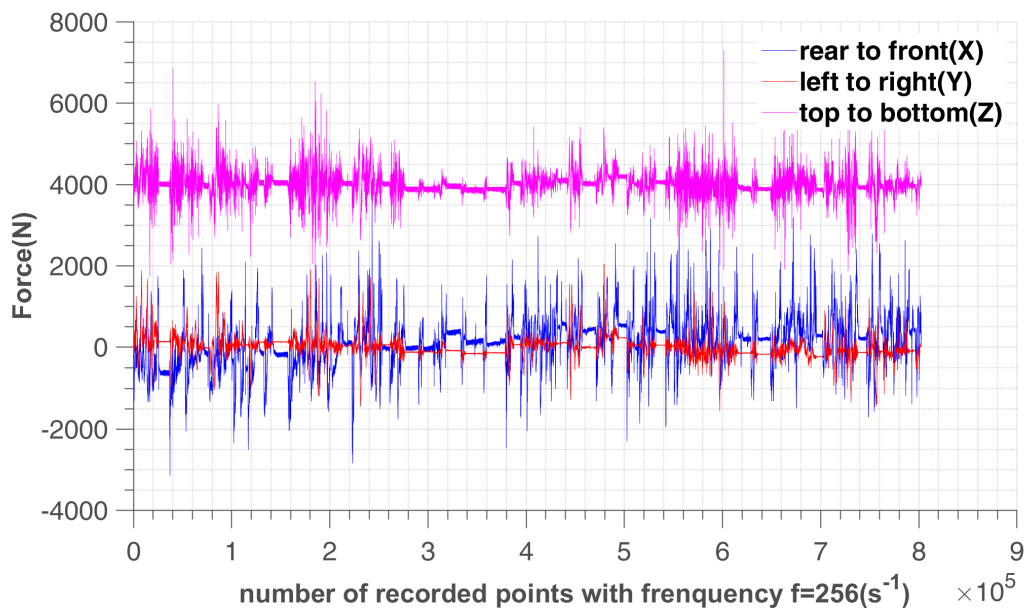


Fig. 31: Complex loading of a car suspension arm (data from PSA tests)

As we mentioned before, the mean value of α depends on the loading pattern (sinusoidal, linear division points between max and min stresses in unit cycle,...), but our optimal time step numerical strategy is not loading pattern dependent because it equally divides the range of α during the load history, which means the variation amplitude of stress intensity. So in random loading case with only recorded maximum and minimum load history, we first divide linearly between every 2 recorded points into 100 time steps, and then perform numerical tests with optimal time step method.

The first tests are performed on aluminum batches, the characteristics of the sample are shown in Tab.4.

There are 12 validated uniaxial fatigue tests on the AW-6106 T6 aluminum sample, in which 2 are of constant amplitude load case and 10 involve random load case. The cyclic stress of test number 1(ep01) and test number 2(ep02) are respectively 131.9 MPa and 97.0 MPa. We first identify the parameters from these two tests.

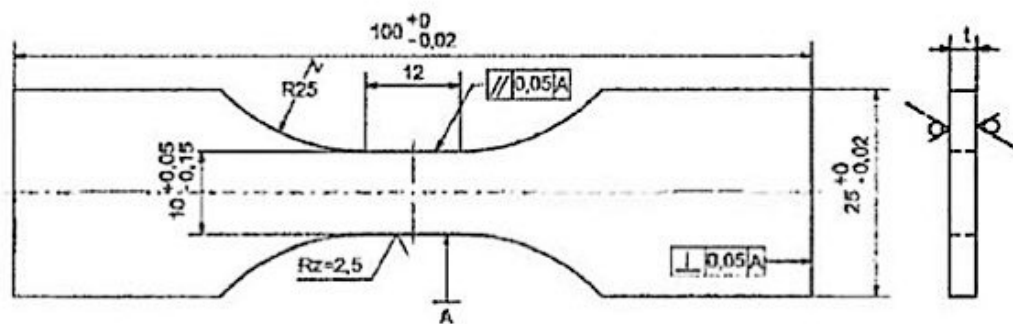
Specimen geometry for fatigue and corrosion fatigue tests ($t < 3.5$ mm):


Fig. 32: Specimen geometry for fatigue tests of AW-6106 T6 aluminum (sample given by PSA)

| Parameters | Value |
|--------------------------|----------------------|
| Young's modulus | $E = 72$ GPa |
| Hardening parameter | $k = 8.5$ MPa |
| Macroscopic yield stress | $\sigma_y = 230$ MPa |
| Thickness | $e = 2.9\text{mm}$ |
| Width | $l = 9.95\text{mm}$ |

Table 4: Material parameters of AW-6106 T6 aluminum

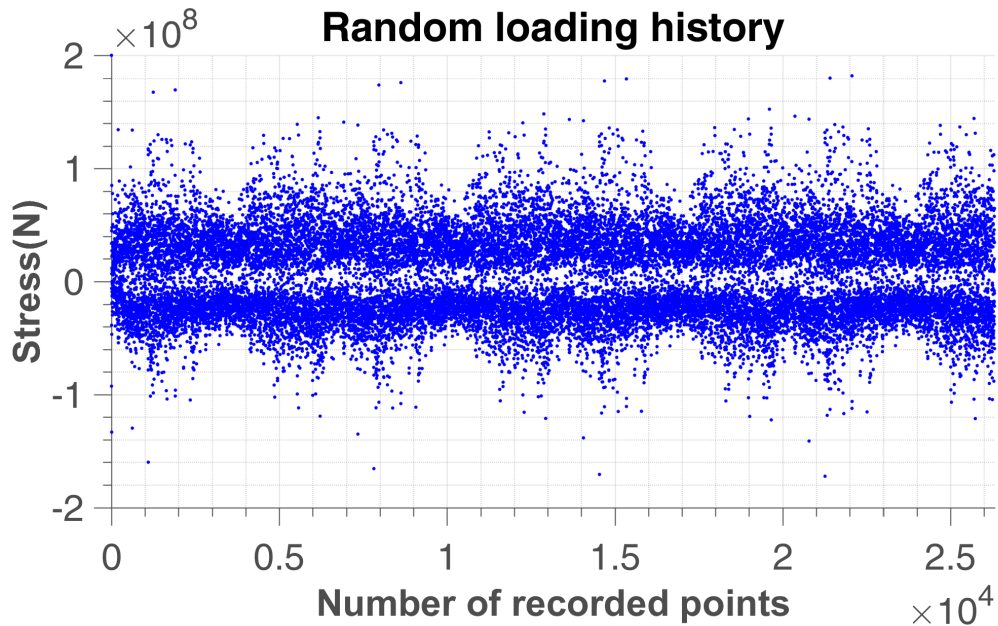


Fig. 33: Random loading history on BATCH_A_06 of AW-6106 T6 aluminum (see Tab.5)

The detailed tests information are shown in Tab.5. There are $27000(\pm 2.4\%)$ recorded points per repetition.

We assume the material parameters like Young's modulus E , hardening parameter k , hydrostatic

| Specimen | Fmax (kN) | Σ_{max} in the block | Number of repetition | Number of points |
|------------|-----------|-----------------------------|----------------------|------------------|
| BATCH_A_01 | 3.375 | | | 99892 |
| BATCH_A_02 | 2.475 | | | 414298 |
| BATCH_A_04 | nom | 225.88 | 95 | 2500000 |
| BATCH_A_05 | nom | 225.88 | 156 | 4105263 |
| BATCH_A_06 | nom | 225.88 | 145 | 3815789 |
| BATCH_A_07 | nom | 225.88 | 90 | 2368421 |
| BATCH_A_08 | nom | 225.88 | 194 | 5105263 |
| BATCH_A_09 | nom | 225.88 | 197 | 5184211 |
| BATCH_A_10 | nom x 0,9 | 203.292 | 515 | 13552632 |
| BATCH_A_11 | nom x 0,9 | 203.292 | 385 | 10131579 |
| BATCH_A_12 | nom x 0,9 | 203.292 | 424 | 11157895 |
| BATCH_A_13 | nom x 0,9 | 203.292 | 409 | 10763158 |
| BATCH_B_01 | nom | 225.88 | 121 | 3184211 |
| BATCH_B_02 | nom x 0,8 | 180.704 | 380 | 10000000 |
| BATCH_B_03 | nom x 0,8 | 180.704 | 380 | 10000000 |
| BATCH_B_04 | nom x 0,9 | 203.292 | 406 | 10684211 |
| BATCH_B_05 | nom x 0,9 | 203.292 | 454 | 11947368 |
| BATCH_B_06 | nom x 0,9 | 203.292 | 518 | 13631579 |
| BATCH_B_07 | nom x 0,9 | 203.292 | 553 | 14552632 |
| BATCH_B_08 | nom x 0,9 | 203.292 | 612 | 16105263 |
| BATCH_B_09 | nom | 225.88 | 253 | 6657895 |
| BATCH_B_10 | nom | 225.88 | 196 | 5157895 |
| BATCH_B_11 | nom | 225.88 | 178 | 4684211 |
| BATCH_B_12 | nom | 225.88 | 123 | 3236842 |

Table 5: Fatigue tests result on AW-6106 T6 aluminum, test data provided by CETIM

pressure sensitivity λ_+ (for $\bar{\Sigma}_H = 0$ in all cases), macroscopic yield stress σ_y and sequence effect sensitivity a are known. We first identify the weakening scales distribution β , and dissipated energy to failure W_0 from cyclic tests ep01 and ep02. Then fit the major damage effect parameter f to see if our assumption is correct or need to be changed.

The numerical fitting process show that the damage is caused mainly by large stresses (see later). The definition of major stress which affects the value of α now needs to be specified according to the material. To take into account this effect we first find out the proportion stress above a certain value in the repetition signal of random loading, as shown in Tab.6. Here ep_a and ep_b are the same material. Since the samples were extracted from aluminum profiles of industrial products, the two batches correspond to two different times of sampling in the production. The variation is supposed to be representative of the regular tolerances you might have in the production. ep_a_01 and ep_a_02 are constant amplitude loading which helps identify the power of weakening scale distribution β . ep_a_03 is low cycle fatigue data. ep_b_02 and ep_b_03 have infinite life time. The data in the table are grabbed from random signal high cycle fatigue loading history.

From Tab.8 and Tab.9 we can see f has positive correlation with β in high cycle fatigue which is the regime we focus on. However, very large value of f may ignore the small stress variations in the loading history, which goes against our assumption that small stresses also contribute to material damage. So we give $f = 1.1$ in high cycle random loading case to minimize the relative error. The sensitivity of parameters is calculated by dividing the percentage of variation of number of points to failure with respect to the reference number of points to failure, by the percentage of variation of parameter with respect to the reference parameter, as shown in Eq.(48).

$$sensitivity = \frac{(Max_n - Min_n) / Ref_n}{(Max - Min) / Ref}. \quad (48)$$

| Stress(MPa)> | 70 | 90 | 110 | 130 | 150 | 170 | 190 |
|--------------|--------|--------|--------|--------|--------|--------|--------|
| S_a (MPa)> | 57.15 | 73.48 | 89.81 | 106.14 | 122.47 | 138.80 | 155.13 |
| ep_a_04 | 1.962% | 0.904% | 0.077% | 0.037% | 0.018% | 0.007% | |
| ep_a_05 | 1.604% | 0.784% | 0.044% | 0.030% | 0.007% | 0.007% | |
| ep_a_06 | 1.645% | 0.784% | 0.045% | 0.030% | 0.007% | 0.007% | |
| ep_a_07 | 1.632% | 0.788% | 0.048% | 0.029% | 0.007% | 0.007% | |
| ep_a_08 | 1.644% | 0.787% | 0.048% | 0.037% | 0.007% | 0.007% | |
| ep_a_09 | 1.655% | 0.800% | 0.048% | 0.037% | 0.007% | 0.007% | |
| ep_a_10 | 0.768% | 0.134% | 0.007% | 0.000% | 0.000% | 0.000% | |
| ep_a_11 | 0.772% | 0.145% | 0.007% | 0.000% | 0.000% | 0.000% | |
| ep_a_12 | 0.779% | 0.133% | 0.011% | 0.000% | 0.000% | 0.000% | |
| ep_a_13 | 0.775% | 0.141% | 0.007% | 0.000% | 0.000% | 0.000% | |
| ep_b_01 | 4.739% | 1.737% | 0.840% | 0.224% | 0.049% | 0.034% | 0.004% |
| ep_b_04 | 1.999% | 0.745% | 0.156% | 0.034% | 0.004% | 0.000% | 0.000% |
| ep_b_05 | 2.010% | 0.749% | 0.148% | 0.034% | 0.008% | 0.000% | 0.000% |
| ep_b_06 | 1.999% | 0.790% | 0.118% | 0.034% | 0.008% | 0.000% | 0.000% |
| ep_b_07 | 2.029% | 0.756% | 0.152% | 0.034% | 0.008% | 0.000% | 0.000% |
| ep_b_08 | 1.999% | 0.737% | 0.137% | 0.034% | 0.008% | 0.000% | 0.000% |
| ep_b_09 | 4.663% | 1.687% | 0.798% | 0.205% | 0.049% | 0.034% | 0.004% |
| ep_b_10 | 4.712% | 1.744% | 0.809% | 0.224% | 0.046% | 0.034% | 0.004% |
| ep_b_11 | 4.636% | 1.664% | 0.790% | 0.209% | 0.049% | 0.034% | 0.004% |
| ep_b_12 | 0.775% | 0.141% | 0.007% | 0.000% | 0.000% | 0.000% | 0.000% |

Table 6: Proportion of stress(MPa) above different threshold with $\Sigma_y=230$ MPa, test data provided by CETIM on AW-6106 T6 aluminum.

| Random amplitude sensitivity test with $f(\beta) = \beta$ | | | | | | |
|---|--------|--------|---------|---------|---------|-------------|
| Ref | Min | Max | Ref_n | Min_n | Max_n | Sensitivity |
| β | 1.1 | 1.05 | 4220452 | 7469257 | 1799585 | -3.28 |
| λ | 0.1 | 0.05 | 4220452 | 4566335 | 2175991 | -0.13 |
| W_0 | 3.27e8 | 1.00e8 | 5.00e8 | 4220452 | 1321761 | 6420810 |
| a | 0.1 | 0.05 | 0.15 | 4220452 | 7156622 | 2827894 |
| $f(\beta)$ | | | | | | -1.03 |

Table 7: Parameters sensitivity at random loading of ep05 on AW-6106 T6 aluminum

| Constant amplitude sensitivity test with $f(\beta) \neq \beta$ | | | | | | |
|--|--------|--------|--------|--------|--------|-------------|
| Ref | Min | Max | Ref_n | Min_n | Max_n | Sensitivity |
| β | 1.1 | 1.05 | 1.50 | 414233 | 797377 | 213682 |
| λ | 0.1 | 0.05 | 0.50 | 414233 | 449598 | 443376 |
| W_0 | 3.27e8 | 1.00e8 | 5.00e8 | 414233 | 137498 | 687209 |
| a | 0.1 | 0.05 | 0.15 | 414233 | 672869 | 324754 |
| $f(\beta)$ | 1.1 | 1.05 | 1.5 | 414233 | 441661 | 511644 |

Table 8: Parameters sensitivity at cyclic loading of ep02 on AW-6106 T6 aluminum

After the fitting process, the reference parameters value we use are in Tab.10.

The best fitted results with constant α are shown in Fig. 34. The dispersion is relatively large. In conclusion, we are not able to predict the random stress amplitude fatigue life with fixed α , because random stresses not only cause different energy dissipations, but also show a distinctive load sequence effect. So we have to update the value of α at each time step.

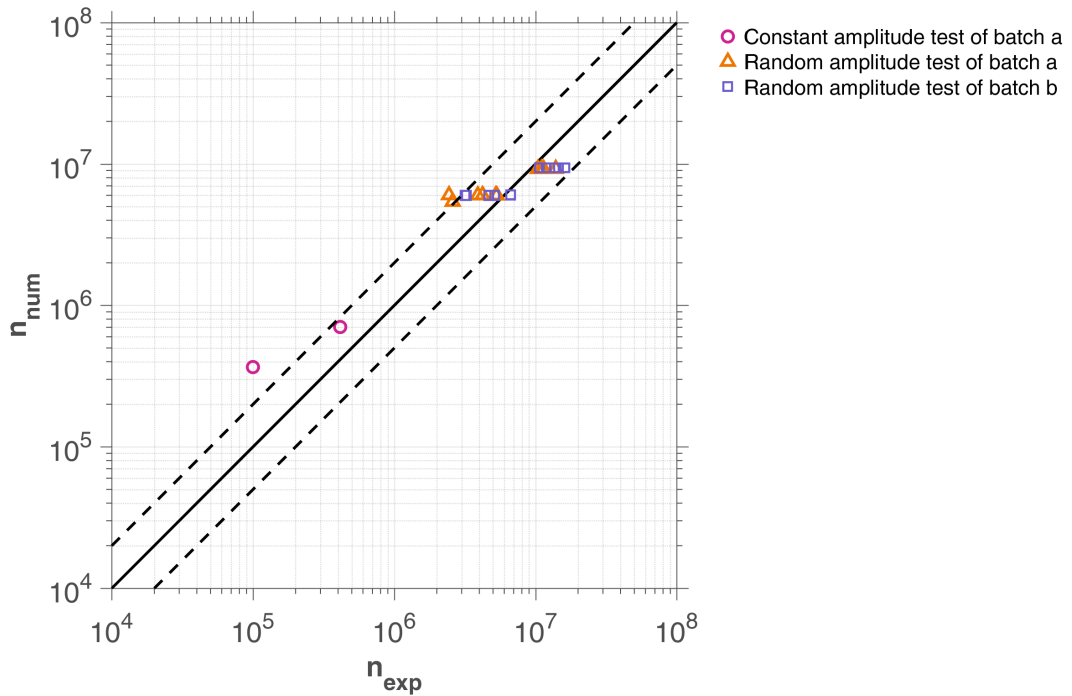
We can find that the numerical results are satisfactory when we introduce a major damage influence through the construction of a load dependent α . The dispersion figure with distinction of

| Random amplitude sensitivity test with $f(\beta) \neq \beta$ | | | | | | | |
|--|--------|--------|--------|---------|---------|-------------|-------|
| Ref | Min | Max | Ref_n | Min_n | Max_n | Sensitivity | |
| β | 1.1 | 1.05 | 1.50 | 4220452 | 7254554 | 2472791 | -2.77 |
| λ | 0.1 | 0.05 | 0.50 | 4220452 | 4566335 | 2175991 | -0.13 |
| W_0 | 3.27e8 | 1.00e8 | 5.00e8 | 4220452 | 1321761 | 6420810 | 0.99 |
| a | 0.1 | 0.05 | 0.15 | 4220452 | 7156622 | 2827894 | -1.03 |
| $f(\beta)$ | 1.1 | 1.05 | 1.5 | 4220452 | 4341560 | 3052299 | -0.75 |

Table 9: Parameters sensitivity at random loading of ep05 on AW-6106 T6 aluminum

| Constant α | W_0 (MPa) | $\lambda_+ = \lambda_-$ | β | α | f |
|-------------------|-------------|-------------------------|---------|----------|-----|
| | 326.9 | 0.1 | 1.1 | 0.7 | 1.1 |
| Changing α | W_0 (MPa) | $\lambda_+ = \lambda_-$ | β | a | f |
| | 326.9 | 0.1 | 1.1 | 0.1 | 1.1 |

Table 10: The parameters in 1D cyclic and random loading on AW-6106 T6 aluminum fatigue tests by Cetim

Fig. 34: Comparison between experimental and numerical results of 1D cyclic and random loading on aluminum fatigue tests by CETIM with constant α from the first row of Tab.10

major damage is depicted in Fig. 35. Here it is necessary to control the parameter a to make sure $\alpha > 0$ in the most severe situation.

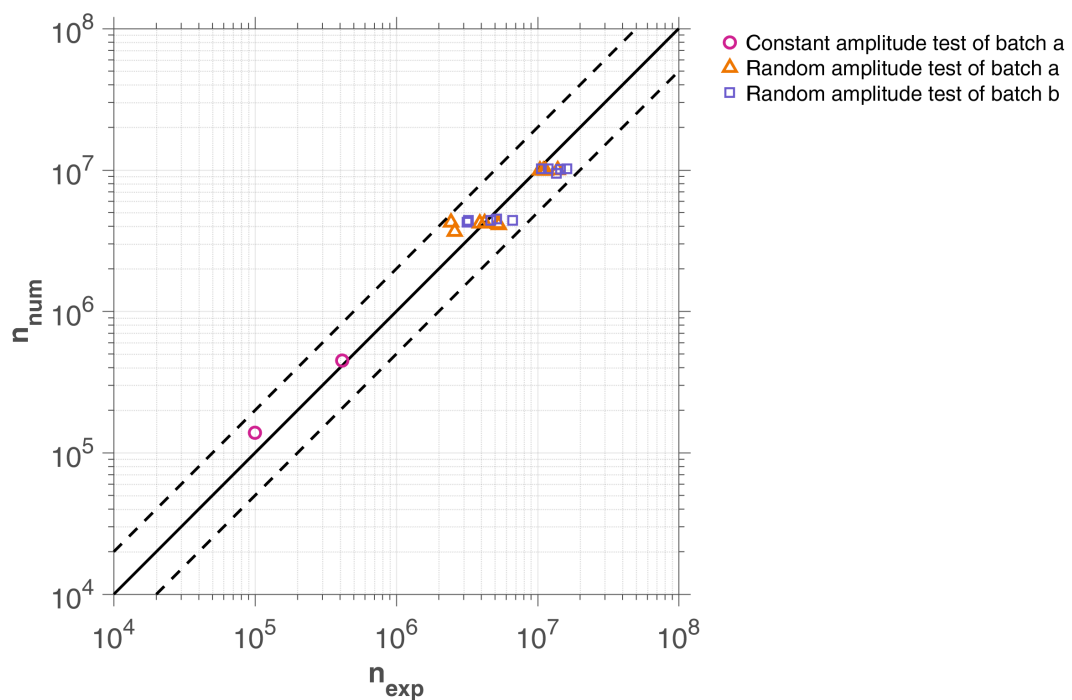


Fig. 35: Comparison between experimental and numerical results of 1D cyclic and random loading on aluminum fatigue tests by Cetim with load dependent α . Coefficients data are given in the second row of Tab.10

8 Experimental validation of the model on aluminum 6082 T6

8.1. Presentation of aluminum 6082 T6

The material tested is aluminum 6082 T6, used by [6] to validate their method of lifetime prediction. The mechanical properties of this material are summarized in Tab.11.

| E [GPa] | σ_y [MPa] | σ_u [MPa] | ν |
|-----------|------------------|------------------|-------|
| 69.4 | 298 | 343 | 0.33 |

Table 11: Mechanical and dynamic characteristics of aluminum 6082 T6 ([6])

Specimens of aluminum 6082 T6

The specimens were made from the drawn bars (diameter 30 mm) and the geometrical shape of which is given in Fig. 36. They are successively polished with $6 - \mu\text{m}$ diamond compounds until a good mirror-like finish is obtained.

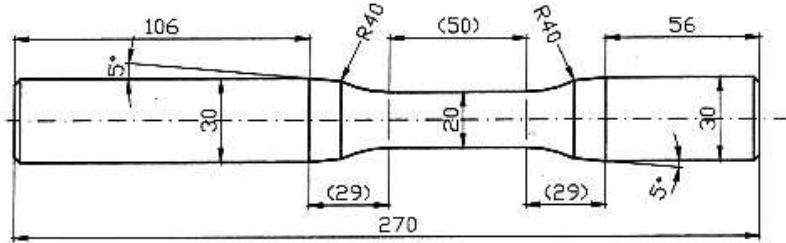


Fig. 36: Specimen geometry for fatigue tests of aluminum 6082 T6 (dimension in millimeters)??

8.2. Fatigue tests on aluminum 6082 T6

The simulated tests are purely alternate and summarized in Tables 12 and 13. They consist of simple tests in bending, torsion and bending-torsion in phase and out-phase for two cases of biaxial stress ratio, $\lambda = \tau_{xy,a}/\sigma_{x,a}$ ($\lambda > 1$ and $\lambda < 1$). The expected lifetimes range from 10^4 to 1.5×10^6 cycles.

In the Tables 12 and 13, $\sigma_{x,a}$ is the normal stress amplitude, $\tau_{xy,a}$ is the torsion amplitude, λ is the biaxial stress ratio, δ is the phase shift between the components of applied stresses and $N_{f,5\%}$ represents the number of cycles at break, defined by a 5% decrease in flexural or torsional stiffness.

It is interesting to note that a reduced amount of plasticity was measured by strain gauges in the PC10T2, PC14T2 and P36BT11 tests ([6]). They are therefore located in the field of oligocyclic fatigue. Therefore, they are not simulated as we only deal with the field of polycyclic fatigue3.

| Batch N° | $\sigma_{x,a}$ [MPa] | $\tau_{xy,a}$ [MPa] | λ | δ [°] | $N_{f,5\%}$ [Cycles] |
|-----------------|----------------------|---------------------|-----------|--------------|----------------------|
| P1B1 | 190 | 0 | 0 | 0 | 160000 |
| P2B2 | 180 | 0 | 0 | 0 | 248518 |
| P3B3 | 164 | 0 | 0 | 0 | 444411 |
| P4B4 | 144 | 0 | 0 | 0 | 1069220 |
| P5B5 | 224 | 0 | 0 | 0 | 56285 |
| P6B4 | 145 | 0 | 0 | 0 | 1238325 |
| P7B1 | 187 | 0 | 0 | 0 | 200480 |
| P8B3 | 161 | 0 | 0 | 0 | 423590 |
| PC9T1 | 0 | 117 | ∞ | 0 | 534032 |
| PC10T2 | 0 | 155 | ∞ | 0 | 26987 |
| PC11T3 | 0 | 127 | ∞ | 0 | 76665 |
| PC12T3 | 0 | 127 | ∞ | 0 | 132295 |
| PC13T1 | 0 | 117 | ∞ | 0 | 203535 |
| PC14T2 | 0 | 155 | ∞ | 0 | 16195 |
| PC15T4 | 0 | 106 | ∞ | 0 | >1.1E6 |
| PC16T4 | 0 | 104 | ∞ | 0 | 565150 |

Table 12: Simple bending and torsion tests ($R = -1$), data from [6]

| Batch N° | $\sigma_{x,a}$ [MPa] | $\tau_{xy,a}$ [MPa] | λ | δ [°] | $N_{f,5\%}$ [Cycles] |
|-----------------|----------------------|---------------------|-----------|--------------|----------------------|
| P17BT1 | 57 | 100 | 1.75 | 0 | 266435 |
| P18BT2 | 51 | 84 | 1.65 | 0 | 1119254 |
| P19BT2 | 51 | 84 | 1.65 | 0 | 1416225 |
| P20BT3 | 71 | 118 | 1.66 | 0 | 83000 |
| P21BT3 | 70 | 118 | 1.69 | 0 | 75695 |
| P22BT1 | 59 | 99 | 1.68 | 0 | 630325 |
| P23BT4 | 132 | 97 | 0.73 | 0 | 157210 |
| P24BT4 | 132 | 99 | 0.75 | 0 | 126470 |
| P25BT5 | 144 | 107 | 0.74 | 0 | 35450 |
| P26BT5 | 149 | 105 | 0.7 | 0 | 68465 |
| P27BT6 | 122 | 90 | 0.74 | 0 | 252658 |
| P28BT7 | 116 | 83 | 0.72 | 0 | 316149 |
| P30BT8 | 148 | 66 | 0.45 | 90 | 278836 |
| P31BT9 | 152 | 47 | 0.31 | 90 | 465010 |
| P32BT8 | 149 | 68 | 0.46 | 90 | 118965 |
| P33BT9 | 155 | 72 | 0.46 | 90 | 447525 |
| P34BT10 | 190 | 105 | 0.55 | 90 | 47940 |
| P35BT10 | 189 | 106 | 0.56 | 90 | 30995 |
| P36BT11 | 79 | 129 | 1.63 | 90 | 23080 |
| P37BT12 | 69 | 110 | 1.59 | 90 | 202807 |
| P38BT13 | 68 | 99 | 1.46 | 90 | 262980 |
| P39BT13 | 68 | 99 | 1.46 | 90 | 398615 |
| P41BT15 | 79 | 116 | 1.47 | 90 | 46045 |

Table 13: In-phase and out-of-phase bending-torsion tests ($R = -1$), data from [6]

8.3. Identification of model parameters on aluminum 6082 T6

Once the average coefficient α_m is fixed in constant amplitude cyclic loading, it has the same influence as W_0 . The parameters remain to calibrate are λ_+ on the mean stress sensitivity which

makes a distinction between bending and torsion, and the exponent β on the slope of $S - N$ curve. The identification strategy is as described in Section 6.

In Fig. 39a and Fig. 39b the diagonal represents a good correlation between the experimental and predicted lifetimes. The line segments on either side of the diagonal correspond to a fatigue lifetime error of a factor of two. The parameters of the 6082 T6 aluminum model are given in Tab.14.

| β | λ_+ | λ_- | W_0 | a | f |
|---------|-------------|-------------|--------|-----|-----|
| 5.126 | 0.9 | 0 | 1E8 Pa | 0.4 | 1.1 |

Table 14: Parameter identification of AL6082T6 steel

Non-proportional Hardening

Non-proportional hardening is used to describe loading paths where the principal strain axes rotate during cyclic loading. The simplest example would be a bar subjected to alternating cycles of tension and torsion loading. Between the tension and torsion cycles the principal axis would rotate 45°. Out-of-phase loading is a special case of non-proportional loading and is used to denote cyclic loading histories with sinusoidal or triangular waveforms and a phase difference between the loads. ([?])

Materials show additional cyclic hardening during this type of loading that is not found in uniaxial or any proportional loading path. Here is an example for 90° out-of-phase tension-torsion loading. (Fig. 37)

The 90° out-of-phase loading path has been found to produce the largest degree of non-proportional hardening. The magnitude of the additional hardening observed for this loading path as compared to that observed in uniaxial or proportional loading is highly dependent on the microstructure and the ease with which slip systems develop in a material. A non-proportional effective stress, $S_{a90} = \sqrt{\sigma_{11}^2 + \tau_{12}^2}$, can be introduced which is defined as the equivalent stress under 90° out-of-phase loading at high plastic strains in the flat portion of the stress-strain curve. This term reflects the maximum degree of additional hardening that might occur for a given material.

The model predictive results for the periodic loads of constant amplitude with a radial path are in good agreement with the durations of experimental life. For the latter condition, 90 deg out-of-phase loading was also investigated(Fig. 39c). These tests indicated a dramatic change in the number of cycles to failure, N_F , as a result of out-of-phase loading. The influence of the plastic strain path on life is thus clearly demonstrated. It is shown that the total strain energy density, $W_t = W_e + W_p$ ([7]), correlates with both the in-phase and out-of-phase cyclic tests, and therefore is a proper damage parameter to be used for life predictions. Our microplasticity model does not take this strain path effect into account and we get inaccurate results on this test.

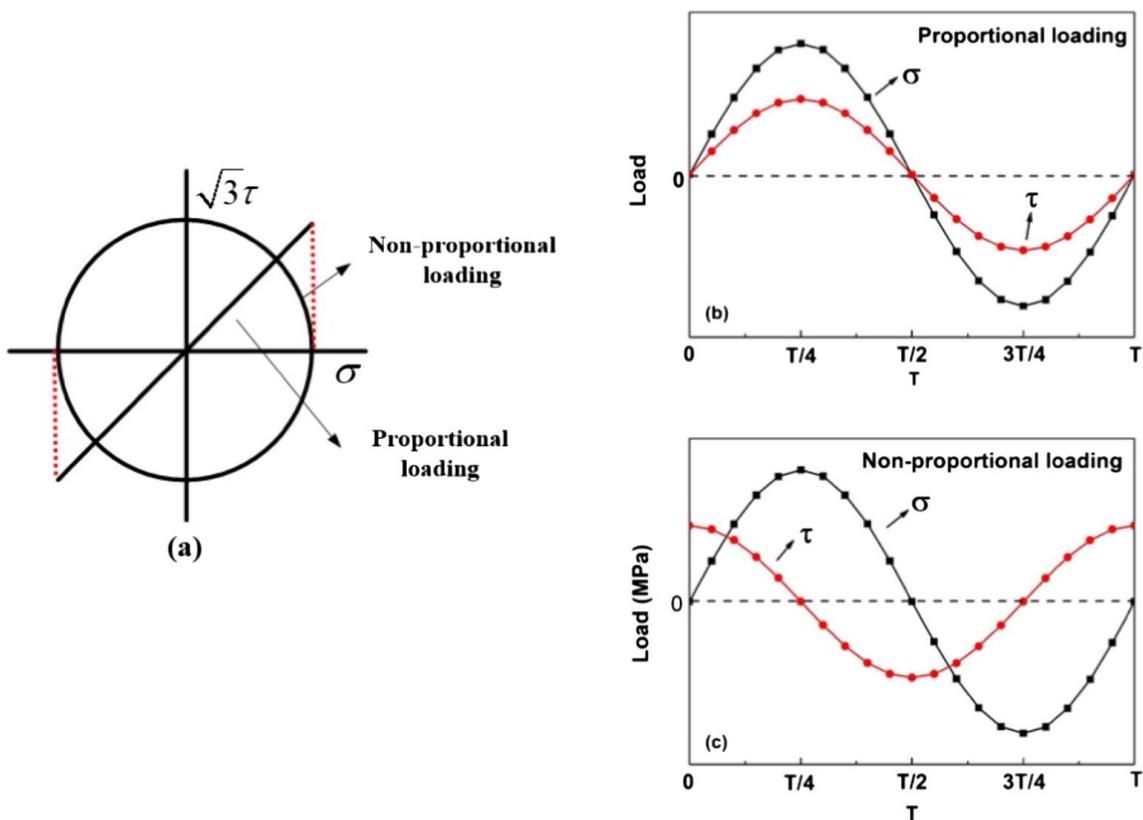


Fig. 37: The loading path and loading waveform of multiaxial corrosion fatigue (stress control) (a) loading path of proportional and non-proportional, (b) loading waveform of proportional loading, (c) loading waveform of non-proportion ([?]).

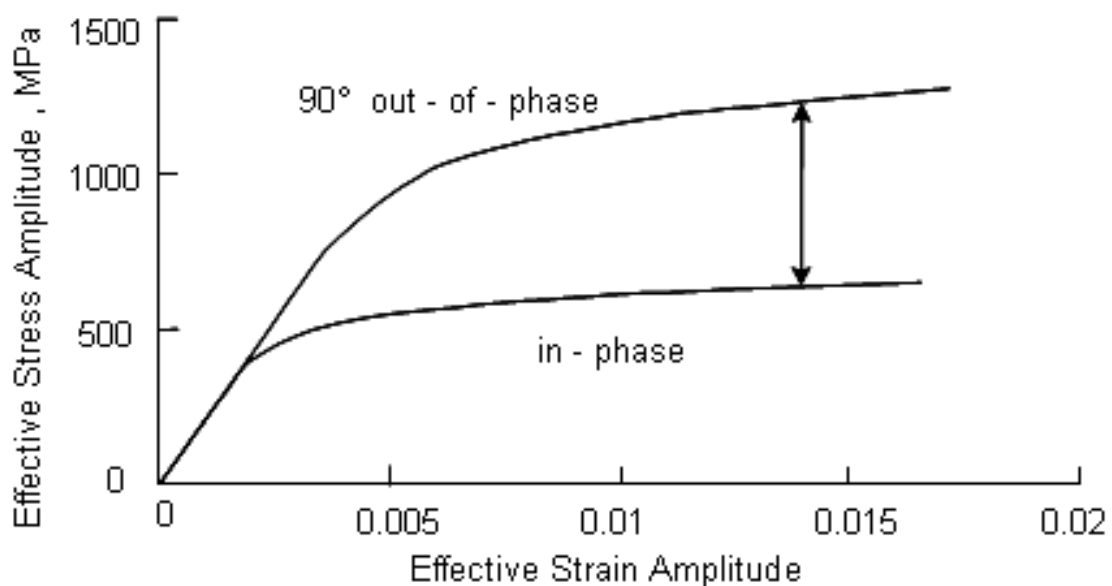


Fig. 38: The 90° out-of-phase loading path has been found to produce the largest degree of non-proportional hardening. ([?]).

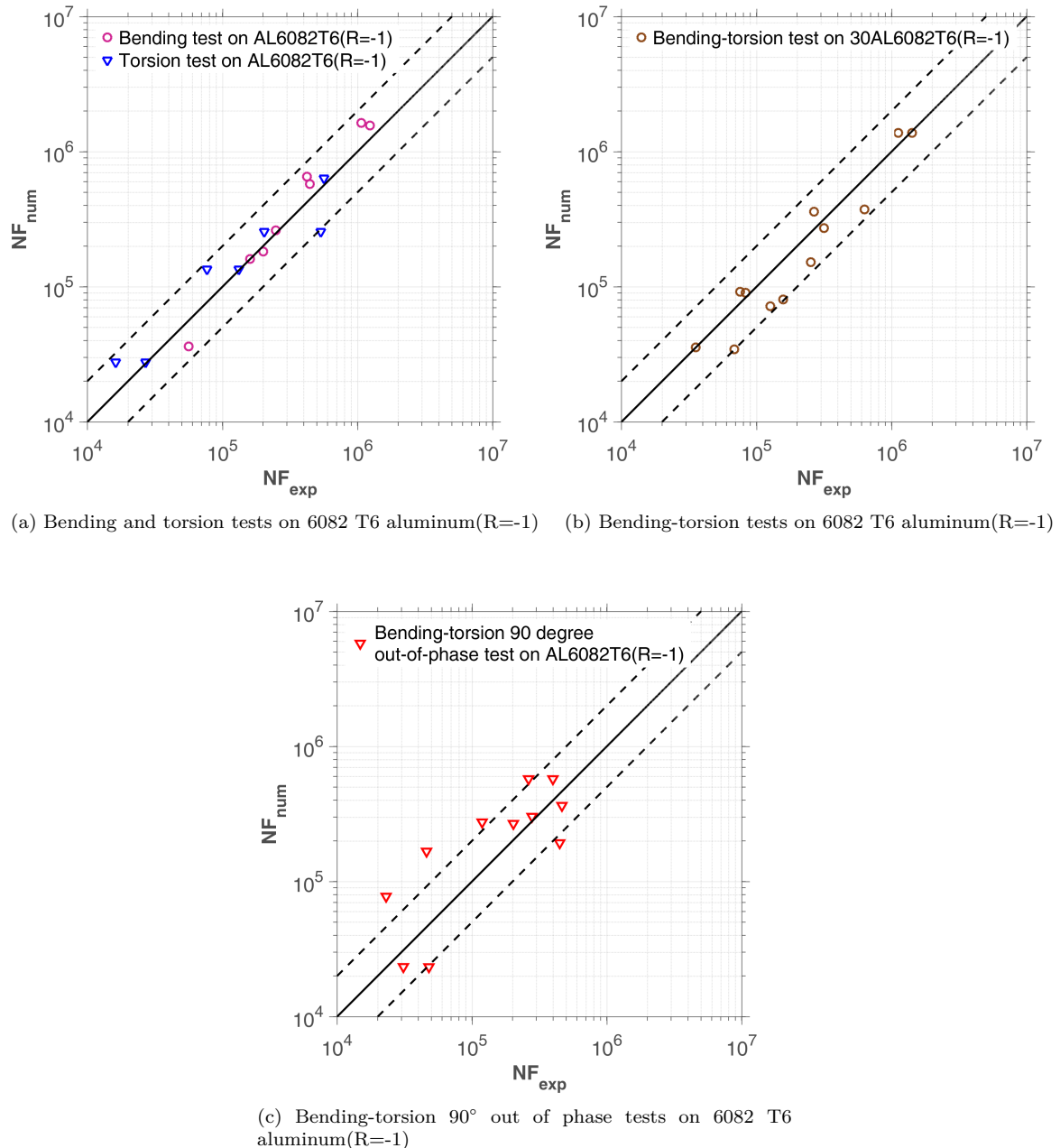


Fig. 39: Calibration on 6082 T6 aluminum ([6]). Comparison between experimental results and our model used with coefficients given in Tab.14. We obtain a good correlation in bending and torsion tests. The out of phase test are not satisfactory in these batches: P32BT8, P41BT15, P36BT11.

9 Experimental validation of the model on 30NCD16 steel

9.1. Presentation of steel 30NCD16

Tests with blocks of loading from database are compared to our model predictions. The material for testing is steel 30NCD16. The mechanical characteristics relating to each lot were determined by Dubar ([8]) by effecting monotonic tensile test batch. He eventually define “average material” one who has characteristics listed in Tab.15:

| $\sigma_{y0.02\%}$ [MPa] | $\sigma_{y0.2\%}$ [MPa] | σ_u [MPa] | σ_{-1} [MPa] | τ_{-1} [MPa] | E [GPa] |
|--------------------------|-------------------------|------------------|---------------------|-------------------|-----------|
| 895 | 1080 | 1200 | 690 | 428 | 191 |

Table 15: Mechanical and dynamic characteristics of 30NCD16 steel [8]

9.2. Fatigue tests performed by Dubar on steel 30 NCD 16

Tests carried out under simple bending and torsional stresses are grouped together in Tab.16 and 17.

| Bending Tests (R=-1) | N [Cycles] | $\sigma_{x,m}$ [MPa] | $\sigma_{x,a}$ [MPa] |
|-------------------------|---------------|-------------------------|-------------------------|
| 1 | 51000 | 0 | 820 |
| 2 | 80000 | 0 | 795 |
| 3 | 90000 | 0 | 790 |
| 4 | 95000 | 0 | 785 |
| 5 | 100000 | 0 | 780 |
| 6 | 120000 | 0 | 765 |
| 7 | 140000 | 0 | 752 |
| 8 | 200000 | 0 | 725 |
| 9 | 210000 | 0 | 720 |
| 10 | 230000 | 0 | 715 |
| 11 | 250000 | 0 | 708 |

Table 16: 30NCD16 steel fully reversed bending tests [8]

| Torsion Tests (R=-1) | N [Cycles] | $\tau_{xy,a}$ [MPa] |
|-------------------------|---------------|------------------------|
| 16 | 51000 | 527 |
| 17 | 80000 | 505 |
| 18 | 90000 | 500 |
| 19 | 95000 | 497 |
| 20 | 100000 | 495 |
| 21 | 120000 | 482 |
| 22 | 140000 | 470 |
| 23 | 200000 | 450 |
| 24 | 210000 | 446 |
| 25 | 230000 | 445 |
| 26 | 250000 | 440 |

Table 17: 30NCD16 steel fully reversed torsion tests ([8])

The results of combined bending-torsion tests in phase with or without mean stress $\sigma_{x,m}$ are given in the Tab.17 and Tab.18:

| Bending Tests (R=-1) | N [Cycles] | $\sigma_{x,m}$ [MPa] | $\sigma_{x,a}$ [MPa] | $\tau_{xy,a}$ [MPa] |
|-------------------------|---------------|-------------------------|-------------------------|------------------------|
| 27 | 80000 | 0 | 600 | 335 |
| 28 | 200000 | 0 | 548 | 306 |
| 29 | 120000 | 290 | 0 | 460 |
| 30 | 120000 | 450 | 0 | 460 |
| 31 | 250000 | 450 | 0 | 430 |
| 32 | 95000 | 450 | 490 | 285 |
| 33 | 120000 | 290 | 500 | 290 |

Table 18: 30NCD16 steel bending-torsion tests ([8])

9.3. Identification of model parameters for steel 30 NCD 16

The identification of the parameters consists in minimizing the relative difference between the experimental lifetimes and calculated ones for purely alternating bending tests (R = -1). Following the identification strategy of section 6, it is clearly indicated in Fig. 40a by obtaining a good correlation between these different lifetimes

| β | λ_+ | λ_- | W_0 | a | f |
|---------|-------------|-------------|-----------|-----|-----|
| 5.3 | 0.55 | 0 | 4.97E8 Pa | 0.4 | 1.1 |

Table 19: Parameter identification of 30NCD16 steel

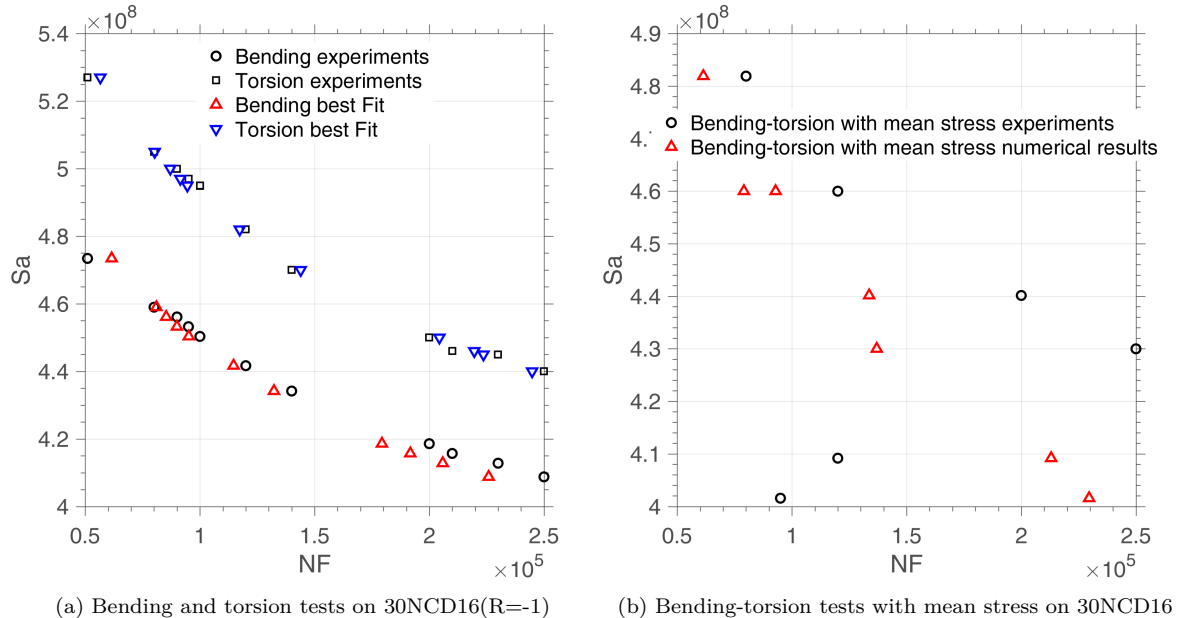


Fig. 40: Calibration on 30NCD16 ([8]). We can observe that the bending-torsion experimental values are largely dispersed

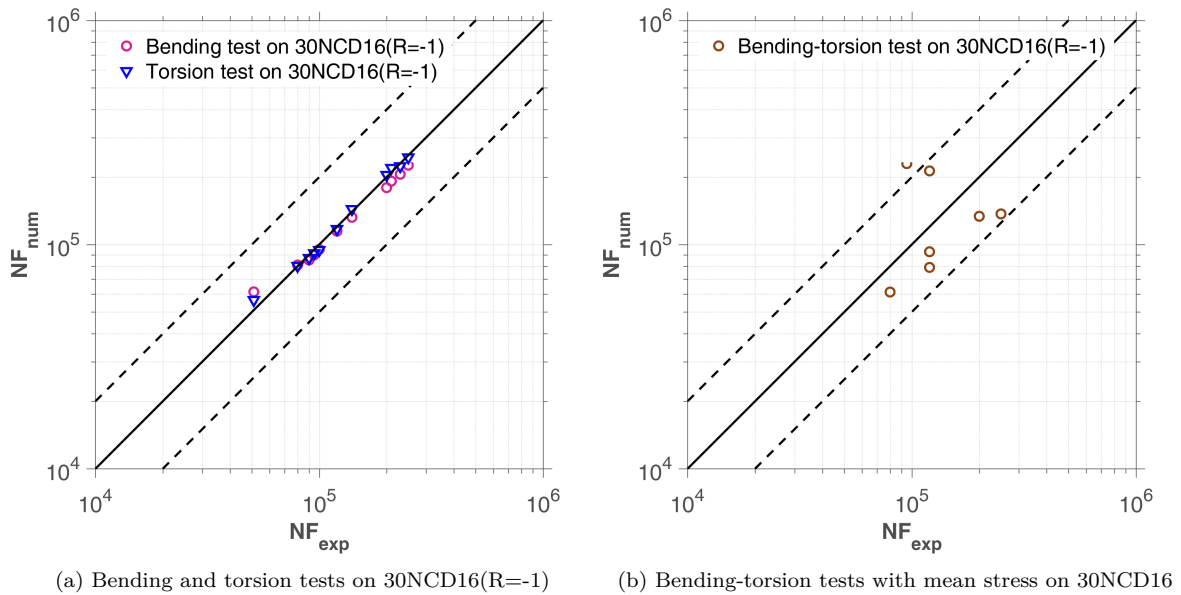


Fig. 41: Calibration on 30NCD16 ([8]). In figure (c) data 29(same N_F with data30 but with smaller $\sigma_{x,m}$) and 32(2-D with large mean stress) from Tab.18 are more dispersed. The numerical tests are carried out using the coefficients of Tab.19

10 Experimental validation of the model on SM45C steel

10.1. Presentation of steel SM45C

This is a structural steel widespread use for the crankshafts and the structural components. The chemical composition and mechanical properties of this material is given in Tab. 20 and Tab. 21.

| C | Mn | P | S | Si | Ni | Cr | Cu |
|------|------|------|-------|------|------|------|------|
| 0.42 | 0.73 | 0.02 | 0.012 | 0.28 | 0.14 | 0.18 | 0.13 |

Table 20: Chemical composition of SM45C steel

| σ_y [MPa] | σ_u [MPa] | E [GPa] | G [GPa] | ν | A |
|---------------------|---------------------|------------|------------|-------|----|
| 638 | 824 | 213 | 82.5 | 0.29 | 22 |

Table 21: Mechanical and dynamic characteristics of SM45C steel

E: Young's modulus,

G: Shear modulus,

ν : Poisson ratio,

A: Elongation at break.

10.2. Fatigue tests performed by Dubar on steel SM45C

Preliminary fatigue tests in purely alternating torsion and purely alternating flexion were performed by [9]. These two types of tests were carried out with test pieces of the same geometric shape. In addition, the author had performed moderate stress bending fatigue tests to study its effect on the lifetime of SM45C steel. All uniaxial fatigue tests performed by [9] are illustrated in Fig. 42. This figure shows a reduction in bending life of SM45C steel in the presence of a positive mean stress. Crack initiation was detected when the stiffness of the specimen or specimen used was reduced by 10%.

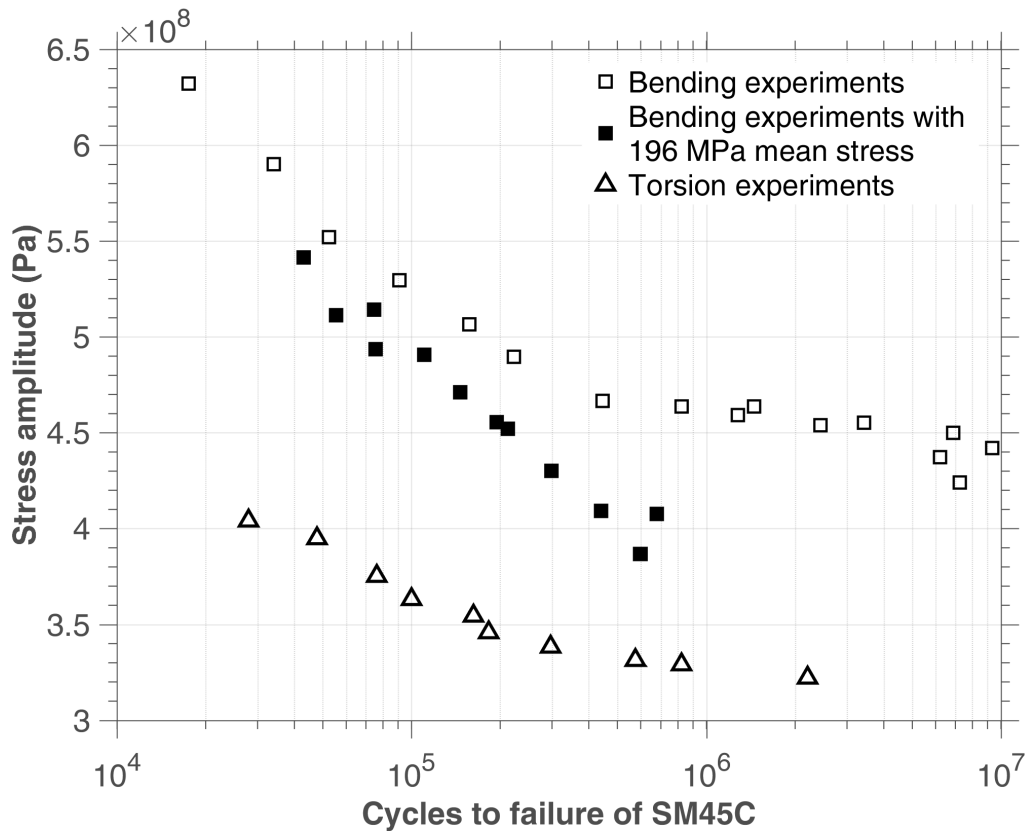


Fig. 42: Fatigue curves on SM45C steel by [9]

Preliminary fatigue tests were carried out under fully reversed bending and torsion separately.

| Bending Tests R=-1 | N [Cycles] | $\sigma_{x,a}$ [MPa] | $\sigma_{x,m}$ [MPa] |
|-----------------------|---------------|-------------------------|-------------------------|
| 1 | 17520 | 632.1 | 0 |
| 2 | 33991 | 590.1 | 0 |
| 3 | 52427 | 552.0 | 0 |
| 4 | 91077 | 529.5 | 0 |
| 5 | 156882 | 506.5 | 0 |
| 6 | 222261 | 489.8 | 0 |
| 7 | 446115 | 466.7 | 0 |
| 8 | 822487 | 463.8 | 0 |
| 9 | 1279414 | 459.2 | 0 |
| 10 | 1453321 | 463.8 | 0 |
| 11 | 2440360 | 454.0 | 0 |
| 12 | 3428115 | 455.2 | 0 |
| 13 | 6880791 | 450.0 | 0 |
| 14 | 6213809 | 437.3 | 0 |
| 15 | 9342857 | 441.9 | 0 |
| 16 | 7240667 | 424.1 | 0 |
| 1 | 43043 | 541.5 | 196 |
| 2 | 55523 | 511.5 | 196 |
| 3 | 74725 | 514.4 | 196 |
| 4 | 75362 | 493.6 | 196 |
| 5 | 110407 | 490.7 | 196 |
| 6 | 146090 | 471.1 | 196 |
| 7 | 194951 | 455.5 | 196 |
| 8 | 212218 | 452.0 | 196 |
| 9 | 297990 | 430.1 | 196 |
| 10 | 440286 | 409.3 | 196 |
| 11 | 678727 | 407.6 | 196 |
| 12 | 597603 | 386.8 | 196 |

Table 22: SM45C steel fully reversed bending tests(extracted from [9])

| Torsion Tests R=-1 | N [Cycles] | $\tau_{xy,a}$ [MPa] | $\sigma_{x,m}$ [MPa] |
|-----------------------|---------------|------------------------|-------------------------|
| 1 | 27957 | 404.1 | 0 |
| 2 | 47749 | 394.9 | 0 |
| 3 | 76194 | 375.3 | 0 |
| 4 | 100000 | 363.1 | 0 |
| 5 | 162305 | 354.5 | 0 |
| 6 | 182807 | 345.8 | 0 |
| 7 | 296705 | 338.3 | 0 |
| 8 | 575636 | 331.4 | 0 |
| 9 | 822487 | 329.1 | 0 |
| 10 | 2203806 | 322.2 | 0 |

Table 23: SM45 steel fully reversed torsion tests(extracted from [9])

10.3. Identification of model parameters for steel SM45C

We use the same identification strategy as described in Section 6. The fitted curve using experimental data in Tab.24 and data with mean stress effect is shown in Fig. 44b. The tests on

| Group | N [Cycles] | τ_a [MPa] | σ_a [MPa] | σ_m [MPa] |
|-------|---------------|-------------------|---------------------|---------------------|
| A | 29.9E3 | 282 | 449 | 0 |
| | 35.7E3 | 334 | 354 | 0 |
| | 50E3 | 223 | 485 | 0 |
| | 73.8E3 | 309 | 357 | 0 |
| | 106E3 | 217 | 449 | 0 |
| | 106E3 | 285 | 370 | 0 |
| | 112E3 | 199 | 449 | 0 |
| | 131E3 | 194 | 457 | 0 |
| | 333E3 | 252 | 354 | 0 |
| | 431E3 | 154 | 437 | 0 |
| B | 53E3 | 215 | 441 | 196 |
| | 59.2E3 | 309 | 286 | 196 |
| | 70.1E3 | 155 | 464 | 196 |
| | 86.3E3 | 136 | 473 | 196 |
| | 89.9E3 | 334 | 173 | 196 |
| | 92.1E3 | 209 | 403 | 196 |
| | 102E3 | 177 | 437 | 196 |
| | 135E3 | 321 | 167 | 196 |
| | 351E3 | 179 | 357 | 196 |
| | 394E3 | 274 | 182 | 196 |

Table 24: Effect of mean bending stress on out-of-phase(90°) fatigue of SM45C steel ([9])

SM45C steel have illustrated that the mean bending stress has an influence on both uniaxial and multiaxial fatigue life.

Although the uniaxial experimental data we extracted from Lee's curve ([9]) of SM45C steel are slightly dispersed, we can find our model quite satisfactory in the case of SM45C steel. As for multiaxial 90 degree out of phase, fully reversed bending-torsion fatigue tests, our model is able to evaluate the cycles to failure.

| $\beta(LCF/HCF)$ | λ_+ | λ_- | $W_0(LCF/HCF)$ | a | f |
|------------------|-------------|-------------|----------------|-----|-----|
| 6/15.8 | 1.4 | 0 | 2.6E8/5.6E5 Pa | 0.1 | 1.1 |

Table 25: Parameter identification of SM45C steel

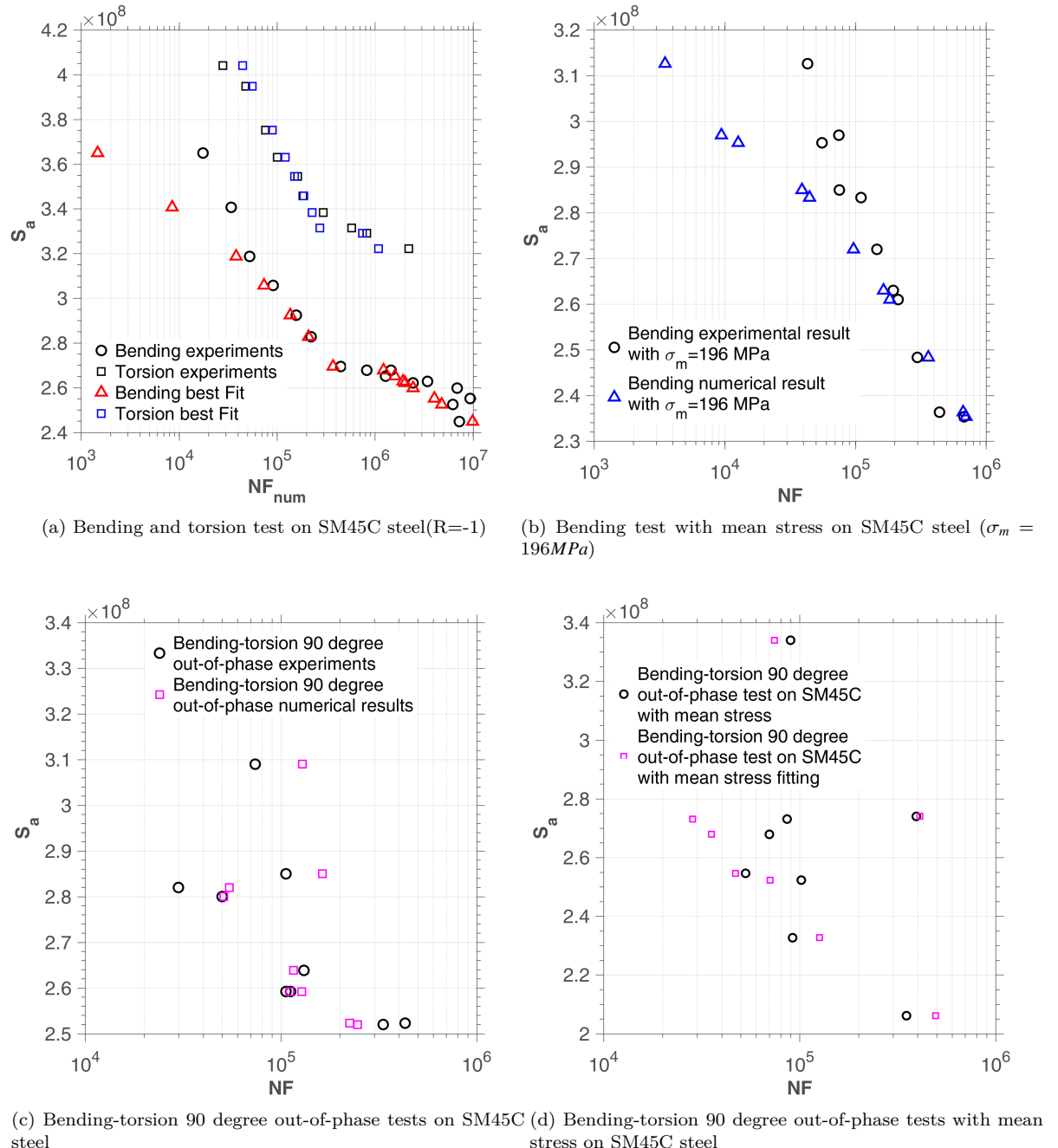


Fig. 43: Calibration on SM45C

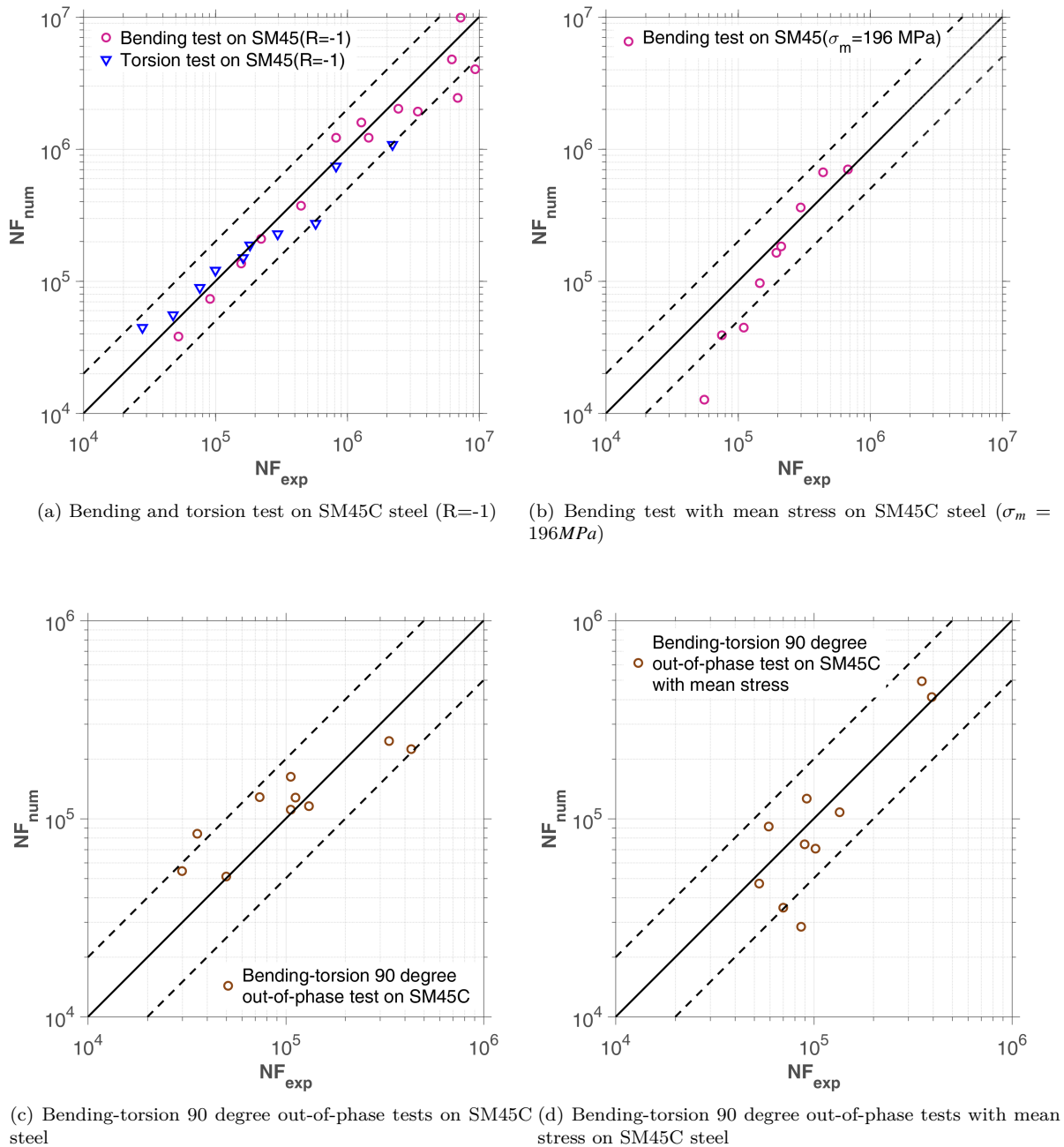


Fig. 44: Calibration on SM45C. The numerical tests are carried out using the coefficients of Tab.25

11 Experimental validation of the model on 10 HNAP steel

11.1. Presentation of the material

Fatigue tests were performed on the HNAP steel. It is a very low carbon steel which resembles the 10 CN 6. In Tab.26, its chemical composition is given: The mechanical properties of this steel

| C | Mn | Si | P | S | Cr | Cu | Ni | Fe |
|-------|-------|-------|-------|-------|-------|-------|-------|----------|
| 0.12% | 0.71% | 0.41% | 0.08% | 0.03% | 0.81% | 0.30% | 0.50% | the rest |

Table 26: Chemical composition of 10 HNAP steel, data from [10]

are given in Tab.27:

| $Re_{0.2\%}$ | R_m | A | ν | E |
|--------------|---------|-----|-------|------------|
| 418 MPa | 566 Mpa | 32% | 0.29 | 215000 Mpa |

Table 27: Mechanical characteristics of steel 10 HNAP, data from [10]

where

- $Re_{0.2\%}$: elastic limit at 0.2% of plastic deformation,
- R_m : maximum tensile strength,
- A : elongation at break,
- ν : Poisson's coefficient,
- E : Young's modulus.

11.2. Description of fatigue tests on 10 HNAP steel

The Macha team performed a large number of fatigue tests on the HNAP steel. Thus, it performed not only simple tensile compression and torsion tests ($R = -1$) in order to establish the corresponding Wöhler curves but also tests under variable loading on cylindrical specimens of the same material ([11]). [12] carried out tensile tests on this material for various mean stress values. It has established the Wöhler curve in repeated traction in order to validate on this steel the method of Robert whose use requires three Wöhler curves in symmetrical alternating traction, symmetrical alternating torsion and repetitive traction.

Wöhler curve in tension-compression

The model chosen by Macha and recovered by [13] for the tensile-compression Wöhler curve is that of Basquin:

$$\ln N = 68.361 - 9.82 \ln (\sigma_{-1}), \quad (49)$$

Wöhler curve in symmetrical alternating torsion

The symmetric alternating torsion Wöhler curve was recovered by [13] using following equation:

$$\ln N = 21.55 - 0.0385 \tau_{-1}. \quad (50)$$

Tensile fatigue tests for various mean stress values

[12] carried out tensile tests on HNAP steel for various values of mean stress. The results are summarized in Tab.28. They allowed us to plot the Wöhler curves for different values of the mean stress σ_m .

Fatigue testing under variable loading

| N_F | $\Sigma_{xx,a}$ | σ_m | $\Sigma_{xx,a}$ | σ_m | $\Sigma_{xx,a}$ | σ_m | $\Sigma_{xx,a}$ | σ_m |
|----------|-----------------|------------|-----------------|------------|-----------------|------------|-----------------|------------|
| 1.00E+05 | 311.30 | 75 | 224.42 | 150 | 257.98 | 225 | 251.82 | 300 |
| 2.00E+05 | 289.36 | 75 | 208.40 | 150 | 242.47 | 225 | 224.42 | 300 |
| 3.00E+05 | 276.53 | 75 | 197.03 | 150 | 233.40 | 225 | 208.40 | 300 |
| 4.00E+05 | 267.43 | 75 | 188.21 | 150 | 226.96 | 225 | 197.03 | 300 |
| 5.00E+05 | 260.37 | 75 | 181.00 | 150 | 221.97 | 225 | 188.21 | 300 |
| 6.00E+05 | 254.60 | 75 | 174.91 | 150 | 217.89 | 225 | 181.00 | 300 |
| 7.00E+05 | 249.72 | 75 | 169.63 | 150 | 214.44 | 225 | 174.91 | 300 |
| 8.00E+05 | 245.49 | 75 | 164.97 | 150 | 211.46 | 225 | 169.63 | 300 |
| 9.00E+05 | 241.77 | 75 | 160.81 | 150 | 208.82 | 225 | 164.97 | 300 |
| 1.00E+06 | 238.43 | 75 | 233.29 | 150 | 206.47 | 225 | 160.81 | 300 |

Table 28: Experimental results of tensile tests for various values of σ_m , data from [12]

Random multiaxial loading fatigue tests were performed on cylindrical HNAP steel specimens ([11]). The load considered is proportional and results from a combination of bending and torsion. The random signal is stationary and has a normal distribution as a probability distribution. Tests of this type have been analyzed and simulated by Carpinteri et al. ([14]). They were provided to us in the form of tests carried out on the HNAP steel for two values of the angle α' : $\alpha' = \pi/8$ and $\alpha' = \pi/4$. α' is the angle made by the resultant moment M with the bending moment M_B (see Fig. 45). The angle is kept constant during each individual test.

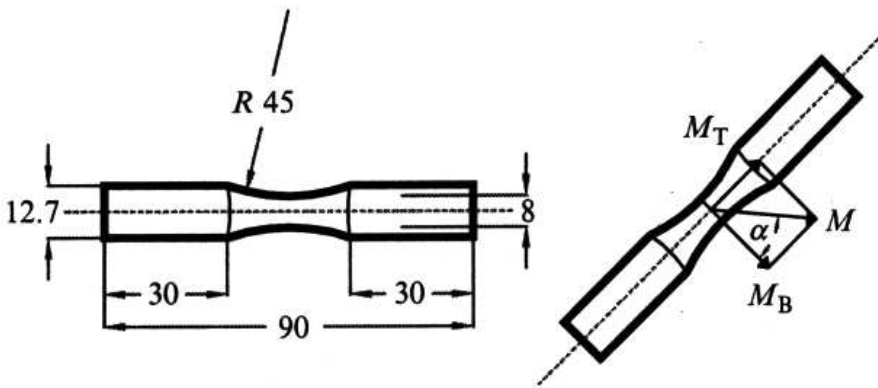


Fig. 45: Bending-torsion fatigue tests on cylindrical specimens ([14])

The stationary random loading sequence contains 49152 values recorded by a time interval of 0.00375 seconds (frequency = 266.67 Hz). It is shown in Fig. 46. Its total duration is 184.32 seconds. This sequence is multiplied by load coefficients corresponding to bending $f(\sigma_{xx})$ and torsion $f(\tau_{xy})$ in order to obtain random multiaxial loading sequences. As the signal is stationary, the breaking life is determined in terms of number of sequences with break N_{Sq} . Knowing N_{Sq} and the total time in seconds of the sequence studied, it is easy to express the lifetime of the piece in seconds. The results of fatigue tests under variable loads are summarized in Tab.29 and Tab.30 as a function of angle α' and ratio r ; $r = f(\tau_{xy})/f(\sigma_{xx})$.

1st type of tests: $\alpha' = \pi/8$ and $r = f(\tau_{xy})/f(\sigma_{xx}) = 0.2$.

2nd type of tests: $\alpha' = \pi/4$ and $r = f(\tau_{xy})/f(\sigma_{xx}) = 0.5$.

In Fig. 47, an example of a random multiaxial loading sequence is given.

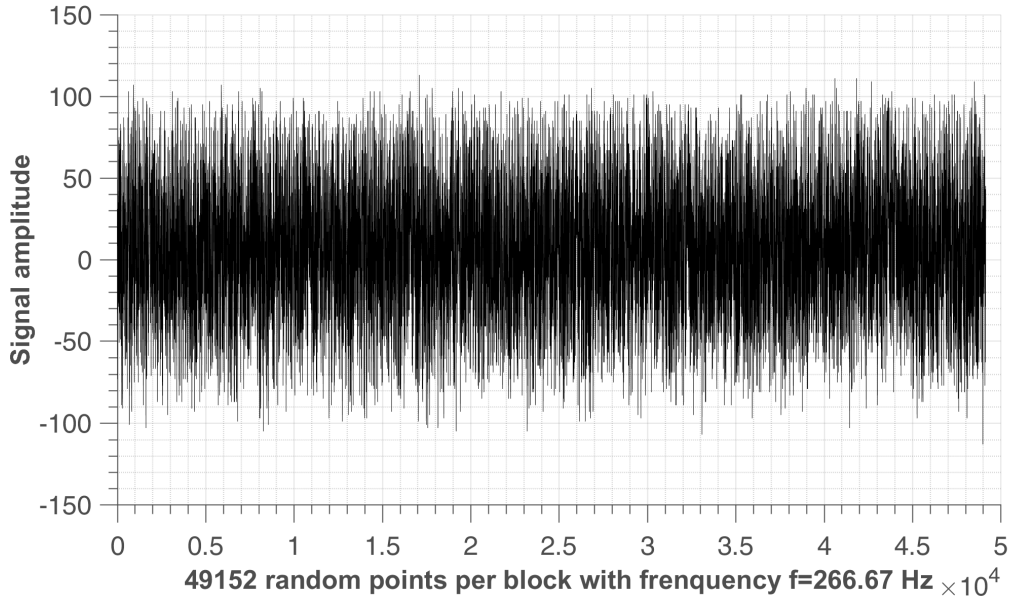


Fig. 46: Bending-torsion fatigue tests on cylindrical specimens ([14])

| N^o | $f(\sigma_{xx})$ | $f(\tau_{xy})$ | r | $T_{exp}(s)$ |
|-------|------------------|----------------|-----|--------------|
| 1 | 5.7084 | 1.1822 | 0.2 | 16843.2 |
| 2 | 5.2917 | 1.0959 | 0.2 | 17780.1 |
| 3 | 4.8337 | 1.0010 | 0.2 | 24416.5 |
| 4 | 5.2674 | 1.0909 | 0.2 | 24858.2 |
| 5 | 5.4534 | 1.1294 | 0.2 | 26518.3 |
| 6 | 5.2002 | 1.0769 | 0.2 | 36162.3 |
| 7 | 4.7944 | 0.9929 | 0.2 | 47600.4 |
| 8 | 4.3862 | 0.9084 | 0.2 | 57993.9 |
| 9 | 4.6241 | 0.9576 | 0.2 | 60428 |
| 10 | 4.0194 | 0.8324 | 0.2 | 73373.3 |
| 11 | 4.0127 | 0.8310 | 0.2 | 87609.1 |
| 12 | 4.2292 | 0.8758 | 0.2 | 89185.2 |
| 13 | 3.9213 | 0.8121 | 0.2 | 106900 |
| 14 | 3.7731 | 0.7814 | 0.2 | 117358 |
| 15 | 4.1148 | 0.8521 | 0.2 | 118902 |
| 16 | 3.6150 | 0.7486 | 0.2 | 132448 |
| 17 | 3.3135 | 0.6862 | 0.2 | 170571 |
| 18 | 4.1298 | 0.8553 | 0.2 | 178215 |
| 19 | 3.4761 | 0.7199 | 0.2 | 225288 |
| 20 | 3.3430 | 0.6923 | 0.2 | 352635 |
| 21 | 3.0135 | 0.6241 | 0.2 | 355720 |

Table 29: Fatigue results under variable loads for $\alpha' = \pi/8$ and $r = f(\tau_{xy})/f(\sigma_{xx}) = 0.2$

11.3. Identification of model parameters of 10HNAP steel

As the previous tests, we identify the slope β in pure torsion tests without the mean stress effect. Then fit λ_+ and W_0 with bending tests ($R = -1$). The parameters of the HNAP steel model can be identified by referring to Tab.31. They are grouped in Tab.31:

| N^o | $f(\sigma_{xx})$ | $f(\tau_{xy})$ | r | $T_{exp}(s)$ |
|-------|------------------|----------------|-----|--------------|
| 1 | 4.2519 | 2.126 | 0.5 | 15379.4 |
| 2 | 4.0567 | 2.0284 | 0.5 | 21465.7 |
| 3 | 3.8982 | 1.9491 | 0.5 | 25350.4 |
| 4 | 3.7823 | 1.8912 | 0.5 | 45949 |
| 5 | 3.5963 | 1.7982 | 0.5 | 62434.8 |
| 6 | 3.4497 | 1.7249 | 0.5 | 75225.7 |
| 7 | 2.9423 | 1.4712 | 0.5 | 115009 |
| 8 | 2.8814 | 1.4407 | 0.5 | 136794 |
| 9 | 2.3299 | 1.165 | 0.5 | 203365 |
| 10 | 2.8399 | 1.42 | 0.5 | 221370 |
| 11 | 2.8493 | 1.4247 | 0.5 | 244757 |
| 12 | 2.2542 | 1.1271 | 0.5 | 251723 |
| 13 | 2.3651 | 1.1826 | 0.5 | 288080 |
| 14 | 2.4215 | 1.2108 | 0.5 | 405444 |

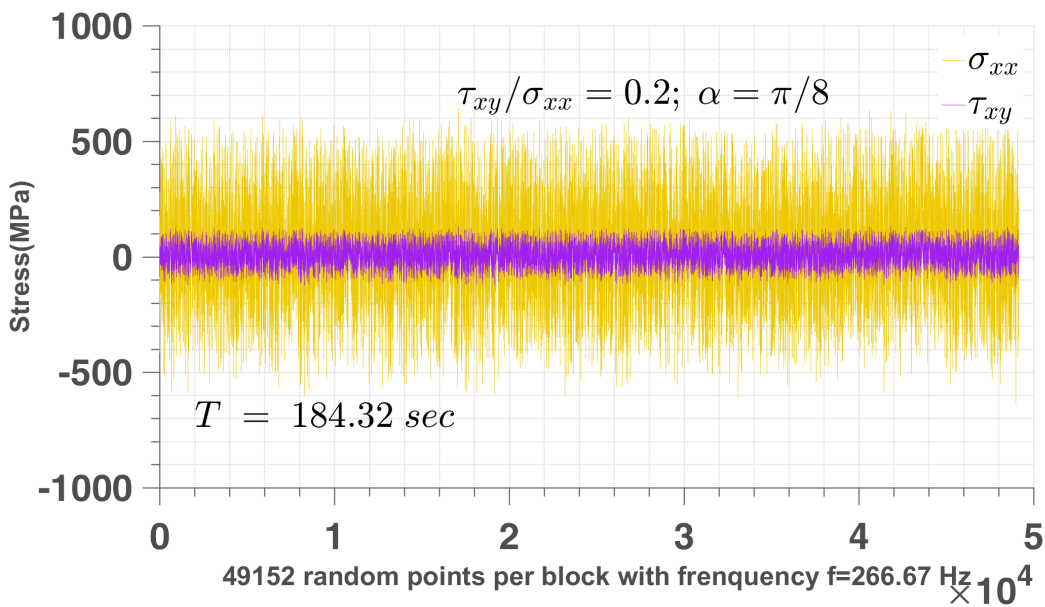
Table 30: Fatigue results under variable loads for $\alpha' = \pi/4$ and $r = f(\tau_{xy})/f(\sigma_{xx}) = 0.5$ 

Fig. 47: Multiaxial random loading sequence

| β | λ_+ | λ_- | W_0 | a | f |
|---------|-------------|-------------|-----------|-----|-----|
| 5.3 | 1.7 | 0 | 6.48E8 Pa | 0.4 | 1.1 |

Table 31: Model parameters for 10HNAP steel

The constant amplitude loading tests corresponds to number of cycles to failure in the range of $1E5 \sim 1E6$. However, in random loading case, the total reversals to failure are $2E6 \sim 5E7$ (calculated from Tab.29 and 30). These two cases belongs to different mechanisms, so their sensitivity of sequence effect and mean stress effect can be different as shown in Tab.31 and 32.

| β | λ_+ | λ_- | W_0 | a | f |
|---------|-------------|-------------|----------|-------|-----|
| 5.3 | 0.3 | 0 | 2.2E8 Pa | 0.001 | 1.1 |

Table 32: Model parameters for 10HNAP steel (random loading)

11.4. Simulation of fatigue tests performed on 10HNAP steel

The constant amplitude unidimensional tests data are show in Tab.33 and 34.

| N^o | N_F | $\Sigma_{xx,a}$ |
|-------|----------|-----------------|
| 1 | 1.00E+05 | 326.69 |
| 2 | 2.00E+05 | 304.42 |
| 3 | 3.00E+05 | 292.11 |
| 4 | 4.00E+05 | 283.68 |
| 5 | 5.00E+05 | 277.30 |
| 6 | 6.00E+05 | 272.20 |
| 7 | 7.00E+05 | 267.96 |
| 8 | 8.00E+05 | 264.34 |
| 9 | 9.00E+05 | 261.19 |
| 10 | 1.00E+06 | 258.41 |

Table 33: Constant amplitude bending tests performed on 10HNAP steel, data from [12]

| N^o | N_F | $\Sigma_{xy,a}$ |
|-------|----------|-----------------|
| 1 | 1.00E+05 | 260.70 |
| 2 | 2.00E+05 | 242.70 |
| 3 | 3.00E+05 | 232.17 |
| 4 | 4.00E+05 | 224.70 |
| 5 | 5.00E+05 | 218.90 |
| 6 | 6.00E+05 | 214.16 |
| 7 | 7.00E+05 | 210.16 |
| 8 | 8.00E+05 | 206.69 |
| 9 | 9.00E+05 | 203.63 |
| 10 | 1.00E+06 | 200.90 |

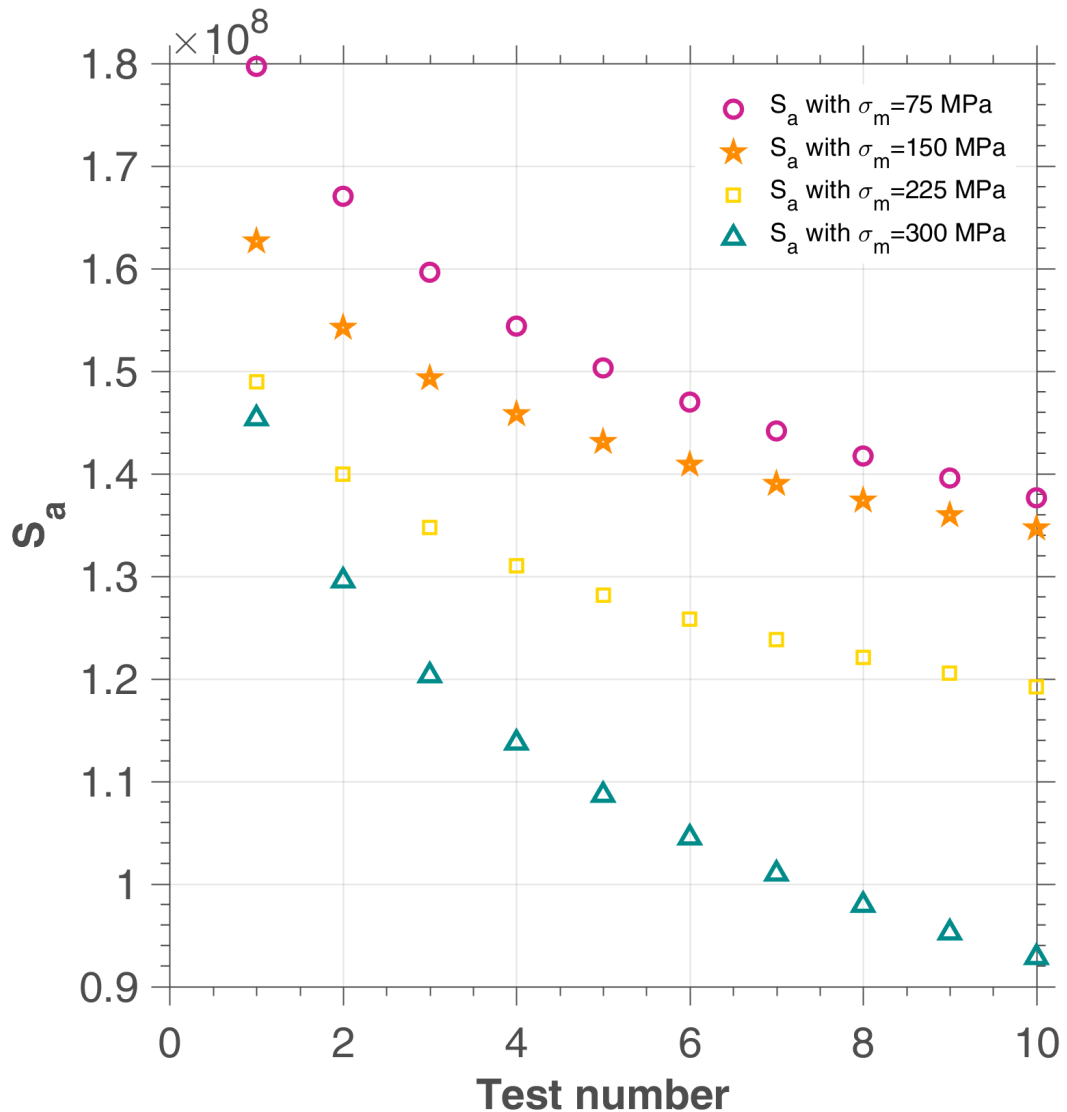
Table 34: Constant amplitude torsion tests performed on 10HNAP steel, data from [12]

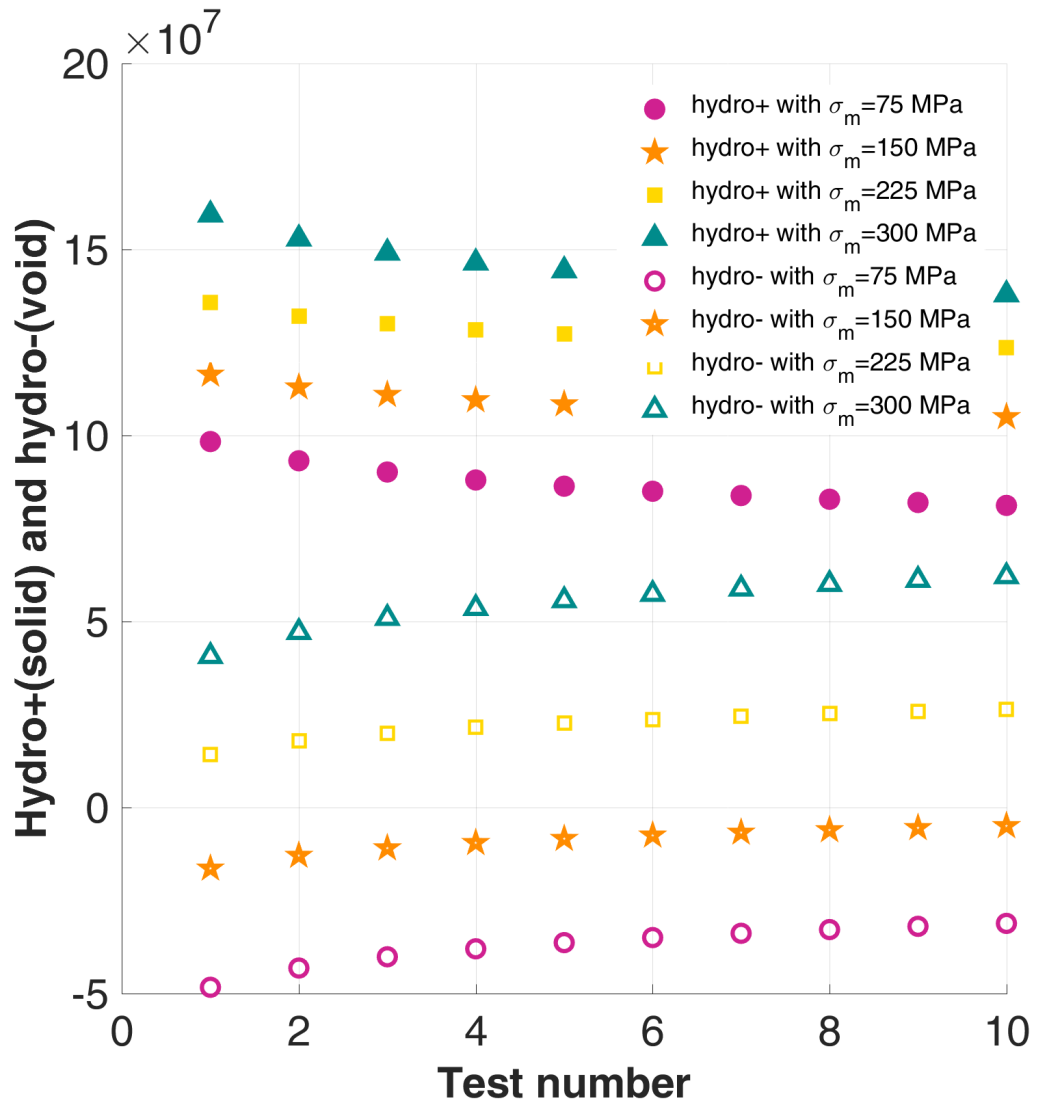
After determining the parameters of the 10HNAP steel model for each of the batches tested, the number of priming cycles can be obtained by directly applying equation (41) for the proportional periodic loads of constant amplitude and for multiaxial loadings of variable amplitude.

In Fig. 52 and Fig. 53, we give the prediction results of the torsion tests used to identify β and W_0 of the model, then we use the bending with various mean stress to get the parameter λ_+ . These are to be taken with caution because of the effect of the gradient because the specimens stressed in tension and in torsion are not of the same nature.

The prediction results of the tensile tests for various values of the mean stress σ_m are summarized in Fig. 53. These results correlate well with the experimental lifetimes.

The tests of multiaxial loadings of variable amplitude are plotted in Fig. 54 and Fig. 55 as a function of the angle α_M and the ratio r . In these figures, the prediction results of the proposed model and that presented by [14]. For the first type of tests ($\alpha_M = \pi/8$ and $r = 0.2$), and the second type of tests ($\alpha_M = \pi/4$ and $r = 0.5$), the predictions of [14] are both good.

Fig. 48: S_a of bending tests with mean stress on 10HNAP

Fig. 49: Hydro_{+-} of bending tests with mean stress on 10HNAP

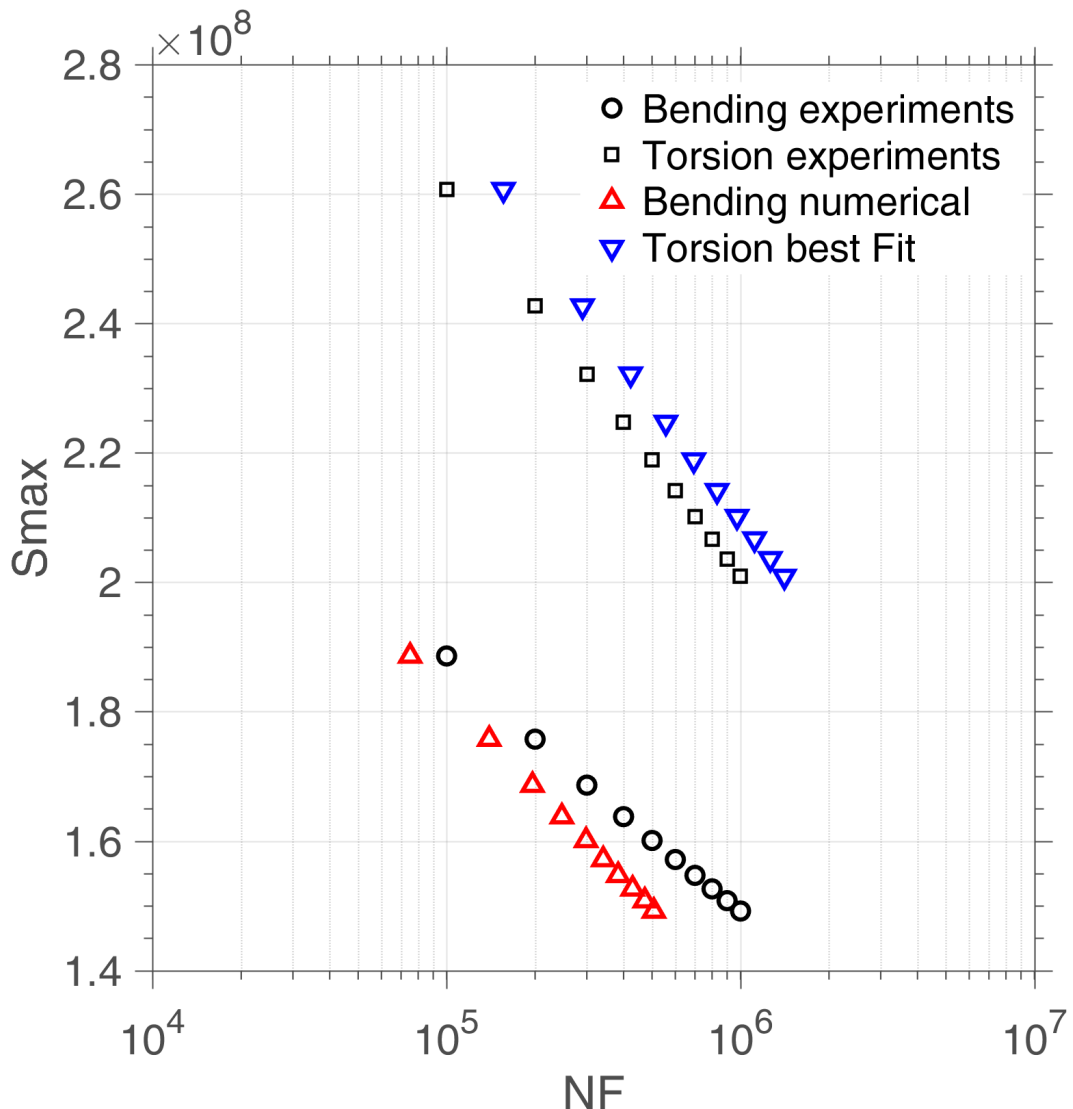


Fig. 50: Bending and torsion test on 10HNAP steel($R=-1$). Data are presented in Tab.33 and 34. The torsion best fit and the bending numerical results(optimal time step of method 2 deduced in Chapter ??) are obtained with the coefficients of Tab.31

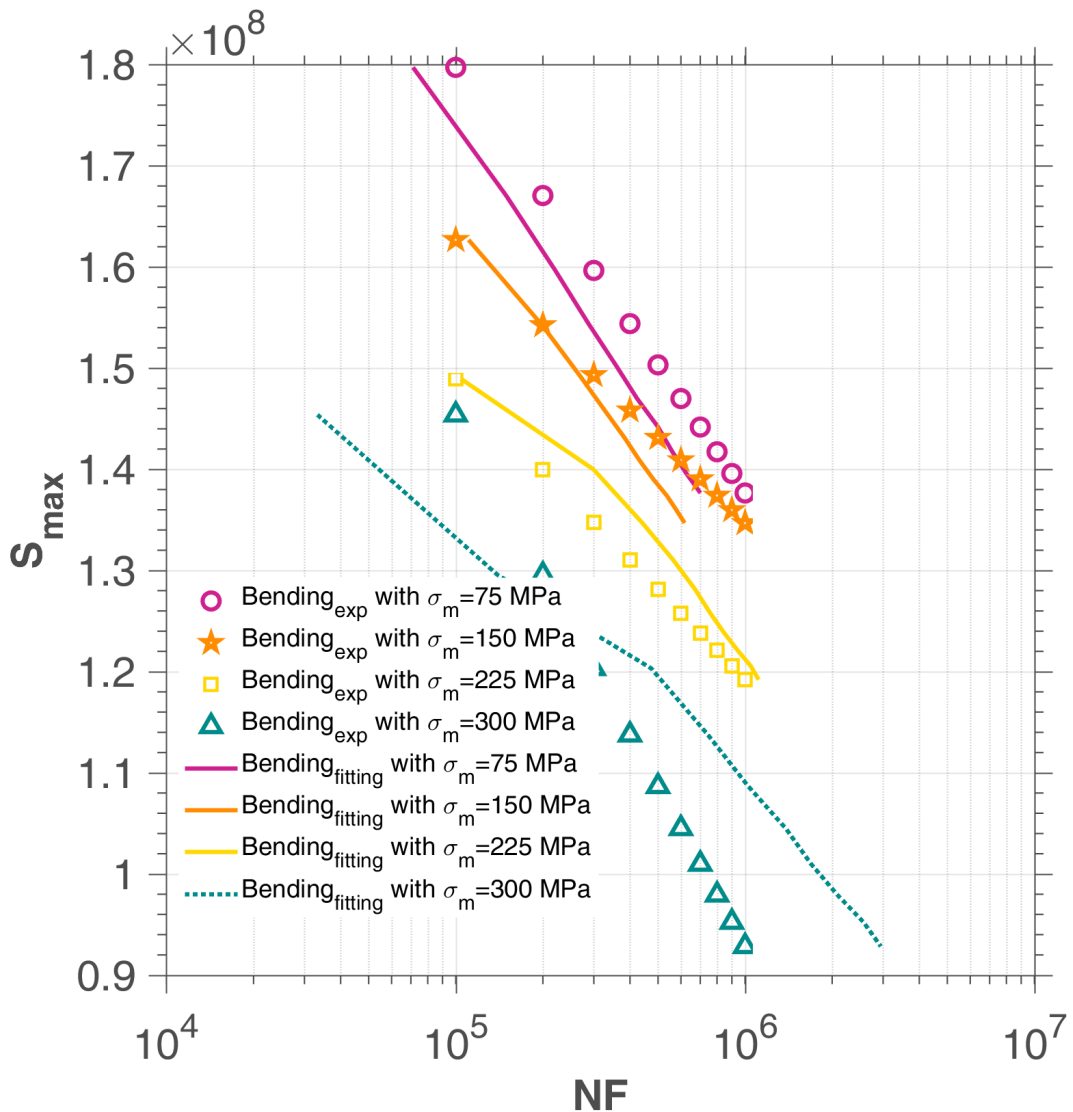


Fig. 51: Wöhler tensile curves for various mean stress values. Data are presented in Tab.28 and results are obtained with the coefficients of Tab.31

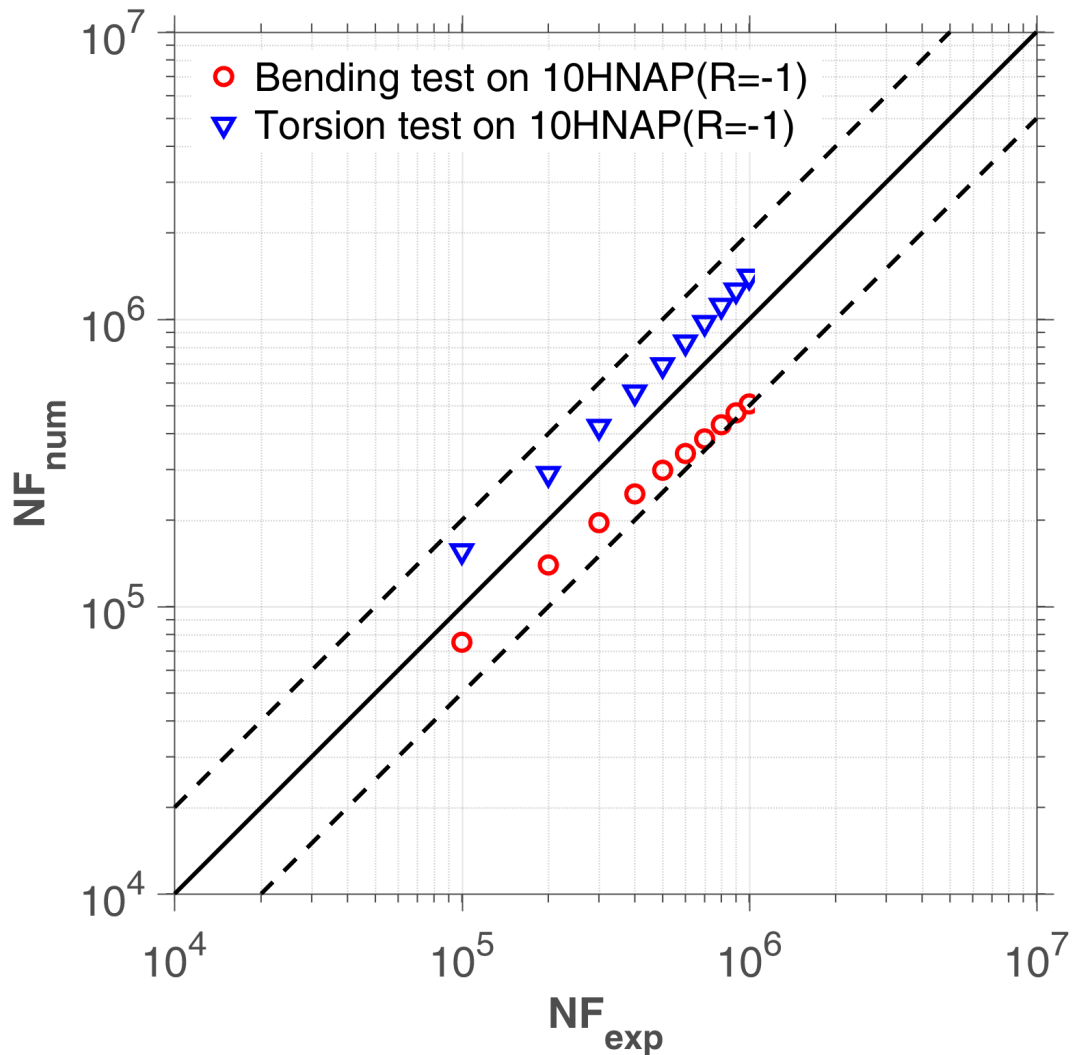


Fig. 52: Calibration on 10HNAP steel, bending and torsion tests on 10HNAP($R=-1$). Data are presented in Tab.33 and 34 and results obtained with the coefficients of Tab.31

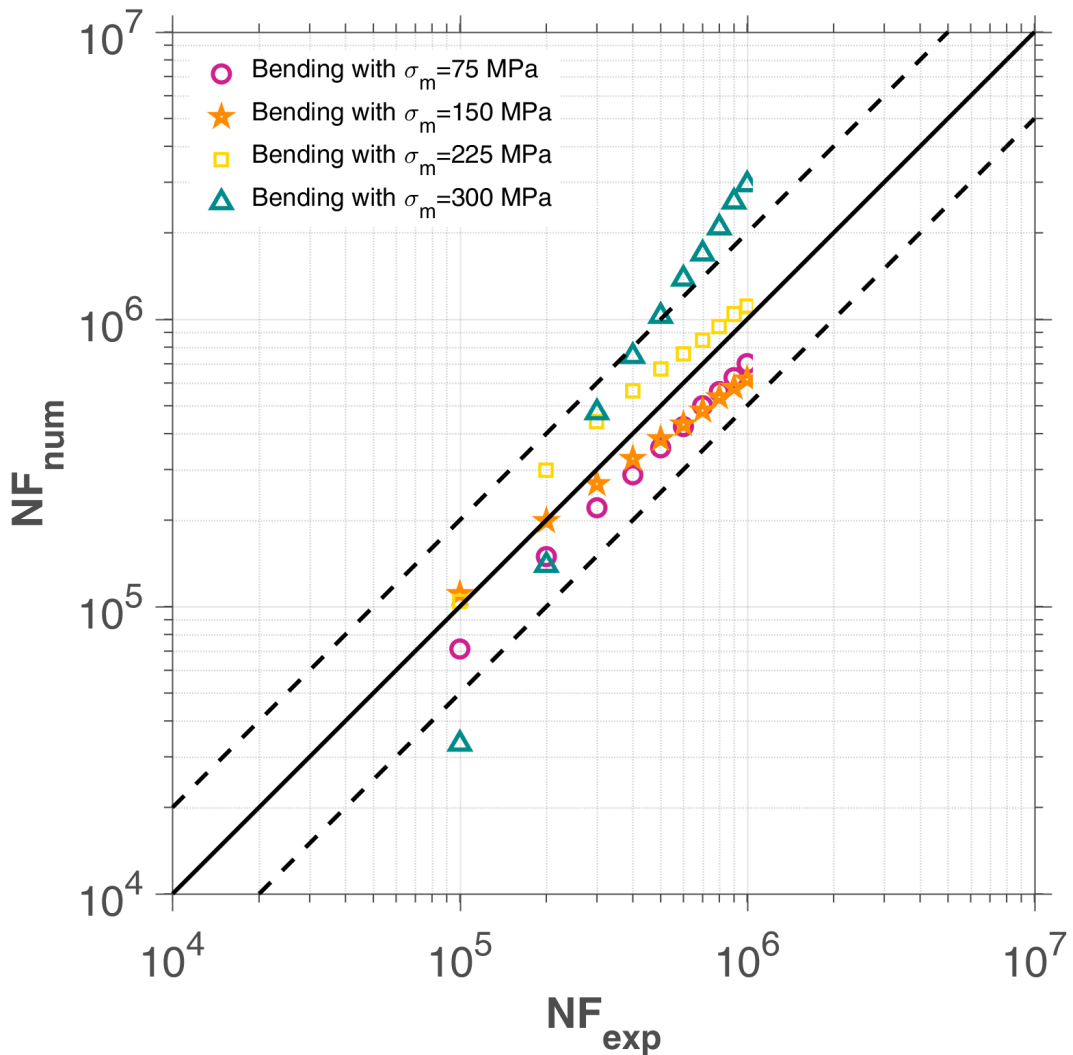


Fig. 53: Calibration on 10HNAP steel, bending tests with various mean stress on 10HNAP, data from Tab.28 and results obtained with the coefficients of Tab.31

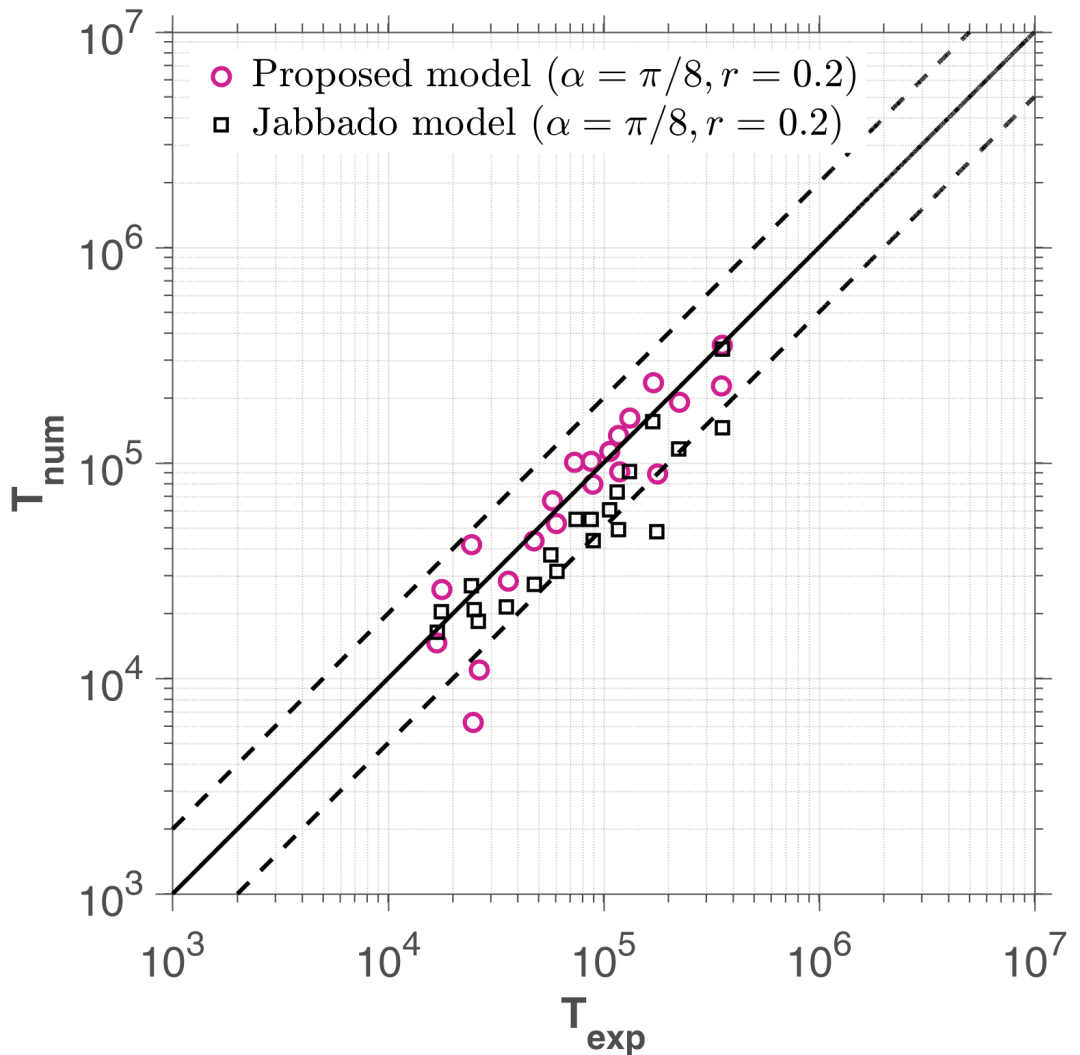


Fig. 54: Random bending-torsion 2D tests on 10HNAP, data from Tab.29 and [13]. Results are obtained with the coefficients of Tab.32 ($\alpha_M = \pi/8$ and $r = 0.2$)

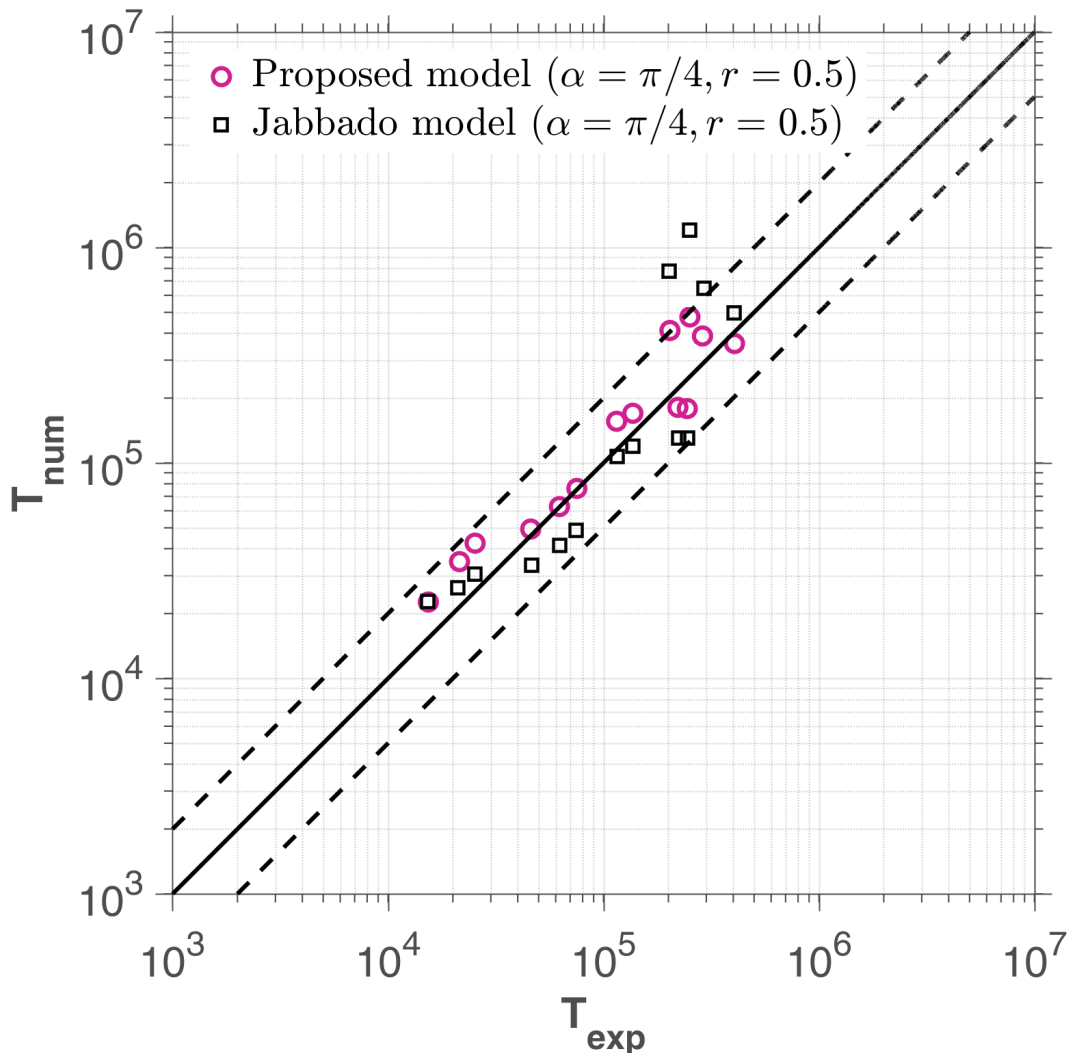


Fig. 55: Random bending-torsion 2D tests on 10HNAP, data from Tab.30 and [13]. Results are obtained with the coefficients of Tab.32 ($\alpha_M = \pi/4$ and $r = 0.5$)

12 Conclusions

We work on the stress tensor directly in 3D analysis in stead of using the multidimensional equivalent stress. The strategy can be made more complex by introducing a local space averaging process in the calculation of the local damage, and by taking more general plastic flows. The energy based fatigue approach takes into account impurities and hardness in the material and is applicable to any type of micro plasticity law and multiaxial load geometry. The time implicit strategy gets rid of cycle counting which is hardly applicable to complex loading, big fluctuation is magnified which reflects the real situation.

There are several advantages and drawbacks of our proposed model. The time implicit method does not take the unit of cycle so as to avoid cycle counting and relevant methods such as rain-flow filter. The possibility to handle different S-N curves corresponding to various materials and load conditions via changing the parameters. We also have the random loading suitability with nonlinear damage accumulation. The drawback is this strategy requires a scale by scale analysis which can be complicated for very high cycle fatigue. However, as introduced above, we can use the optimal time step method to calculate precisely the representative loading history sequence and use scalar integration for the rest of fatigue life. In this way the numerical cost can be dramatically reduced without losing the precision.

Since our method is based on the Dang Van paradigm, to deal with mean stress effect and multiaxial loads we only have the parameter λ_{+-} , which is insufficient to fit the experiments. In fact, our microplasticity model is probably too crude to handle situations where there is a clear strain path effect.

Also, we need more experimental data and comparison with other results from the literature.

Acknowledgments

We are grateful for the financial and technical support of Chaire PSA.

References

- [1] M. Maitournam, C. Krebs, A. Galtier, **A multiscale fatigue life model for complex cyclic multiaxial loading**, International Journal of Fatigue 33 (2) (2011) 232 – 240. doi:<http://dx.doi.org/10.1016/j.ijfatigue.2010.08.017>.
URL <http://www.sciencedirect.com/science/article/pii/S0142112310001933>
- [2] S. Bosia, A. Constantinescu, **Fast time-scale average for a mesoscopic high cycle fatigue criterion**, International Journal of Fatigue 45 (2012) 39 – 47. doi:<http://dx.doi.org/10.1016/j.ijfatigue.2012.06.015>.
URL <http://www.sciencedirect.com/science/article/pii/S0142112312002162>
- [3] M. Zepeng, Structures under multiaxial fatigue taking consideration of gradients of the constraints with time and space variation.
- [4] J. Lemaitre, J.-L. Chaboche, Mechanics of solid materials, Cambridge university press, 1990.
- [5] Legendre Gauss Quadrature weights and nodes, <https://www.mathworks.com/matlabcentral/fileexchange/4540-legendre-gauss-quadrature-weights-and-nodes>, accessed: 2004-05-11.
- [6] L. Susmel, N. Petrone, Multiaxial fatigue life estimations for 6082-t6 cylindrical specimens under in-phase and out-of-phase biaxial loadings, European Structural Integrity Society 31 (2003) 83–104.
- [7] F. Ellyin, K. Golos, Z. Xia, In-phase and out-of-phase multiaxial fatigue, ASME J. Eng. Mater. Technol 113 (1991) 112.
- [8] L. DUBAR, Fatigue multiaxiale des aciers - passage de l'endurance à l'endurance limitée -prise en compte des accidents géométriques., Thèse de Doctorat, Ecole Nationale Supérieure d'Arts et Métiers, Toulouse, France.
- [9] S.-B. Lee, Out-of-phase combined bending and torsion fatigue of steels, ICBMFF2.
- [10] W. Bedkowski, Determination of the critical plane and effort criterion in fatigue life evaluation for materials under multiaxial random loading. experimental verification based on fatigue tests of cruciform specimens (1994) s.435–447.
- [11] B. W. G. J. M. E. ACHTELIC, H., Fatigue life of 10hnsp steel under synchronous random bending and torsion. (1994) 421–434.
- [12] E. VIDAL, Prévision de la durée de vie en fatigue multiaxiale sous sollicitations d'amplitude variable à l'aide d'un critère global.
- [13] M. Jabbado, **High-Cycle Fatigue of Metallic Structures : Lifetime Duration under Variable Loadings.**, Theses,

Ecole Polytechnique X (Mar. 2006).

URL <https://pastel.archives-ouvertes.fr/pastel-00002116>

- [14] A. Carpinteri, A. Spagnoli, S. Vantadori, A multiaxial fatigue criterion for random loading, *Fatigue & Fracture of Engineering Materials & Structures* 26 (6) (2003) 515–522.